Sorption of non-ionic organic compounds by carbon-based nanomaterials – Systematic characterization, modeling, and application

Dissertation

zur Erlangung des akademischen Grades eines
Doktors der Naturwissenschaften
– Dr. rer. nat. –

vorgelegt von

Thorsten Hüffer

geboren in Beckum

Lehrstuhl für Instrumentelle Analytische Chemie
der
Universität Duisburg-Essen

2014

Die vorliegende Arbeit wurde im Zeitraum von Mai 2010 bis Oktober 2013 im Arbeitskreis von Prof. Dr. Torsten C. Schmidt am Lehrstuhl für Instrumentelle Analytische Chemie der Universität Duisburg-Essen durchgeführt.

Tag der Disputation: 08.01.2014

Gutachter:	Prof. Dr. Torsten C. Schmidt
	Prof. Dr. Thilo Hofmann
	Prof. Dr. Stephan Barcikowski
Vorsitzender:	Prof. Dr. Thomas Schrader

2700

Für KPMN

Danksagung

Mein besonderer Dank gilt Herrn Prof. Dr. Torsten C. Schmidt, der mir die Möglichkeit gegeben hat, diese Arbeit anzufertigen. Wissenschaftlich gab er mir stets den größtmöglichen Freiraum und stand bei Bedarf immer mit Rat und Tat zur Seite. Desweiteren möchte ich Herrn Prof. Dr. Thilo Hofmann für die Übernahme des Zweitgutachtens und für den sehr erfolgreichen Start in mein Promotionsprojekt danken. Herrn Prof. Dr. Stephan Barcikowski danke ich für die Erstellung des Drittgutachtens.

Ausdrücklich möchte ich mich bei Frau Dr. Mélanie Kah (Universität Wien), Herrn Beat Schiling (BGB Analytik), Herrn Prof. Dr. Karl Molt, Herrn Dr. Maik A. Jochmann und Frau Xochitli Osorio (alle Universität Duisburg-Essen) für die hervorragende Zusammenarbeit danken. Die dadurch hervorgehenden Manuskripte legten den Grundstein für diese Arbeit. Herrn Dr. Satoshi Endo (UFZ Leipizg) danke ich für seine konstruktive Kritik an Kapitel 5. Dank gebührt auch Frau Sarah Schroth und Herrn Florian Metzelder, deren Bachelor- bzw. Masterarbeit ich betreuen durfte.

Allen derzeitigen und auch ehemaligen Mitarbeitern des Lehrstuhls Instrumentelle Analytische Chemie (Universität Duisburg-Essen) und des Departments für Umweltgeowissenschaften (Universität Wien) möchte ich für die immer freundliche und produktive Zusammenarbeit danken. Besonders danken möchte ich dabei der „Kochgruppe“ an der Uni Wien (Susanne Laumann, Dr. Elisabeth Neubauer und Dr. Christian Mühlegger) für die freundschaftliche Aufnahme und die sehr schöne Zeit in Wien sowie der Gruppe „AOP+X“ (Alexandra Beermann, Alexandra Fischbacher, Holger Lutze und Dr. Maike Cyris). Dies gilt ganz besonders auch für PD Dr. Uschi Telgheder (Universität Duisburg-Essen). Ich danke Euch für die immer offenen Türen, die Spitznamen und das Aufmuntern!

Dank gebührt ebenfalls der Deutschen Forschungsgemeinschaft, die meinen Antrag auf Förderung bewilligte und mir damit den nötigen finanziellen Freiraum für diese Arbeit gab.

Desweiteren möchte ich ganz besonders meinen Eltern, Sabine und Bernd, sowie meinem Bruder Martin, aber natürlich auch meinen Freunden danken, die mich in all den Jahren, aber ganz besonders in den letzten Monaten, immer unterstützt und stets zu mir gehalten haben.

Summary

The interaction (i.e., sorption) of hydrophobic organic compounds (HOC) and carbon-based nanomaterials (CNM) has already been studied to some extent; however, a fundamental and systematic understanding of the relevant sorption mechanisms is yet missing. As a result of their increasing application, CNM will inevitably be released to the environment. Consequently, the interaction of HOC and CNM is of major importance for example for the environmental risk assessment on how CNM may influence the fate and transport of HOC. A qualitative and quantitative understanding of the interactions between HOC and CNM is thus of crucial importance. To this end, this thesis aims at a comprehensive and systematic investigation of sorption of carefully selected sorbates as molecular probe compounds by various CNM.

The influence of environmentally relevant parameters such as irradiation, redox conditions, or the presence of natural organic matter (NOM) on sorption by CNM was investigated. Both the presence of oxygen and irradiation significantly changed surface properties of aqueous dispersed fullerenes (nC60) and consequently reduced the sorption affinity and capacity of nC60 for polycyclic aromatic hydrocarbons. Furthermore, the presence of NOM was shown to result in a reduction of sorption affinity and non-linearity by multi-walled carbon nanotubes (MWCNTs). Nevertheless, the use of *n*- and cycloalkanes as molecular probes showed that a potential change in sorption mode from *ad*sorption by MWCNTs to *ab*sorption into NOM-coated MWCNTs did not occur. Overall, the studied parameters indicated a decreased sorption by CNM after a release of these sorbents into the environment.

Sorption isotherms of a diverse set of molecular probes covering compounds of various polarities were determined to develop a poly-parameter linear free-energy relationship (ppLFER) for sorption by MWCNTs. This approach gave useful insights into the relevant interactions and their contribution to overall sorption. The development of a ppLFER allowed a significantly improved prediction of distribution coefficients between water and MWCNTs compared to commonly used predictions based on a correlation of sorption by MWCNTs with hydrophobicity parameters of sorbates, such as the octanol-water partitioning coefficient.

Finally, MWCNTs were explored for their potential application in solventless in-tube microextraction for the preconcentration of BTEX compounds from aqueous samples. For

method development, a design of experiments was used for a systematic investigation of relevant extraction parameters and their interactions. The results of method validation emphasized the strong interaction of MWCNTs with BTEX and the promising potential of the sorbent in analytical chemistry compared to currently available sorbent material. In addition, the method was successfully applied to various real samples.

This thesis demonstrates that systematic approaches in combination with selected probe sorbates present useful insights into the molecular interaction of CNM with non-ionic organic compounds.

Zusammenfassung

Sorption nicht-ionischer organischer Verbindungen an kohlenstoff-basierten Nanomaterialien – Systematische Charakterisierung, Modellierung und Anwendung

Die Wechselwirkung (Sorption) von hydrophoben organischen Verbindungen (HOC) und kohlenstoffbasierenden Nanomaterialien (CNM) wurde bereits in gewissem Umfang untersucht. Ein grundlegendes und systematisches Verständnis der relevanten Sorptionsmechanismen fehlt aber bisher. Zudem wird als Folge ihrer zunehmenden Anwendung ein Eintrag von CNM in die Umwelt unweigerlich wahrscheinlicher. Folglich ist die Wechselwirkung von HOC und CNM auch unter umweltrelevanten Aspekten von großer Bedeutung: zum Beispiel zur Risikoabschätzung, ob CNM in der Umwelt den Verbleib und Transport von HOC beeinflussen. Ein qualitatives und quantitatives Verständnis der Wechselwirkungen zwischen HOC und CNM ist dafür von entscheidender Bedeutung. Zu diesem Zweck war das Ziel dieser Arbeit eine umfassende und systematische Untersuchung der Sorption von ausgewählten Sorbaten als molekulare Sonden an verschiedenen CNM.

Der Einfluss umweltrelevanter Parameter, wie Redox-Bedingungen, die Bestrahlung mit Licht und das Vorhandensein von natürlichem organischem Material (NOM), auf die Sorption an CNM wurde untersucht. Durch Anwesenheit von Sauerstoff und Bestrahlung änderten sich die Oberflächeneigenschaften von wässrig dispergiertem Fulleren (nC60) erheblich. Folglich reduzierte sich die Sorptionsaffinität und –kapazität polyzyklischer aromatischer Kohlenwasserstoffe an nC60. Zudem führte die Anwesenheit von NOM zu einer Reduzierung der Sorptionsaffinität und –nichtlinearität an mehrwandigen Kohlenstoffnanoröhren (MWCNTs). Hingegen zeigte die Verwendung von n- und Cycloalkanen als molekulare Sonden keine Änderung des Sorptionsmodus von *Ad*sorption an die Oberfläche von MWCNTs zu *Ab*sorption in NOM-beschichtete MWCNTs. Insgesamt lassen die Ergebnisse der untersuchten Parameter auf eine verringerte Sorption an in die Umwelt eingetragenen CNM schließen.

Sorptionsisothermen wurden für eine Vielzahl diverser Molekularsonden unterschiedlicher Polarität experimentell bestimmt, um die Sorption an MWCNTs mittels poly-parameter linearer freie-Energie Beziehungen zu beschreiben. Dieser Ansatz gab nützliche Einblicke in

die relevanten Wechselwirkungen und deren Beitrag zur Gesamtsorption. Die Entwicklung einer ppLFER erlaubte eine deutlich verbesserte Vorhersage der Verteilungskoeffizienten im Vergleich zu gängigen Vorhersagemodellen mittels einer Korrelation der Sorption an MWCNTs und Hydrophobizitätsparametern, wie der Oktanol-Wasser Verteilungskonstanten.

Schließlich wurden MWCNTs hinsichtlich einer möglichen Anwendung als gepackte Phasen in der lösemittelfreien In-tube Mikroextraktion zur Anreicherung von BTEX aus wässrigen Proben untersucht. Zur Methodenentwicklung wurde eine statistische Versuchsplanung verwendet, die eine systematische Untersuchung der relevanten Extraktionsparameter und deren potentieller Wechselwirkung erlaubte. Die Ergebnisse der Methodenvalidierung betonten die starke Wechselwirkung von MWCNTs und BTEX und damit das vielversprechende Potential von CNM als Sorbentmaterial in der analytischen Chemie im Vergleich zu derzeit verfügbaren Extraktionsphasen. Zudem wurde das Verfahren erfolgreich an verschiedenen Realproben angewandt.

Die vorliegende Arbeit zeigt, dass systematische Verfahren in Kombination mit ausgewählten Sorbatsonden, wertvolle Einblicke in die molekularen Wechselwirkungen von CNM mit nicht-ionischen organischen Verbindungen bieten.

Table of contents

Chapter 1 General Introduction

1.1 Theoretical Background

1.1.1 Sorption

In principle, *sorption* is regarded as the process, where a chemical (*sorbate*) becomes associated with a solid phase (*sorbent*) [1]. In solid-water systems, sorption at equilibrium conditions (i.e., no net-change of concentration) is described by the distribution coefficient (K_d), which is given by the ratio between the equilibrium concentrations of the sorbate sorbed by the sorbent (C_s) and its aqueous concentration (C_w):

$$K_d = C_s / C_w \qquad \text{(Eq. 1-1)}$$

The unit of K_d is commonly given by the volume of water over the dry weight of the sorbent. However, due to the fact that K_d may depend on various factors, such as sorbate and sorbent properties, aqueous chemical conditions and in certain cases sorbate concentration, a comparison of K_d values reported may be difficult to achieve. The relationship between the two concentrations is generally considered as *sorption isotherm* [1]. In practice, sorption isotherms are commonly determined by batch experiments, in which a given mass of sorbent is mixed with water, spiked with the sorbate, and then the system is equilibrated by agitation at constant temperature. After equilibration, the solid and the aqueous phase are separated and the sorbate concentration in the aqueous phase is determined. The sorbed concentration of the sorbate can then be obtained by mass balance:

$$m_T = m_w + m_s \qquad \text{(Eq. 1-2)}$$

where m_T, m_w, and m_s denote the total mass of sorbate in the system, in water, and associated on the solid, respectively. The sorption isotherm is then obtained by plotting C_s versus C_w. If a linear sorption isotherm is given, K_d is constant and independent from the considered concentration range. Otherwise, at non-linear sorption, K_d is regarded as the sorption coefficient and depends on the aqueous concentration of the sorbate. In that case various sorption models have been developed to explain sorption, which are further explained in section 1.1.2.

An important question for the phase transfer of organic molecules is the clarification of the dominant sorption mode. Here, generally two modes are discussed: the *ad*sorption onto the surface of a sorbent, or on the other hand, *ab*sorption, i.e., the distribution into a condensed phase. To clarify the dominant sorption mode only a few experimental approaches are available. While Goss & Bronner studied sorption of highly fluorinated compounds [2], another approach was developed by Endo et al., where distribution coefficients of linear and cyclic alkanes were compared in order to differentiate between *ad*- and *ab*sorption [3]:

$$K_n / K_c = \frac{K_{\text{d of n-alkane}}}{K_{\text{d of cycloalkane}}} \qquad \text{(Eq. 1-3)}$$

This comparison of sorption of n- and cyclo-alkanes is based on the fact that linear alkanes preferably *ad*sorb onto surfaces, as in case of non-planar cyclohexane, not all carbon atoms may interact with the sorbent surface, which is the case for planar n-hexane [4, 5]. In contrast, the partitioning (i.e., *ab*sorption) of cyclo-alkanes from air into a condensed phase is stronger than for their linear homologues as the molar volume of cyclic alkanes is generally smaller, which results in less free-energy required for cavity formation during partitioning processes [6]. However, a direct comparison of the sorbent-water distribution coefficients for alkane pairs as given in equation 1-3 is not feasible as the calculated coefficients do not only result from interactions between sorbent and sorbate, but also the interaction with water is included. Thus, a normalization of the determined distribution coefficients by the air-water partitioning constant (K_{aw}) is necessary:

$$K_n / K_c = \frac{K_d / K_{aw} \text{ of n-alkane}}{K_d / K_{aw} \text{ of cycloalkane}} \qquad \text{(Eq. 1-4)}$$

From the given derivation of equation 1-4, it can be concluded that if $K_n/K_c < 1$ *ab*sorption is the dominant sorption mode, while for $K_n/K_c \geq 1$ the sorption process can be considered as *ad*sorption. Steric effects have to be considered, as for microporous materials the interaction can be significantly stronger, where the molecular shape of compounds fit precisely into the pores of the given material. Furthermore, in case where sorbates are larger than the pore sizes, size exclusion effects may have to be taken into account. Overall, this leads to the restriction that significant steric effects can lead to $K_n/K_c >> 1$; for example, for some zeolites or

activated carbons K_n/K_c values of 100 and higher were obtained [3]. The concept of distinguishing between the two sorption modes was applied for literature data to determine the dominant sorption mode of various sorbents for sorption from air [3] as well as to characterize the sorbent properties of soil organic matter and carbonaceous geosorbents [7].

1.1.2 Sorption models and mechanisms

In order to explain non-linear sorption, various models have been derived in literature, of which only the most relevant for sorption in aqueous systems should briefly be discussed here. For example, non-linear sorption models have successfully been applied for *ad*sorption by organic and inorganic surfaces, such as activated carbon [8] and clay minerals [9]. Among the most frequently considered sorption models is the empirically derived relationship by Freundlich, in which it is assumed that various types of sorption sites are available for sorption in parallel in combination with total site abundance. In general, the FM assumes that there is no limited sorption capacity, while each sorption site offers different free-energy for interaction. The mathematical relationship of the *Freundlich Model* (FM) is given by:

$$C_s = K_F C_w^{\ n} \qquad \text{(Eq. 1-5)}$$

where K_F is the Freundlich coefficent, commonly expressed in the corresponding units of C_s and C_w, and n is the Freundlich exponent. In case where n = 1, the sorption isotherm is linear and a homogeneous free-energy distribution of sorption sites can be assumed. In that case equation 1-5 simplifies to equation 1-1 and K_F equals K_d. When n < 1, sorption free-energy decreases with increasing sorbate concentration and the sorption isotherm has a concave like shape. Furthermore, when n > 1, the free-energy increases with increasing sorbate concentration and the isotherm becomes convex shaped [1].

In contrast, the *Langmuir Model* (LM) assumes a homogeneous distribution of sorption free-energy in combination with the formation of a monolayer on the sorbent surface, i.e., surface saturation, due to a limited number of available sorption sites. This is described by:

$$C_s = \frac{Q_{max} K_L C_w}{1 + K_L C_w} \qquad \text{(Eq. 1-6)}$$

where Q_{max} represents the maximum sorption capacity and K_L is referred to as the Langmuir affinity coefficient. It should be noted that Q_{max} is sorbate specific as the total number of available sorption sites may be occupied by less molecules of a rather large compound, while more molecules of a small compound may be sorbed [1].

Another model mainly applied to describe sorption of hydrophobic sorbates is the *Polanyi-Manes Model* (PMM). In brief, the sorption potential (ε) of a given sorbate that exists close to the area of a sorbent surface, depends on its vicinity to the sorbent surface and the properties of the sorbate [10]. The application of Polanyi theory relies on the postulate that organic sorbates of limited miscibility with water will separate as liquid-like or solid like sorbates, when the sorbate sorption potential suffices to concentrate them to saturation [11]. For sorption of partially miscible solutes from aqueous solution, the effective sorption potential (ε_{sw}, kJ mol^{-1}) can be defined as:

$$\varepsilon_{sw} = RT \ln(S_w / C_w) \qquad \text{(Eq. 1-7)}$$

where S_w represents the aqueous solubility, C_w is the aqueous concentration of the sorbate at absolute temperature T [K], and R is the universal gas constant [kJ mol^{-1} K^{-1}]. It should be noted that ε_{sw} is the sorption potential corrected for the sorption potential of an equal volume of water on a non-polar sorbent, such as activated carbon [11-12]. In the PMM, sorption isotherms are expressed in terms of the sorbate volume and the sorption potential density, ε_{sw}/V_s. With the molar volume used as a correlating divisor [13], the empirically derived relation can be used to describe the sorption isotherms by carbonaceous sorbents for a wide variety of sorbates [14-15].

$$\log C_s = \log Q_{max} + a\left(\varepsilon_{sw} / V_s\right)^b \qquad \text{(Eq. 1-8)}$$

where C_s is the sorbed sorbate concentration, Q_{max} is the maximum sorption capacity, a and b are fitting parameters, and V_s is the bulk molar volume of the sorbate at temperature of sorption.

1.1.3 Linear free-energy relationships (LFER)

The interpretation and prediction of molecular interactions is of major importance to understand phase distribution processes in environmental chemistry. However, the determination of distribution coefficients of all compounds of interest is not possible due the high number of both used compounds and relevant phases. Thus, a correlation between the distribution of compounds between natural phases on the one hand (i.e., the free-energy of transfer, $\Delta_{12}G_i$), and their specific physico-chemical properties on the other hand is common practice in environmental chemistry. These so-called linear free-energy relationships are most frequently used for the correlation of phase transfer with hydrophobic parameters, such as the octanol-water partitioning constant, K_{ow}, (equation 1-9) or the aqueous solubility, S_w, (Equation 1-10).

$$\log K_i = a \log K_{ow} + b \qquad \text{(Eq. 1-9)}$$

$$\log K_i = a' \log S_w + b' \qquad \text{(Eq. 1-10)}$$

where a, a', b, and b' are regression coefficients/constants. Despite the fact that these one-parameter LFER may be powerful tools for the prediction of sorption processes if cautiously used, there are a number of important limitations: the correlations shown in equations 1-9 and 1-10 are only valid for a specific compound class and may be used only for the prediction for phases the fitting parameters a and b were determined for. Furthermore, the precision of the derived prediction model depends on the precision of the raw data and for some physico-chemical properties, such as K_{ow}, the literature data may vary [16]. These disadvantages may be overcome by linear salvation-energy relationships (LSER), which are the most commonly used poly-parameter linear free-energy relationships (ppLFER). LSER developed by Abraham et al. are promising approaches as they decompose the free-energy of transfer of a given compound *i* between two phases, 1 and 2, into terms of relevant interactions in a single equation [17-18]. Each term in LSER represents the contribution of individual intermolecular interactions by properties of the sorbate, so-called solute descriptors, and the sorbent, phase descriptors. For sorption of non-ionic organic compounds, only non-specific van-der-Waals and specific electron-donor-acceptor (EDA) interactions, such as hydrogen bonding, are relevant interactions to be considered. In the majority of studies two types of ppLFER were fitted to the experimental data sets:

$$\log K_{i,12} = eE + sS + aA + bB + vV + c \quad \text{(Eq. 1-11)}$$

$$\log K_{i,12} = eE + sS + aA + bB + lL + c \quad \text{(Eq. 1-12)}$$

The notations in equations 1-11 and 1-12 are as follows: E, the excess molar refraction; S, the dipolarity/polarizability parameter, A; the solute hydrogen (H)-bond acidity; B, the solute H-bond basicity; V, the molar volume; and L, log of the hexadecane-air partitioning constant. The regression coefficients e, s, a, b, v, and l in equations 1-11 and 1-12 characterize the phase capabilities of corresponding molecular interactions with solutes. The phase descriptors and the constant c are determined by linear multiple regression analysis (MRA) after the experimental determination of several tens to hundreds of distribution coefficients. The solute descriptors can be obtained from literature for many thousands of compounds [19-21]. For a detailed review on the theoretical aspects of ppLFER, the reader is referred to Goss & Schwarzenbach [22]. To date ppLFER have successfully been applied to qualitatively and quantitatively describe sorption of organic compounds from air by snow [23], from aqueous solutions by activated carbon [24] and solid-phase microextraction (SPME) fibers [25], and natural organic matter (NOM) in soils and sediments [26-27]. Aside from the precise prediction of phase distribution by ppLFER, they are powerful tools to characterize the properties of sorbents [28].

1.2 Carbon-based nanomaterials (CNM)

Based on their composition, nanomaterials (NM) can be divided into inorganic and carbon-based nanomaterials (CNM). Furthermore, NM can be distinguished between natural and anthropogenic, engineered nanomaterials (ENM). A schematic overview of nanomaterials is given in Figure 1-1.

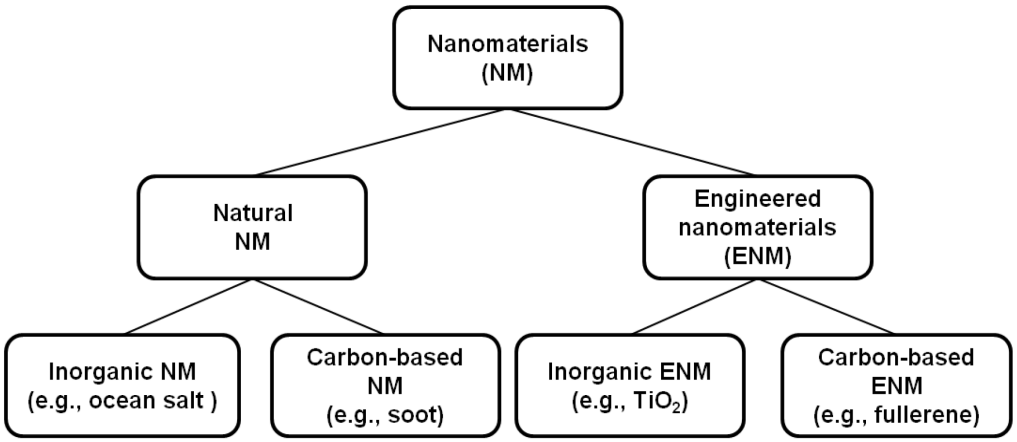

Figure 1-1: Schematic categorization of nanomaterials. Adapted from [29].

CNM can be further sub-divided in fullerenes (C60) and carbon nanotubes (CNTs) (Figure 1-2). CNTs consist of cylindrically rolled graphene layers that can measure several micrometers in length and a few nanometers in diameter. In addition, the walls of CNTs can be made of a single graphite layer, so-called single-walled carbon nanotubes (SWCNTs), or several graphite layers, which are nested concentrically, so-called multi-walled carbon nanotubes (MWCNTs) [30]. Since their first discovery in 1991 by arc-discharge, several production processes have been developed [31], so that today CNTs with various properties (e.g., chirality, diameter, length, and functionalization) can be produced industrially and are commercially available.

Figure 1-2: Carbon-based nanomaterials: Fullerene (left), SWCNT (middle), and MWCNT (right). Adapted from [32].

As a result of varying synthesis, purification, and functionalization, CNM have very diverse and unique properties [33], which allow a wide range of application. CNM are, among others, used in nanoelectronics as storage materials, sensors, and catalysts, whereas CNM are used in medicine to investigate the fate and transport of drugs [34]. Environmentally relevant applications of CNM are in areas of antimicrobial agents, sorbents, environmental sensors, and renewable energy [32]. In the field of analytical chemistry, CNM are increasingly used as sorbents and separation phases [35]. In many of these areas, the understanding of sorption properties and relevant mechanisms of different CNM is of great importance.

Because of the broad application fields of CNM, the annual production capacity of SWCNTs was estimated to have reached 4500 t in 2011 [36], whereby the entry of these materials into the environment is likely to increase. However, there are no data or studies concerning the presence of CNM in the environment, which is partly due to still very few available analytical methods, which are mainly based on microscopy. A modeling experiment using a probabilistic material flow analysis showed low CNM concentrations in all compartments modeled compared with other ENM (i.e., nano-TiO_2, -ZnO, -Ag) [37]. The already mentioned increasing production and wider application of CNM in combination with the hitherto not existing regulation regarding their disposal, suggest not only an increase in environmental concentrations but also a change in potential entry pathways in natural water bodies [38]. Despite the non-regulation, NM in general have been recorded on the list of “Emerging Pollutants” [39].

1.3 Environmental behavior of CNM

The aforementioned increasing production and application of CNM raises the question of their environmental behavior. Among the most important issues in terms of the environmental relevance of CNM are the questions regarding their i) toxicity, ii) stability (i.e., aggregation), and iii) impact on the transport of contaminants [38, 40]. In the following only the latter two aspects are considered as the toxicity was not within the scope of this study.

Generally, CNM tend to aggregate in aquatic environments due to their strong hydrophobic character. The stabilization of CNM dispersions can be achieved either by functionalization of the CNM surface in order to reduce their hydrophobicity, e.g., by oxidation, or with the addition of stabilizing agents such as surfactants or NOM. In this process, the stabilization of CNM is achieved either by direct contact between the nanoparticle and the dispersion agent's molecules, which leads to a disaggregation of the nano bundles into smaller aggregates, or individual "particles" [41]. Furthermore, it has been shown that both the presence of mono- and divalent cations and pH have a major impact on the stability of CNM dispersions [42-43]. In addition, the stability of an aqueous CNM dispersion varies among different kinds of CNM. Lin et al. investigated the stability of pristine MWCNTs in fresh water samples after the addition of stabilizing agents and showed that with one exception none of the investigated mixtures were stable over the observed period of one week [44]. It has recently been shown that the aggregation of CNM and their sorptive behavior have to be considered simultaneously [45-46].

Assessing the impact of the presence of CNM on the transport of contaminants requires a systematic understanding of their interaction with, among others, hydrophobic organic compounds (HOC). With regard to sorption of HOC by CNM in the environment, it can be assumed that the interaction between sorbent and sorbate is strongly affected by environmental factors. Sorption of individual compounds or several compounds of one compound class has been the subject of several studies, whereas Pan and Xing summarized previous work on sorption mechanisms of organic compounds by CNTs [47]. Overall, sorption of HOC by CNM is a non-linear process. Various sorption models have been discussed to explain sorption by CNM (e.g., Freundlich Model, FM [48]; Langmuir Model, LM [49]; and Polanyi-Manes Model, PMM [50]). From this, it can be concluded that generally non-linear sorption by CNM cannot be described by a single sorption coefficient.

Essentially, two reasons are given for explanation: i) the presence of high-energy sorption sites due to surface defects [51], functional groups [52], and regions in gaps and joints of CNM bundles [53] and ii) condensation of the sorbate on the sorbent surface and in capillaries [54].

The outer surface of CNM provides hydrophobic sorption sites. While hydrophobic interactions have previously been discussed, for example, for sorption of acidic herbicides by CNTs [54], an explanation of sorption due to hydrophobic interactions alone resulted in an inadequate prediction of sorption by hydrophobic parameters such as the octanol-water partitioning constant (K_{ow}). A general relationship between K_{ow} of the sorbate and the measured sorption by CNM could not be observed [47], which clearly shows that hydrophobicity alone cannot comprehensively explain sorption by CNM [55].

Chin et al. (2010) compared sorption of various substituted non-polar benzene derivates by pristine and functionalized SWCNTs to investigate the influence of sorbate properties on the interaction with CNTs. Unlike benzene, toluene showed a lower sorption capacity after the oxidation of SWCNTs, which was explained by steric hindrance of the electron donor-acceptor (EDA) interactions resulting from the surface modification of the sorbent [56]. Furthermore, a linear relationship between the oxygen concentration on the surface of MWCNTs and their sorption capacity for naphthalene was observed [57]. Thus, the influence of properties of the sorbate and the sorbent on sorption needs to be taken into account.

There are two main limitations to so far published studies on sorption of non-ionic organic compounds by CNM. Firstly, a relatively high concentration range with respect to the aqueous solubility of the sorbate is usually investigated (Table 1-1). However, as sorption by CNM has in most cases found to be non-linear, the investigated concentration range is a crucial aspect when assessing sorption strength and thus impact of CNM on transport of HOC. In fact, Kah et al. showed that sorption of PAHs by MWCNTs is linear in a low concentration range (pg-ng L^{-1}) over three orders of magnitude, while the formation of a mono-layer (i.e., non-linear sorption) was observed for high concentrations [58]. In combination, this led to the best isotherm fit by a combination of linear and Langmuir-based model sorption over the full concentration range of six orders of magnitude. This further emphasizes importance of the investigated concentration range. In addition, sorption is most

often investigated over a concentration range smaller than three orders of magnitude. A meaningful discussion of sorption data and an interpretation of the sorption mechanism are hardly possible, especially in concentration ranges only one or two orders of magnitude below the aqueous solubility [58]. Secondly, the sorbate concentration in the aqueous phase is analyzed in the supernatant after a separation of the sorbent from the aqueous phase, which in sorption batch experiments is commonly achieved by various methods, such as filtration [59], sedimentation [60-61], or centrifugation [55, 62]. These techniques may be sufficient for phase separation if the nanoparticles are highly aggregated [58]. In size ranges, where particles show properties not observed in the bulk material (< 30 nm) [63], these methods may fail due to an incomplete separation of the sorbent from the aqueous phase, which could lead to a subsequent underestimation of the distribution coefficient (K_d). Alternative approaches such as the introduction of a third phase, e.g., with non-depletion solid-phase microextraction (nd-SMPE) [64] or polyoxymethylene solid-phase extraction (POM-SPE) [45, 58], have exemplarily been applied to investigate sorption by CNM; however, they have yet hardly been used in common practice.

Table 1-1: Selected studies of sorption by CNM reported in literature.

Sorbate	Sorbent	Phase separation	C_w/S_w [a]	Reference
Naphthalene	C60	Filtration	10^{-2}-10^{-1}	[59]
PAH	MWCNTs	Sedimentation	10^{-1}-10^{-3}	[60]
Benzene	CNTs	Sedimentation	10^{0}-10^{-3}	[61]
Phenanthrene	CNM	Centrifugation	10^{0}-10^{-3}	[62]
Bisphenol A	CNM	Centrifugation	10^{-1}-10^{-4}	[55]

[a] C_w/S_w: aqueous concentration to solubility ratio.

In a recently published statement by the German Federal Environment Agency on "nanotechnology for humans and the environment" an urgent information gap and research needs especially in the area of "interaction [….] with chemicals dependent of their form, size, charge, coating, and/or surface shape" is stated [65]. In addition, in the more recently published revised OECD "Guidance manual for testing of manufactured nanomaterials", a future research focus on sorption by NM is determined [66]. To date available studies on sorption of organic compounds by CNM mainly deal with the analysis of individual mechanisms. For example, Chen et al. evaluated sorption of polar and non-polar aromatic compounds by CNM and found poor correlation with the hydrophobicity of the sorbates [62].

This investigation considered one of the most diverse probe compound sets available in literature for sorption by CNM. Nevertheless, out of the ten tested probe sorbates, nine were aromatic compounds, out of which six compounds were non-polar and three were mono-polar aromatics. However, sorption of a much broader probe compound set should be analyzed for the quantitative determination of the contribution of individual mechanisms to overall sorption. Such an approach would be necessary for the comprehensive understanding and general prediction of the sorption of organic compounds by CNM. Very recently, Apul et al. developed a ppLFER model for sorption by MWCNTs. The probe compound set used for the ppLFER model contained 29 non-, mono-, and bi-polar aromatic compounds [67]. For a more comprehensive modeling the incorporation of aliphatic compounds of various polarities would be necessary. In addition, the previously reported investigations of the influence of CNM properties on sorption emphasize the need for quantitative and qualitative information on the contribution of individual properties of sorbent and sorbate to overall sorption [47].

1.4 Application of CNM

The promising properties and their broad application area have made CNM highly desirable sorbents in analytical chemistry with attractive properties. Fundamental prerequisites in terms of sorbent application are, among others, a high sorption capacity and efficient desorption properties. Due to their large aspect ratio and easily accessible sorption sites on the outer surface and interstitial spaces, CNM have high sorption capacity and efficient desorption [68]. To date, the main applications of CNM in analytical chemistry have been as sorbents in SPE [e.g., 69-70] and SPME [e.g., 71-72] and as chromatographic stationary phases [e.g., 73-74].

Compared to widely used traditional sorbents in SPE, such as C-18, MWCNTs were shown to sorb by several orders of magnitude higher amounts of TCDD (2,3,7,8-tetrachlorodibenzo-p-dioxin) [69]. In addition, the incorporation of MWCNTs into a micro-scale SPE (μSPE) resulted in significantly higher enrichment factors of polar and non-polar aromatic compounds than for C-18 under similar conditions [70]. Furthermore, a comparison of sol-gel-CNT with commercial PDMS fibers for SPME showed that CNT-implemented SPME fibers had much better headspace extraction efficiencies for both polar and non-polar analytes [71]. Other approaches have shown high recoveries and low detection limits if CNTs were used for SPME [72]. Packed columns of CNTs have been investigated as stationary phases in gas chromatography. Compared to other, commercially available, phases with similar properties (e.g., Carbopack), CNTs showed stronger retention, higher capacity factors [74-75], and higher breakthrough volumes [76] for analytes with various functional groups. A detailed overview on the analytical application of CNM as chromatographic stationary phases was recently published by Speltinin et al. [77].

The above overview indicates the great potential of the application of CNM in analytical chemistry. Despite the fact that CNM compared to common sorbent materials are yet much more cost intensive in production, they have been proposed to be the next-generation, high performance sorbents [68]. Furthermore, the fact that they are used in much lower quantity compared to classical sorbent materials, lowers the importance of their costs per gram.

1.5 References

1. Schwarzenbach, R.P.; Gschwend, P.M.; Imboden, D.M. *Environmental Organic Chemistry;* John Wiley and Sons: Hoboken, NJ, U.S.A., 2003.
2. Goss, K.U.; Bronner, G. *Journal Physical Chemistry A* **2006**, 110, 9518-9522.
3. Endo, S.; Grathwohl, P.; Schmidt, T.C. *Environmental Science & Technology* **2008**, 42, 3989-3995.
4. Smiciklas, I.D.; Milonjic, S.K.; Zec, S. *Journal of Materials Science* **2000**, 35, 2825-2828.
5. Onjia, A.E.; Milonjic, S.K.; Rajakovic, L.V. *Journal of the Serbian Chemical Society* **2001**, 66, 259-271.
6. Goss, K.U. *Critical Reviews in Environmental Science & Technology* **2004**, 34, 339-389.
7. Endo, S.; Grathwohl, P.; Haderlein, S.B.; Schmidt, T.C. *Environmental Science & Technology* **2009**, 43, 393-400.
8. Streat, M.; Patrick, J.W.; Perez, M.J.C. *Water Research* **1995**, 29, 467-472.
9. Haderlein, S.B.; Weissmahr, K.W.; Schwarzenbach, R.P. *Environmental Science & Technology* **1996**, 30, 612-622.
10. Manes, M.; Hofer, L.J.E. *Journal of Physical Chemistry* **1969**, 73, 584-590.
11. Manes, M. Activated Carbon Adsorption Fundamentals. In *Encyclopedia of Environmental Analysis and Remediation;* Meyers R.A., Ed.; John Wiley and Sons: New York, U.S.A., 1998.
12. Xia, G.; Ball, W.P. *Environmental Science & Technology* **1999**, 33, 262-269.
13. Dubinin, M.M. *Chemical Reviews* **1960**, 60, 235-241.
14. Sontheimer, H.; Crittenden, J.C.; Summers, S. *Activated Carbon for Water Treatment*; DVGW-Forschungsstelle, 1988.
15. Crittenden, J.C.; Hand, D.W.; Arora, H.; Lykins, B.W.Jr. *Journal of the American Water Works Association* **1987**, 79, 74-82.
16. Goss, K.U. *UWSF-ESPR-Beitragsreihe*. **2003**, 15, 273-279.
17. Abraham, M.H. *Chemical Society Reviews* **1993**, 22, 73-83.
18. Abraham, M.H.; Ibrahim, A.; Zissimos, A.M. *Journal of Chromatography A* **2004**, 1037, 29-47.
19. Abraham, M.H.; Andonian-Haftvan, J.; Whiting, G.S.; Leo, A.; Taft, R.S. *Journal of the Chemical Society – Perkin Transaction 2* **1994**, 8, 1777-1791.
20. Abraham, M.H.; Chadha, H.S.; Whiting, G.S.; Mitchell, R.C. *Journal of Pharmaceutical Sciences* **1994**, 83, 1085-1100.
21. Abraham, M.H. *Journal of Physical Organic Chemistry* **1993**, 6, 660-684.
22. Goss, K.U.; Schwarzenbach, R.P. *Environmental Science & Technology* **2001**, 35, 1-9.
23. Roth, C.M.; Goss, K.U.; Schwarzenbach, R.P. *Environmental Science & Technology* **2004**, 38, 4078-4084.
24. Shih, Y.H.; Gschwend, P.M. *Environmental Science & Technology* **2009**, 43, 851-857.
25. Endo, S.; Droge, S.T.J.; Goss, K.U. *Analytical Chemistry* **2011**, 83, 1394-1400.

26. Endo, S.; Grathwohl, P.; Haderlein, S.B.; Schmidt, T.C. *Environmental Science & Technology* **2008**, 42, 5897-5903.
27. Bronner G.; Goss, K.U. *Environmental Science & Technology* **2011**, 45, 1307-1312.
28. Poole, S.K.; Poole, C.F. *Journal of Chromatography A* **1999**, 845, 381-400.
29. Pan, B.; Xing, B.S. *Advances in Agronomy* **2010**, 108, 137-181.
30. Sing, I.; Rehni, A.K.; Kumar, P.; Kumar, M.; Aboul-Enein, H.Y. *Fullerenes, Nanotubes and Carbon Nanostructures* **2009**, 17, 361-377.
31. Iijima, S. *Nature* **1991**, 354, 56-58.
32. Mauter, M.S.; Elimelech, M. *Environmental Science & Technology.* **2008**, 42, 5843-5859.
33. Balasubramania, K.; Burghard, M. *Small* **2005**, 1, 180-192.
34. Kam, N.W.S.; O'Connell, M.; Wisdon, J.A.; Dai, H. *Proceedings of the National Academy of Sciences of the United States of America* **2005**, 102, 11600-11605.
35. Boonjob, W.; Miró, M.; Segundo, M.A.; Cerdà, V. *Analytical Chemistry* **2011**, 83, 5237-5244.
36. De Volder, M.F.L.; Tawfick, S.H.; Baughman, R.H.; Hart, A.J. *Science* **2013**, 339, 535-539.
37. Gottschalk, F.; Sonderer, T.; Scholz, R.W.; Nowack, B. *Environmental Science & Technology* **2009**, 43, 9216-9222.
38. Nowack, B.; Bucheli, T.D. *Environmental Pollution* **2007**, 150, 5-22.
39. Richardson, S.D.; Ternes, T.A. *Analytical. Chemistry* **2011**, 83, 4614-4648.
40. Klaine, S.J.; Alvarez, P.J.J.; Batley, G.E.; Fernandes, T.F.; Handy, R.D.; Lyon, D.Y.; Mahendra, S.; McLaughlin, M.J.; Lead, J.R. *Environmental Toxicology and Chemistry* **2008**, 27, 1825-1851.
41. Hyung, H.; Fortner, J.D.; Hughes, J.B.; Kim, J.H. *Environmental Science & Technology* **2007**, 41, 179-184.
42. Smith, B.; Wepasnick, K.; Schrote, K.E.; Bertele, A.R.; Ball, W.P.; O'Melia, C.; Fairbrother, D.H. *Environmental Science & Technology* **2009**, 43, 819-825.
43. Chen, K.L.; Elimelech, M. *Environmental Science & Technology* **2009**, 43, 7270-7276.
44. Lin, D.; Liu, N.; Yang, K.; Xing, B.; Wu, F. *Environmental Pollution* **2010**, 158, 1270-1274.
45. Zhang, X.; Kah, M.; Jonker, M.T.O.; Hofmann, T. *Environmental Science & Technology* **2012**, 46, 7166-7173.
46. Pan, B.; Zhang, D.; Hao, L.; Wu, M.; Wang, Z.; Xing, B.S. *Environmental Science & Technology* **2013**, 47, 7722-7728.
47. Pan, B.; Xing, B.S. *Environmental Science & Technology* **2008**, 42, 9005-9013.
48. Chen, W.; Duan, L.; Wang, L.L.; Zhu, D.Q. *Environmental Science & Technology* **2008**, 42, 6862-6868.
49. Lu, C.S.; Chung, Y.L.; Chang, K.F. *Journal of Hazardous Materials* **2006**, 138, 304-310.
50. Yan, X.M.; Shi, B.Y.; Lu, J.J.; Feng, C.H.; Wang, D.S.; Tang, H.X. *Journal of Colloid and Interface Science* **2008**, 321, 30-38.
51. Shih, Y.H.; Li, M.S. *Journal of Hazardous Materials* **2008**, 154, 21-28.

52. Fagan, S.B.; Souza, A.G.; Lima, J.O.G.; Mendes, J.; Ferreira, O.P.; Mazali, I.O.; Alves, O.L.; Dresselhaus, M.S. *Nano Letters* **2004**, 4, 1285-1288.
53. Zhao, J.J.; Buldum, A.; Han, J.; Lu, J.P. *Nanotechnology* **2002**, 13, 195-200.
54. Gotovac, S.; Song, L.; Kanoh, H.; Kaneko, K. *Colloids and Surfaces A: Physicochemical and Engineering Aspects* **2007**, 300, 117-121.
55. Pan, B.; Lin, D.H.; Mashayekhi, H.; Xing, B.S. *Environmental Science & Technology* **2008**, 42, 5480-5485.
56. Chin, C.J.M.; Shih, M.W.; Tsai, H.J. *Applied Surface Science* **2010**, 256, 6035-6039.
57. Cho, H.H.; Smith, B.A.; Wnuk, J.D.; Fairbrother, D.A.; Ball, W.P. *Environmental Science & Technology.* **2008**, 42, 2899-2905.
58. Kah, M.; Zhang, X.; Jonker, M.T.O.; Hofmann, T. *Environmental Science & Technology* **2011**, 45, 6011-6017.
59. Cheng, X.K.; Kan, A.T.; Tomson, M.B. *Journal of Chemical Engineering Data* **2004**, 49, 675-683.
60. Yang, K.; Wang, X.L.; Zhu, L.Z.; Xing, B.S. *Environmental Science & Technology* **2006**, 40, 5804-5810.
61. Chen, W.; Lin, D.; Zhu, D.Q. *Environmental Science & Technology* **2007**, 41, 8295-8300.
62. Yang, K.; Zhu, L.Z.; Xing, B.S. *Environmental Science & Technology* **2006**, 40, 1855-1861.
63. Auffan, M.; Rose, J.; Bottero, J.Y.; Lowry, G.V.; Jolivet, J.P.; Wiesner M.R. *Nature Nanotechnology* **2009**, 4, 634-641.
64. Ter Laak, T.L.; Durjava, M.; Struijs, J.; Hermens J.L.M. *Environmental Science & Technology* **2005**, 39, 3736-3742.
65. UBA Press release 075/2009. Nanotechnology for mankind and environment – Seize upon opportunities, reduce risks. (www.uba.de).
66. OECD June 8th, 2010. Guidance manual for testing of manufactured nanomaterials: OECD Sponsorship programme; first revision (www.oecd.org).
67. Apul, O.G.; Wang, Q.L.; Shao, T.; Rieck, J.R.; Karafil, T. *Environmental Science & Technology* **2013**, 47, 2295-2303.
68. Hussain, C.M.; Mitra, S. *Analytical and Bioanalytical Chemistry* **2011**, 399, 75-89.
69. Long, R.Q.; Yang, R.T. *Journal of the American Chemical Society* **2001**, 123, 2058-2059.
70. Sae-Khow, O.; Mitra, S. *Journal of Chromatography A* **2009**, 1216, 2270-2274.
71. Jiang, R.; Zhu, F.; Luang, T.; Tong, Y.; Liu, H.; Ouyang, G.; Pawliszyn, J. *Journal of Chromatography A* **2009**, 1216, 4641-4647.
72. Li, Q.; Wang, X.; Yuan, D. *Journal of Chromatography A* **2009**, 1216, 1305-1311.
73. Speltini, A.; Merli, D.; Quartarone, E.; Profumo, A. *Journal of Chromatography A* **2010**, 1217, 2918-2924.
74. Li, Q.; Yuan, D. *Journal of Chromatography A* **2003**, 1003, 203-209.
75. Karwa, M.; Mitra, S. *Analytical Chemistry* **2006**, 78, 2064-2070.
76. Hussain, C.M.; Saridara, C.; Mitra, S. *Analyst* **2008**, 133, 1076-1082.
77. Speltini, A.; Merli, D.; Profumo, A. *Analytica Chimica Acta* **2013**, 783, 1-16.

Chapter 2 Scope and Aim

The state of research described in Chapter 1 shows that aside from the already existing number of individual studies on sorption of hydrophobic organic compounds (HOC) by carbon-based nanomaterials (CNM), there is still a lack of systematic understanding of the relevant interaction mechanisms. From this, the motivation of this study was to increase the knowledge of molecular interactions of CNM with non-ionic organic compounds by a systematic investigation of the sorption behavior by various CNM. To this end, four work packages were carried out as schematically shown in Figure 2-1.

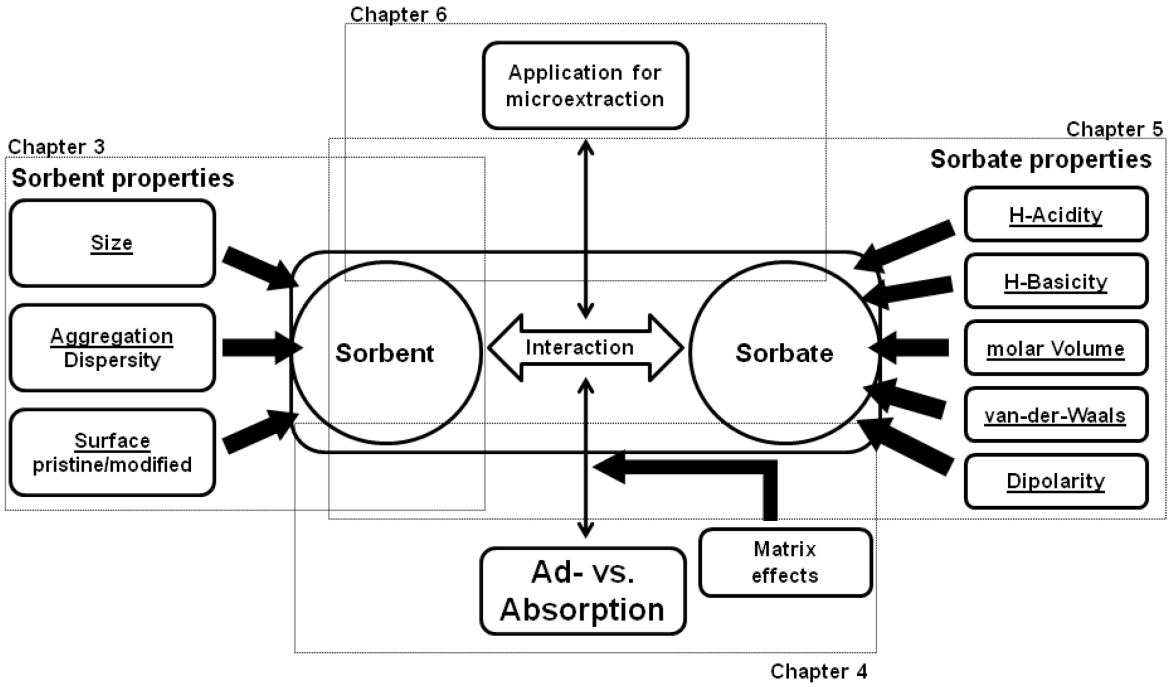

Figure 2-1: Visualization of the scope of this thesis.

The influence of CNM released into the environment on the mobility of HOC is under intense debate among researchers. In this context the question arises regarding the impact of environmental parameters on sorption by CNM. Thus, **Chapter 3** investigates the effect of UV irradiation and presence of oxygen, two environmentally relevant aging factors of CNM, on the surface properties of aqueously dispersed fullerenes and as a consequence on its sorption behavior towards polycyclic aromatic hydrocarbons. The application of POM-SPE as passive sampling method allows the determination of sorption isotherms over a concentration range of four orders of magnitude. Sorption isotherm data are linked with extensive sorbent surface characterization in order to understand the relevant factors that influence the interaction of CNM with HOC.

Results of sorption isotherm fits in Chapter 3 suggested that pore-filling and surface adsorption are the relevant sorption mechanisms. Thus, **Chapter 4** aims at the determination of the dominant sorption mode (i.e., *ad*- or *ab*sorption) by multi-walled carbon nanotubes (MWCNTs). *n*- and cycloalkanes are used as molecular probes, which allows to investigate non-specific interactions, such as van-der-Waals interaction. Potential matrix effects from the presence of natural organic matter (NOM) are explored for their impact on sorption affinity and sorption linearity. In addition, the hypothesis is tested if the mode of sorption changes from *ad*sorption by MWCNTs to *ab*sorption into NOM-coated MWCNTs.

Since in Chapters 3 and 4 it was shown that single sorption mechanisms alone cannot explain sorption behavior of CNM, **Chapter 5** focuses on the characterization of sorption properties of MWCNTs by modeling with poly-parameter linear free-energy relationships (ppLFER). To this end, sorption of a systematically selected probe compound set covering various compound classes (i.e., non-, mono-, and bi-polar aliphatic and aromatic compounds) is determined for the development of a ppLFER for sorption by MWCNTs. This approach allows the systematic investigation of qualitative and quantitative contribution of individual mechanisms to overall sorption for an accurate prediction of interaction**.**

Overall, Chapters 3-5 indicate strong interactions of CNM with HOC. In **Chapter 6**, MWCNTs are therefore explored with respect to their application in microextraction techniques for sample preparation in analytical chemistry. To this end, MWCNTs are used as sorptive packing material for in-tube microextraction for the analysis of non-polar organic

compounds in aqueous samples. Instead of classical method development, the application of a design of experiment allows a systematic investigation on the relevant extraction parameters and their interaction.

In **Chapter 7**, the main results of this study are combined, and an outlook on potential future research questions is given.

Chapter 3 How Redox Conditions and Irradiation Affect Sorption of PAHs by Dispersed Fullerenes (nC60)

Adapted with permission from: Hüffer, T.; Kah, M.; Hofmann, T.; Schmidt, T.C. How Redox Conditions and Irradiation Affect Sorption of PAHs by Dispersed Fullerenes (nC60). *Environmental Science & Technology* **2013**, 47, 6935-6942.
 dx.doi.org/10.1021/es303620c

3.1 Abstract

Surface properties, dispersion state, and sorption behavior of carbon-based nanomaterials will change after being released into the environment. To study these processes, five different scenarios were considered to probe the impact of changes in surface properties of dispersed fullerenes (nC60) on their sorption potential due to irradiation and presence of oxygen. Sorption isotherms of pyrene by nC60 were determined at environmentally relevant concentrations applying a passive sampling method. Isotherms of all dispersion scenarios were best fit with the Dubinin–Ashthakov model. Sorption was strongest for nC60 kept under anoxic condition. Both the presence of oxygen and irradiation significantly decreased the sorption capacity of nC60, while commercially available polyhydroxy fullerenes had the smallest sorption. In addition, competition for sorption sites was never observed in multiple sorbate experiments with four polycyclic aromatic hydrocarbons at small concentration. A strong relationship between sorption coefficients and hydrophobic properties of sorbates suggests that hydrophobic interactions are of major importance. The results emphasize that aging of released fullerenes results in a reduced strength of interactions with nonpolar compounds and, thus, reduces the impact on the environmental transport of hydrophobic pollutants.

3.2 Introduction

Research on carbon-based nanomaterials (CNM) has been increasing over the past decade due to their unique physico-chemical properties (e.g., large surface area to volume ratio). The question of their fate and impact on the environment has also become a major concern due to an expected rise in production of these materials in the future [1]. Even though there is consensus that CNM will eventually reach the environment, their environmental behavior and impact on the fate of other pollutants remains controversial. Predicted fullerene (C60) concentrations (e.g., 0.02 and 0.04 ng L^{-1} in surface waters in Europe and Switzerland, respectively [2]) are likely to increase in the future. This fact substantiates the need of further research on the environmental impact of CNM.

The hydrophobic property of C60 results in the formation of aggregates when C60 is aqueously dispersed. Numerous studies have shown that environmental factors may influence the dispersion of aqueous of fullerenes (nC60) due to changes in surface properties. These changes may result from oxidation (e.g., after exposure to sunlight) or other, non-covalent, surface modifications (e.g., due to the presence of natural organic matter (NOM)) [3-6]. These obvious effects of aging on dispersion properties will inevitably influence the environmental behavior of nC60. The consequences of these changes in surface chemistry on their sorption behavior are yet poorly understood. Recently, Gai et al. [7] showed that sorption of atrazine by nC60 was significantly affected by the dispersion method applied. However, there was no consistent correlation between sorption of atrazine and nC60 particle size. In another study, pH and ionic strength (i.e., NaCl) had no major influence on the sorption of polycyclic aromatic hydrocarbons (PAHs) by nC60, whereas the addition of NOM decreased freely dissolved PAHs concentration [8]. These inconsistent trends between sorbent particle size and their sorption may be assigned to the difference in probe sorbates investigated. Furthermore, irradiation was shown to disaggregate nC60 clusters and form products of smaller hydrophobicity via an oxidative pathway without carbon mineralization [9]. Possible impact(s) of oxidation of nC60 on their sorption potential have not yet been investigated. However, such information is essential as potential surface oxidation represents an important aging factor influencing the impact of fullerenes once they are released to natural systems. Very recently, possible solar transformation of nC60 was proposed to be a critical step for assessing the environmental impact after a potential release into surface waters [10].

The very limited information on the sorption behavior of partially/fully dispersed nC60 systems might be explained by difficulties associated with the generally-applied batch sorption test set-ups. In sorption batch experiments, solid and liquid phases are generally separated by centrifugation, sedimentation, or filtration. Most CNM suspended in aqueous solution may easily be separated from the aqueous phase as they tend to form aggregates due to their hydrophobicity. However, a fraction of dispersed CNM may remain in solution and cause an underestimation of determined distribution coefficients. We thus used a passive sampling technique to accurately measure sorption coefficients applying polyoxymethylene (POM-SPE), which has recently been used to investigate sorption of PAHs by multi-walled carbon nanotubes (MWCNTs) [11]. A complete phase separation when working with (partially) dispersed systems is assured by inserting a third phase into the system that can easily be separated. In addition, the POM-SPE method permits determining freely dissolved aqueous concentration of PAHs down to 1 pg L^{-1} [12]. Studying sorption over a wide concentration range allows a detailed investigation of sorption mechanisms of CNM through robust isotherm analysis. Moreover, sorption can be investigated at sorbate concentrations likely to be found in the environment. The objective of the present study was to analyze the impact of environmental factors (i.e., irradiation and presence of oxygen) known to alter nC60 surface properties on their sorption behavior towards PAHs. Sorption isotherm analysis and extensive solid phase characterization data were combined in order to better understand the interactions likely to occur in natural environments.

3.3 Experimental Section

3.3.1 Materials

Fullerenes (C60, 99.5% purity, Sigma-Aldrich, Steinheim, Germany) and polyhydroxy fullerenes (C60-$(OH)_{18-22}$, BuckyUSA, Houston, TX, USA) were used as purchased. A polyoxymethylene sheet (POM; thickness 0.5 mm; density 1.41 g cm^{-3}) was purchased from Vink Kunststoffen BV (Didam, The Netherlands). The POM sheet was cut into pieces that were cold-extracted in an ultrasonic unit SONOREX SUPER RK106 (Bandelin, Berlin, Germany) once in n-hexane and three times in methanol (each for 30 min), and subsequently air-dried [13].

Pyrene (Pyr, 99.5%) and Pyr-d10 (99.5%, internal standard for quantification) were purchased from Dr. Ehrenstorfer GmbH (Augsburg, Germany). Other PAHs (Phenanthrene, Phen; Benz[a]pyrene, BaP; and Benz[a]anthracene, BaA) were obtained from Sigma-Aldrich (Steinheim, Germany). For quantification of multiple solute experiments, a mixture of deuterated PAHs ("PAH mix 31") containing Acenaphthene-d10 (99.5%), Chrysene-d12 (98.5%), Naphthalene-d8 (99.5%), Perylene-d12 (99.5%), and Phenanthrene-d10 (99.5%) was purchased from Dr. Ehrenstorfer GmbH (Augsburg, Germany). All stock solutions were prepared in methanol. Selected properties of the sorbates are listed in Table A 3-1. Acetone (for analysis), n-hexane, and methanol (both residual analysis grade) were purchased from Acros Organics (Geel, Belgium).

3.3.2 Preparation of nC60 aging scenarios

Approximately 20 mg of C60 and 7 mg of C60-OH were weighed into 50-mL and 20-mL borosilicate glass vials, respectively. Vials were then filled with background solution containing 0.1 mmol NaCl, leaving minimal headspace and subsequently closed with PFTE-lined caps. Four aging scenarios of varying irradiation and atmospheric conditions were prepared with C60. Half of the samples were shaken in the dark (nC60-D) or exposed to lamp light irradiation (nC60-L, two 15 W fluorescent ultraviolet bulbs, Sylvania T8 F15W/BL350, bulbs emitted light at a spectrum of 315 to 400 nm with a peak at 368 nm [14]). Note that previous studies on irradiation of fullerenes were performed in similar glassware and at similar wavelength [15, 16]. Each half of samples was further subdivided into two batches,

one under oxic and the other under anoxic conditions (denoted with subscripts O and A, respectively). Based on previous results of Lee et al. [9] and Hou and Jafvert [15], an irradiation time for pretreatment of 28 d was chosen. Hence, all samples (i.e., oxic and anoxic) were shaken horizontally for 28 d at 150 rpm. Anoxic samples were pretreated, spiked, and equilibrated in a glove box under a constant atmosphere of nitrogen. The glove box was flushed daily with fresh nitrogen to ensure anoxic conditions throughout the experiment. Anoxic NaCl background solution was prepared by autoclaving for 25 min, followed by cooling under nitrogen atmosphere. The solution was transferred to glass bottles sealed with aluminum screw caps and was immediately stored in the glove box.

The fifth scenario consisted in nC60-OH under oxic conditions and without light pretreatment.

3.3.3 POM-SPE batch experiments

POM pieces were added to the nC60 dispersions and pyrene was subsequently spiked at initial concentrations ranging from 0.1 up to 1000 µg L^{-1}. In order to assure reproducibility, two data points of each isotherm were prepared in duplicates. The amount of methanol was 0.2% (v/v) in all samples to minimize the co-solvent effect. Samples were subsequently shaken at 150 rpm in the dark for 28 d to achieve equilibration of the sorbate between the aqueous phase, POM, and nC60 (for further details on the POM-SPE method refer to the Appendix of this chapter). Temperature was kept constant at 25 ± 1 °C during all experiments.

After equilibration, the sorbate concentrations in POM were determined. For this purpose, the POM pieces were withdrawn from the vials and wiped with a wet paper tissue to remove sorbent from POM surface (Figure A 3-1). After the addition of the internal standard, the POM pieces were extracted with methanol by accelerated solvent extraction (ASE 200, Dionex USA; 1500 psi, 100 °C). Methanol was exchanged to hexane under N_2, samples were concentrated, and analyzed by GC-MS (Agilent 7890A gas chromatograph coupled 5975C mass spectrometer; HP-5ms column (30 m x 250 µm x 0.25 µm, J&W Scientific), pulsed splitless mode, and oven program 55 °C for 1 min, then 15 °C min^{-1} up to 300 °C). Analyte quantification was achieved by single ion monitoring (SIM) mode.

The POM-SPE method was also used to determine the sorption coefficients of four PAHs spiked simultaneously at low concentration (10 μg L^{-1}). The only deviations from the protocol described above were (i) the use of multiple deuterated PAH internal standard and (ii) the GC oven program (holding at 55 °C for 1 min, then ramped 10 °C min^{-1} to 320 °C, which was held for 25 min).

The sorbed PAH concentrations on nC60 for single and multiple solute experiments were calculated by mass balance from the measured PAH concentrations on POM (Table A 3-2).

3.3.4 Sorbent characterization

For each pretreatment, the particle size distribution in the whole dispersion was determined using a particle and shape analyzer based on laser light shading (time of transition principle, TOT) and simultaneous microscopy (EyeTech, Ankersmid Lab, Nijverdal, The Netherlands). TOT uses laser obscuration time on the detector and a pulse-length analysis to determine particle size and diameter distribution (with a 95% number based confidence level) [17]. The hydrodynamic diameter, polydispersity index (PdI), and zeta potential (ZP) of the particles remaining in dispersion after four days of sedimentation were determined by dynamic light scattering (DLS) using a Zetasizer Nano-ZS (Malvern Instruments Ltd, UK) and a refractive index of 2.2 for fullerenes [18].

Surface functionalization was determined by attenuated total reflectance Fourier transform infrared spectroscopy (ATR-FTIR; System 2000 FT-IR, Perkin Elmer, Germany) and X-ray photoelectron spectroscopy (XPS; Hemispherical energy analyzer PHOISBOS 100 & high-intensity twin anode X-ray source XR-50, SPECS, Berlin, Germany). Bulk and polyhydroxy fullerenes were analyzed as received whereas samples of dispersions were dried for two days at 80 °C prior to analysis.

3.3.5 Sorption models and statistics

Three sorption models commonly used for CNTs [19, 20] and nC60 [7, 20] were fit to the sorption isotherms (model equations and their fitting parameters are listed in Table A 3-3). Briefly, the Freundlich model (FM) is an empirical relationship that describes well sorbents with heterogeneous distribution of energy of available sorption sites. The Langmuir model

(LM) assumes an even distribution of sorption site energies with the formation of a sorbate monolayer until saturation. The Dubinin-Ashthakov model (DAM) is based on the Polanyi potential theory, in which the sorption potential of a sorbate in a sorption space at the sorbent surface is assumed to depend on the distance between sorbate and sorbent surface (for a detailed description of isotherm models refer to Allen-King et al. [21]). Three additional models were tested: the dual Langmuir model, considering high- and low-energy sorption sites, and two dual mode models based on FM and LM. The latter two models combine linear partitioning and specific sorption modes. However, none of these additional models significantly improved the goodness of fit (data not shown). In fact, the parts of the dual mode models representing partitioning were negligibly small and the model specific sorption coefficients were identical to those derived from single mode models. FM, LM, and DAM showed the best fits; hence, these three models were considered for the discussion below.

Curve fit was evaluated on a three-fold criteria basis including the coefficient of determination (R^2), the mean weighted square error (MWSE), and Akaike's Information Criterion (AIC). R^2, calculated from the sum of the squares of the residuals, does not take the number of fitting parameters into account; hence, MWSE was additionally considered to account for potential over-parameterization. AIC is based on information theory. Probability and evidence ratio were calculated to compare model fits of nC60 dispersions (as in detail described in ref [22]). All statistical tests and model fits were performed with Sigma Plot 12.0 for Windows. Standard errors of model parameters were computed with reduced Chi-square and weighted regression with weighting to reciprocal y^2.

3.4 Results and Discussion

3.4.1 Sorbent characterization

The degree of surface oxidation was assessed for bulk materials of C60 and C60-OH as well as dried samples of nC60 dispersions by FT-IR (Figure 3-1). Intensive peaks at 1427 and 1181 cm^{-1} were observed for bulk C60, which can be assigned to C-C vibrational modes of the C60 molecule [23]. Spectra of bulk C60-OH revealed characteristic peaks for -OH, C-O, and C-OH stretching at wavenumbers of 3319, 1068, and 1408 cm^{-1}, respectively. None of these bands were obtained for bulk C60. Both spectra are consistent with previously reported data for these materials [16]. The spectra of both anoxic dispersions were almost identical (hence only that of nC60-L_A is given in Figure 3-1), showing peaks at C-C vibrations similar to the parent C60. Additionally, a broad band at 3400 cm^{-1} was obtained indicating the presence of remaining water despite drying. The spectra of oxic dispersions showed characteristic peaks also obtained for C60 and C60-OH implying that oxidation occurred at the outer surface of the C60 clusters, whereas no oxidation occurred in the core of the particles [16]. Additionally, XPS spectra of the O(1s) region of the samples C60, nC60-D_O, and nC60-L_O (Figure A 3-2) supported the results of FT-IR that sorbent materials kept under oxic conditions showed an increase in surface oxidation. XPS spectra of the C(1s) region of these samples confirm previous data indicating a shift in binding energy with increasing carbon oxidation (data not shown) [9]. Overall, FT-IR and XPS data indicated that significant oxidation occurred for the samples kept in oxic conditions (especially when combined to lamp light exposure, nC60-L_O).

It has been proposed that extended exposure of C60 to water resulted in the introduction of oxygen containing surface functional groups, whose density on the sorbent surface was not large enough to be detected by titration or elemental analysis [24]. The addition of H_2O to C=C bonds in the aromatic molecule of C60 was excluded by Labille et al. [23] and the rate of C60 transformation was greatly reduced in the absence of oxygen [9]. FT-IR data of the present study showed that oxidation of C60 in anoxic dispersions was minimal. However, oxidation of these sorbents cannot be fully excluded as the mechanisms of hydroxylation of nC60 as well as lamp light assisted nC60 dispersion are not yet fully understood. Nevertheless, our findings are consistent with literature data [15, 16].

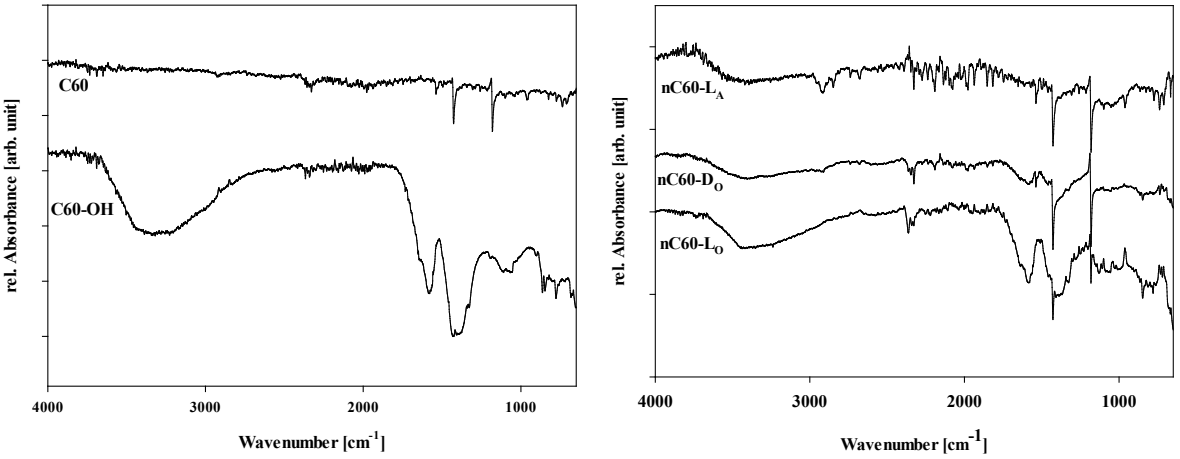

Figure 3-1: ATR-FT-IR spectra of bulk sorbent material (left) and C60 dispersions after different pretreatments (right).

The zeta potential (ZP) of nC60 particles in all dispersion scenarios were significantly more negative ($p < 0.001$) than that of initially dispersed C60 (nC60, Table 3-1). It should be noted that ZP of nC60 suggests that particles in that dispersion are unstable and thus tend to aggregate. Furthermore, ZP of C60 particles in oxic dispersions was significantly smaller ($p < 0.001$) than that of anoxic C60 dispersions. Ionic strength and pH have been previously shown to influence ZP of aqueous nC60 dispersions [24-26]. However, the changes in ZP observed here among dispersion scenarios can be assigned to changes in surface properties of sorbents, as both ionic strength and pH in all nC60 dispersions were identical (pH 6.52 ± 0.36).

The effect of surface functional oxygen groups on the sorption of hydrophobic organic compounds (HOC) has been previously studied for MWCNTs. A linear and negative relationship between the oxygen content of MWCNTs and maximum sorption capacity was observed. A concentration of oxygen of 10% resulted in a 70% decrease in sorption capacity for naphthalene [27]. Similarly, sorption capacities of MWCNTs for benzene, toluene, and *m*-xylene were significantly reduced by an oxygen content larger than 4.7% [28]. The FT-IR and ZP data support a similar trend in the present study as discussed in the next section.

3.4.2 Single solute experiments

Sorption of pyrene generally decreased in the order: nC60-D_A = nC60-L_A > nC60-D_O > nC60-L_O > nC60-OH (Figure 3-2). Sorption isotherms could be grouped into three categories of

decreasing sorption potential: category I > category II > category III. Category I included both sets of samples maintained under anoxic conditions (nC60-L_A and nC60-D_A), for which oxidation processes of sorbent material were minimized. The data suggest that exposure to lamp light in the absence of oxygen had no influence on surface properties and neither on sorption of pyrene (as further discussed below). Category II comprised both nC60 dispersions exposed to oxygen (i.e., nC60-D_O and nC60-L_O), for which exposure to lamp light further decreased sorption of pyrene. Category III consisted of commercial polyhydroxy fullerenes (nC60-OH) with an average number of surface -OH groups of 18-22 per C60 molecule (given by the supplier), for which the smallest sorption was observed. The effects of particle size and change in surface chemistry of the sorbents on their sorption of pyrene are further discussed below.

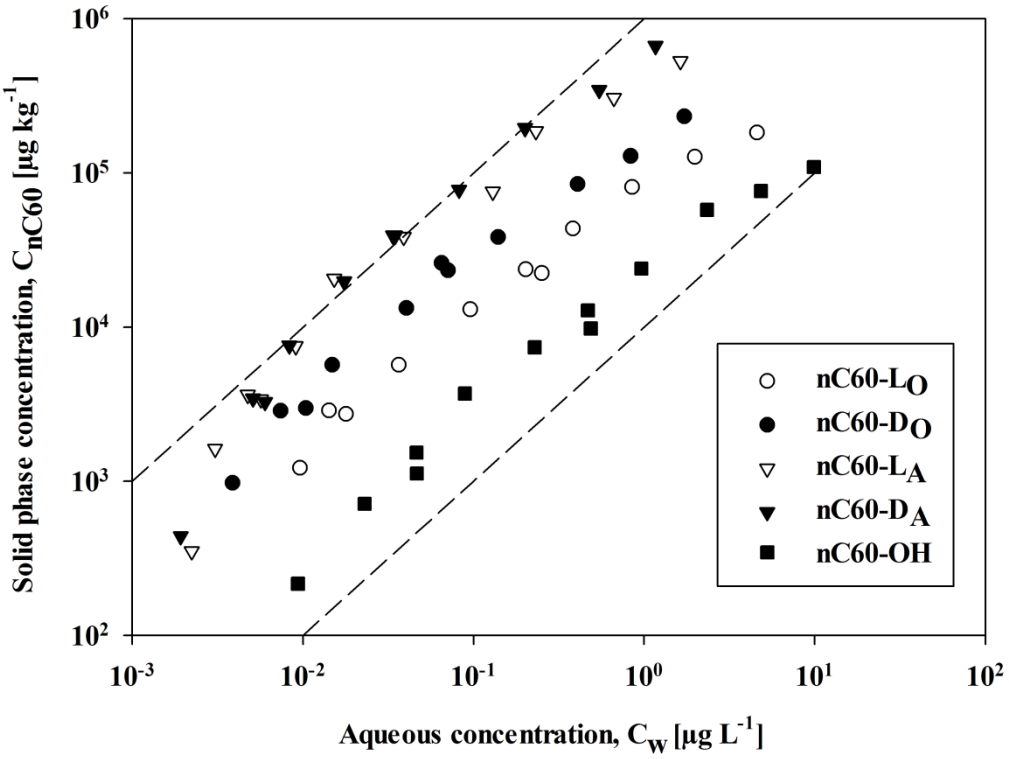

Figure 3-2: Sorption isotherms of single solute pyrene experiments. Dashed lines show linear sorption (n = 1), drawn for visual aid.

3.4.3 Effect of sorbent properties on sorption

Table 3-1 presents the characteristics of the sorbents determined by DLS and TOT. Generally, all C60 dispersions were heterodispersed having a rather large PdI of about 0.21-0.45 (Table 3-1). The PdI decreased for all five C60 dispersion scenarios relative to the initially dispersed bulk material (nC60 in Table 3-1) as a result of shaking [29]. Interestingly, oxic dispersions had larger PdI and particle sizes measured by DLS than those shaken under anoxic conditions. This was in contradiction to the expected as a change in surface chemistry due to presence of oxygen containing functionalities would lead to a decrease in both hydrophobicity and particle size [10]. However, it cannot be excluded that the smaller PdI of particles in anoxic dispersions was rather related to a small size distribution of aggregates.

All pretreatments significantly decreased the particle size ($p < 0.001$) relative to the initial dispersion. Particle sizes of the two anoxic nC60 dispersions were identical ($p > 0.05$). Conversely, lamp light exposure resulted in a significant decrease in particle size for the oxic pretreatment ($p \leq 0.001$). It is known that the large clusters initially formed by C60 in aqueous dispersions can be broken down by extensive mixing [18]. Gai et al. [7] recently reported smaller C60 particle sizes than those observed in the present study. Considering that Gai et al. kept the dispersions in the dark and under oxic conditions for no longer than four weeks, discrepancies with our results can be assigned to differences in the shaking protocol (i.e., magnetic stirring versus horizontal shaking) [30].

Among all samples, nC60-D_A and nC60-L_A had the smallest number-based diameter measured by TOT (D[1,0] of 1.02 and 1.09 µm, respectively, Table 3-1). Therefore, more sorption sites may be available at the particle surface of nC60-D_A and nC60-L_A. In fact these dispersions showed the strongest pyrene sorption affinity (Figure 3-2). Although dispersing fullerene systems was previously observed to result in a stronger sorption potential [7, 31], the relationship between particle size and sorption was not consistent. A similar phenomenon was observed in the present study as plotting particle sizes and sorption showed no relationship (not shown): nC60-OH had the smallest particle size but also exhibited the smallest pyrene sorption. This can be further confirmed by comparing the orders of decreasing sorption from Figure 3-2 (i.e., nC60-D_A = nC60-L_A > nC60-D_O > nC60-L_O > nC60-OH) with the order of increasing particle sizes (i.e., nC60-OH < nC60-D_A ≤ nC60-L_A < nC60-L_O < nC60-D_O).

Consequently, additional factors aside from sorbent particle size play a major role governing sorption and are thus required to explain discrepancies in sorption behavior.

Table 3-1: Main characteristics of the sorbents: hydrodynamic diameter (Z_{ave}), polydispersity index (PdI), intensity-weighted mean (peak), and zeta potential (ZP) were determined by DLS. The number-based diameter of sorbent particles (D[1,0]) was measured by TOT.

Sample	Z_{ave} [nm]	PdI	Peak [nm]	ZP [mV]	D [1,0] [µm]
nC60-OH	218 ± 54	0.373	peak 1 = 216.17 ± 29.30 (peak 2 = 54.03 ± 18.51)	-48.00 ± 2.43	n.d.
nC60-L_O	332 ± 35	0.328	297.76 ± 32.04	-51.60 ± 0.60	1.16 ± 0.02
nC60-D_O	439 ± 47	0.449	350.08 ± 55.35	-52.13 ± 0.40	1.43 ± 0.05
nC60-L_A	281 ± 8	0.215	294.22 ± 14.55	-33.57 ± 1.15	1.09 ± 0.02
nC60-D_A	295 ± 48	0.203	303.27 ± 28.31	-30.50 ± 0.26	1.02 ± 0.01
nC60	(3096 ± 771)	0.860	540.12 ± 111.18	-11.63 ± 2.32	4.18 ± 0.26

±: standard errors (n=5); n.d.: not detectable. pH 6.52 ± 0.36.

3.4.4 Sorption isotherm fit

All isotherms were non-linear; hence, commonly used non-linear isotherm models (i.e., FM, LM, and DAM) were fit to the data obtained for pyrene sorption by five different nC60 dispersions.

DAM provided the best fits for all nC60 dispersions investigated with the largest R^2 (≥ 0.95), smallest MWSE, and AIC (Table 3-2 and Table A 3-4). DAM is based on the Polanyi-Manes theory, which was previously shown to adequately describe the sorption of various sorbates by nC60 and other CNM (for a detailed review, see Pan & Xing [32]). The presence of oxygen-containing groups at the surface allows the formation of hydrogen bonds with surrounding water molecules [33]. Since the water molecules need to be replaced by pyrene, sorption is less favorable. Comparing the capacities for pyrene sorption by nC60 dispersions obtained from DAM fit (Q_{max} as displayed in Table A 3-4), there was a significant decrease following the order: nC60-D_A = nC60-L_A > nC60-D_O = nC60L_O > nC60-OH ($p \leq 0.01$).

Table 3-2: Coefficient of determination (R^2), mean weighted squared error (MWSE), and Akaike's Information Criterion (AIC) determined for three models fitting the sorption isotherms of pyrene by different dispersion scenarios of nC60.

Sample	Freundlich Model (FM)			Langmuir Model (LM)			Dubinin-Ashthakov Model (DAM)		
	R^2	MWSE	AIC	R^2	MWSE	AIC	R^2	MWSE	AIC
nC60-L_O	0.93	0.0538	-24.92	0.96	0.0299	-31.38	0.97	0.0256	-29.16
nC60-D_O	0.92	0.0668	-22.54	0.97	0.0293	-31.59	0.98	0.0175	-33.33
nC60-L_A	0.61	0.3878	-4.55	0.56	0.4383	-3.09	0.95	0.1201	-15.23
nC60-D_A	0.76	0.2443	-8.28	0.66	0.3454	-4.47	0.98	0.0270	-28.58
nC60-OH	0.92	0.0767	-24.82	0.96	0.0440	-31.48	0.97	0.0357	-31.79

Note: Details of curve fit results and quality criteria given in Table A 3-4.

The goodness of fit for sorbents under oxic conditions only slightly increased from two- to three-parameter models (i.e., from FM or LM to DAM); therefore, a potential increase in goodness of fit due to over-parameterization was investigated by calculating AIC (probabilities and evidence ratios are given in Table A 3-5). For anoxic samples, results clearly indicate that the best fit observed by DAM was not due to over-parameterization. This suggests that pore-filling and sorption to flat surfaces are likely the major sorption processes for these sorbents [34]. Both, hydrophobic C60 particles and hydrophilic polyhydroxy fullerenes form amorphous, loosely-associated aggregates in water independent from the degree of hydroxylation [35]. These aggregates would thus allow sorbates to sorb into sorbent pores, which has previously been proposed to be a major sorption mechanism for nC60 [31], unless pore-filling is not hindered by steric [36] or other effects.

The goodness of fit of the used sorption models varied among dispersion scenarios. In fact, sorption by oxic nC60 dispersions was smaller than by anoxic nC60 and LM gave equal or better fits relative to DAM for oxic nC60 (Table A 3-4). This suggests that for oxic nC60 a reduced maximum potential sorption space of these sorbents [34] and thus potential surface saturation should be taken into account as both models (i.e., LM and DAM) include fitting parameters for maximum sorption capacity (Q_{max}). Additionally, functional groups may reduce the accessibility of sorption sites on the surface of sorbent particles [32]. As a consequence, an increased competition between potential sorbates for sorption sites (as further discussed in the next section) [37] and/or the formation of three-dimensional clusters that additionally block sorption sites nearby [38] have to be taken into account influencing the sorption behavior of nC60. Both processes may contribute to the decrease in sorption

observed. By comparing the isotherms of sorbents under oxic and anoxic conditions together with the data from sorbent characterization, the change in sorption can be related to a change in surface properties resulting from functionalization. Surface hydroxyl groups, on both the commercial polyhydroxy fullerenes and lamp light pretreated sorbent material may lead to a disruption of the delocalized electron system and, hence, to a decreased sorbate-sorbent interaction (i.e., to a decrease in sorption), which is consistent with the observed isotherms (Figure 3-2). The results suggest that alterations of nC60 due to the presence of oxygen and irradiation lead to overall decrease in sorption. However, the effect of this change in sorption behavior of nC60 on potential co-transport of other, i.e., ionizable, compounds was not in the focus of the present study but demands further research.

3.4.5 Multiple solute PAHs

Environmental contaminants typically occur simultaneously, which raises the question of altered sorption due to competition for sorption sites. Competition phenomena are known to be concentration dependent [19, 39]. Sorption experiments with four PAHs were conducted at aqueous equilibrium concentrations in the ng L^{-1}-range as PAHs are likely to occur at these concentrations in the environment [40]. Single-point distribution coefficients (log K_{nC60}) of pyrene were obtained from a multiple sorbate experiments, and were compared with single solute log K_{nC60} values derived from DAM fit results for the corresponding aqueous concentration (Table A 3-6). Single and multiple pyrene sorption coefficients were statistically not different for all studied nC60 dispersions. This indicated that no competition for sorption sites among PAHs occurred at the investigated concentration range. The theoretical surface saturation of PAHs on the sorbent (calculated from sorbed concentrations with sorbate molecular area and sorbent surface area of 7.2 m^2 g^{-1} [41] assuming flat surface sorption) ranged between 2 and 4%; thus, sorption competition as a result of over-saturation of the sorbent surface was unlikely to occur. Strong competition for sorption by MWCNTs was previously observed between naphthalene, phenanthrene, and pyrene coexisting at relatively large concentrations [39]. In contrast, sorption coefficients measured for phenanthrene and pyrene in single and multiple sorbate systems together with 11 other PAHs showed no significant competition in the ng L^{-1}-range [19].

Sorption of a number of low-molecular weight PAHs by nC60 dispersions has previously been reported [8, 20, 31]. However, the influence of sorbate properties on the sorption affinity was only briefly discussed. To probe the importance of hydrophobic interactions, the obtained distribution coefficients for five nC60 dispersions were correlated with hydrophobic properties of sorbates (i.e., octanol-water partitioning constant (log K_{ow}), molar volume (MV), and subcooled liquid solubility ($\log S_i$), as given in Table A 3-1). The determined log K_{nC60} values could be significantly correlated ($p < 0.05$) with log K_{ow} (Table A 3-7(a)), which suggests that hydrophobic interactions are of major importance for the studied sorbent-sorbate-systems. For clarity, it has to be stressed that correlations between distribution coefficients (log K_d) and log K_{ow} in some cases have to be considered with caution as log K_{ow} refers to partitioning of a solute between two bulk phases (i.e., *ab*sorption), whereas the distribution of a sorbate to CNM is commonly considered as an *ad*sorption process onto its surface. Nevertheless, log K_{ow} remains the most consulted hydrophobicity parameter in literature for the interpretation of sorption data. Thus, relationships between log K_{nC60} and log K_{ow} were investigated to compare sorption by sorbents used in the present study with previously reported results for similar sorbents. The slopes of log K_{nC60}-log K_{ow} relationships in Figure 3-3 differed from those obtained for other CNM. Generally, the log K_d-log K_{ow} slopes are close to 1 for soils and sediments [42] similar to those in the present study, while slopes for MWCNTs [19] and charcoal [43] were much smaller (e.g., 0.3 for MWCNTs). From this it could be said that once aged nC60 does not seem to behave like other carbonaceous materials but rather ordinary geosorbents. Correlations between log K_{nC60} and hydrophobic properties of sorbates are a first step towards the prediction of sorption of PAHs by nC60.

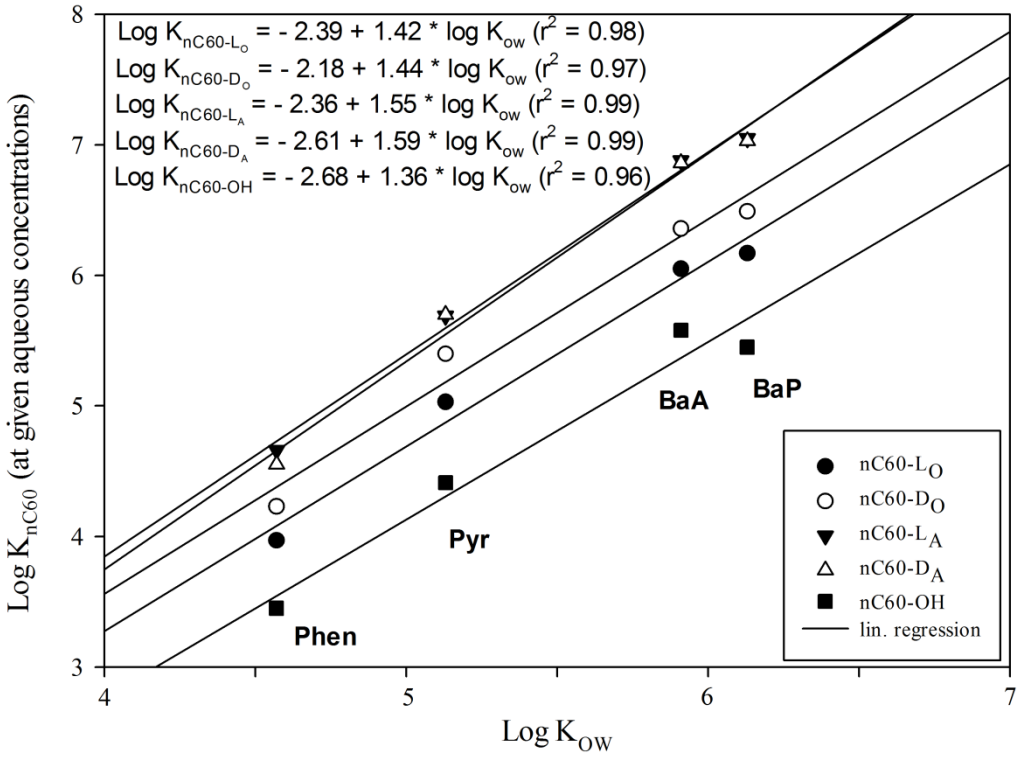

Figure 3-3: Relationships between single-point distribution coefficient (log K_{nC60}) and log K_{ow} (from [42]) of PAHs in C60 dispersions.

Although, BaP is much more hydrophobic than BaA, the distribution coefficients for BaP were only slightly larger for anoxic dispersions than those of BaA (log K_{ow} in Table A 3-1). The difference between log K_{nC60} of BaP and BaA decreased for oxic dispersions, and for nC60-OH log K_{nC60} of BaP was even smaller than that of BaA. This suggests that (i) for oxic C60 dispersions the contribution of hydrophobic interactions decreases, although they probably still dominate, and/or (ii) pores in these nC60 aggregates are too small for larger sorbates as discussed above. Hydrophobic interactions have been used to interpret sorption between HOC and CNM, even though interpretation of sorption data on hydrophobic interactions alone was not sufficient [44]. A number of mechanisms may contribute to the overall sorption to carbon nanotubes (e.g., van-der-Waals and electron donor-acceptor (EDA) interactions) [32]. Similar interactions are expected to play an important role in the dispersion systems presented here. In addition, hydrogen bonding may contribute to sorption when oxygen containing functional groups are present at the sorbent surface [32]. Based on solute descriptors used in poly-parameter linear free energy relationships (ppLFER), PAHs may only act as hydrogen-bonding acceptors (i.e., hydrogen bonding acidity = 0 but basicity > 0 [45]; a detailed description of ppLFER can be found in literature, e.g., ref [46]). The presence of -OH

and -COOH groups on CNM surface makes the sorbent possible hydrogen-bonding donors [44-47], emphasizing the possible contribution of hydrogen bonding.

Hydrophobicity normalized distribution coefficients (i.e., K_{nC60}/K_{ow} ratio) have previously been used as a tool to estimate the fraction of overall sorption that is not due to hydrophobic interaction [19, 36]. Hence, K_{nC60}/K_{ow} was related to polarizability and hydrogen bond basicity (B) of PAHs (as displayed in Table A 3-1) in order to evaluate a possible contribution of hydrogen donor-acceptor interactions (results shown in Table A 3-7(b)). However, a significant correlation could not be observed; neither between K_{nC60}/K_{ow} and polarizability nor B. Thus, considering hydrogen bonds for the interpretation of relevant molecular interactions could not help interpreting the observed differences in log K_{nC60}-log K_{ow} relationships for sorption of PAHs by the studied C60 systems. Endo et al. used ppLFER to identify the most significant type of specific interactions by subtracting ppLFER terms for nonspecific interactions from determined distribution coefficients [48]. However, phase descriptors are not yet available for nC60. Sorption data for a much broader set of probe compounds, covering various chemical classes, are thus necessary to further investigate the contribution of individual molecular interactions to overall sorption (e.g., by ppLFER).

Overall, the findings suggest that molecular interactions with PAHs are independent from the presence of oxygen-containing functional groups on C60 surface. Therefore, hydrogen bonds seem to play a negligible role on sorption behavior of nC60. The presented data set provides a set of scenarios of how aging may affect sorption of dispersed fullerenes in the environment. Changes in surface chemistry led to significant decrease in both sorption capacity, i.e., amount of sorbate to be sorbed by the sorbent, and sorption affinity, i.e., strength of sorption, for non-ionic hydrophobic contaminants. Thus, our results suggest that aging of fullerenes leads to a reduced sorption affinity and capacity, at least for non-polar contaminants.

3.5 References

1. Isaacson, C.W.; Kleber, M.; Field, J.A. *Environmental Science & Technology* **2009**, 43, 6463-6474.
2. Gottschalk, F.; Sonderer, T.; Scholz, R.W.; Nowack, B. *Environmental Science & Technology* **2009**, 43, 9216-9222.
3. Brant, J.; Lecoanet, H.; Wiesner, M.R. *Journal of Nanoparticle Research* **2005**, 7, 545-553.
4. Wiesner, M.R.; Hotze, E.M.; Brant, J.A.; Espinasse, B. *Water Science and Technology* **2008**, 57, 305-310.
5. Li, Q.L.; Xie, B.; Hwang, Y.S.; Xu, Y.J. *Environmental Science & Technology* **2009**, 43, 3574-3579.
6. Li, Q.L.; Mahendra, S.; Lyon, D.Y.; Brunet, L.; Liga, M.V.; Li, D.; Alvarez, P.J.J. *Water Research* **2008**, 42, 4591-4602.
7. Gai, K.; Shi, B.; Yan, X.; Wang, D. *Environmental Science & Technology* **2011**, 45, 5959-5965.
8. Hu, X.L.; Liu, J.F.; Mayer, P.; Jiang, G. *Environmental Toxicology and Chemistry* **2008**, 27, 1868-1874.
9. Lee, J.; Cho, M.; Fortner, J.D.; Hughes, J.B.; Kim, J.H. *Environmental Science & Technology* **2009**, 43, 4878-4883.
10. Turco, R.F.; Bischoff, M.; Tong, Z.H.; Nies, L. *Current Opinion in Biotechnology* **2011**, 22, 527-532.
11. Zhang, X.; Kah, M.; Jonker, M.T.O.; Hofmann, T. *Environmental Science & Technology* **2012,** 46, 7166-7173.
12. Hawthorne, S.B.; Jonker, M.T.O.; van der Heijden, S.A.; Grabanski, C.B.; Azzolina, N.A.; Miller, D.J. *Analytical Chemistry* **2011**, 83, 6754-6761.
13. Jonker, M.T.O.; Koelmans, A.A. *Environmental Science & Technology* **2001**, 35, 3742-3748.
14. Brehm, G.; Axmacher, J.C. *Environmental Entomology* **2006**, 35, 757-764.
15. Hou, W.C.; Jafvert, C.T. *Environmental Science & Technology* **2009**, 43, 362-367.
16. Hwang, Y.S.; Li, Q. *Environmental Science & Technology* **2010**, 44, 3008-3013.
17. Tsai, C.H. *Marine Geology* **1996**, 134, 95-112.
18. Brant, J.A.; Labille, J.; Bottero, J.Y.; Wiesner, M.R. *Langmuir* **2006**, 22, 3878-3885.
19. Kah, M.; Zhang, X.; Jonker, M.T.O.; Hofmann, T. *Environmental Science & Technology* **2011**, 45, 6011-6017.
20. Yang, K.; Zhu, L.Z.; Xing, B.S. *Environmental Science & Technology* **2006**, 40, 1855-1861.
21. Allen-King, R.M.; Grathwohl, P.; Ball, W.P. *Advances in Water Resources* **2002**, 25, 985-1016.
22. Motulsky, H.J.; Christopoulos, A. *Fitting models to biological data using linear and nonlinear regression. A pracitcal guide to curve fitting;* GraphPad Software Inc.: San Diego, CA, U.S.A., 2003.

23. Labille, J.; Masion, A.; Ziarelli, F.; Rose, J.; Brant, J.; Villieras, F.; Pelletier, M.; Borschneck, D.; Wiesner, M.R.; Bottero, J.Y. *Langmuir* **2009**, 25, 11232-11235.
24. Chen, K.L.; Elimelech, M. *Environmental Science & Technology* **2009**, 43, 7270-7276.
25. Chen, K.L.; Elimelech, M. *Langmuir* **2006**, 22, 10994-11001.
26. Qu, X.; Hwang, Y.S.; Alvarez, P.J.J.; Bouchard, D.; Li, Q. *Environmental Science & Technology* **2010**, 44, 7821-7826.
27. Cho, H.H.; Smith, B.A.; Wnuk, J.D.; Fairbrother, D.H.; Ball, W.P. *Environmental Science & Technology* **2008**, 42, 2899-2905.
28. Yu, F.; Ma, J.; Wu, Y. *Journal of Hazardous Materials* **2011**, 192, 1370-1379.
29. Chang, X.; Vikesland, P.J. *Environmental Science & Technology* **2011**, 45, 9967-9974.
30. Duncan, L.K.; Jinschek, J.R.; Vikesland, P.J. *Environmental Science & Technology* **2008**, 42, 173-178.
31. Cheng, X.K.; Kan, A.T.; Tomson, M.B. *Journal of Chemical and Engineering Data* **2004**, 49, 675-683.
32. Pan, B.; Xing, B.S. *Environmental Science & Technology* **2008**, 42, 9005-9013.
33. Brant, J.A. *Fullerol Clusters*; Taylor & Francis: Boca Raton, U.S.A., 2011.
34. Yang, K.; Xing, B.S. *Chemical Reviews* **2010**, 110, 5989-6008.
35. Guirado-López, R.A. *Polyhydroxylated Fullerenes*; Taylor & Francis: Boca Raton, U.S.A., 2011.
36. Wang, X.L.; Tao, S.; Xing, B.S. *Environmental Science & Technology* **2009**, 43, 6214-6219.
37. Ahnert, F.; Arafat, H.A.; Pinto, N.G. *Adsorption-Journal of the International Adsorption Society* **2003**, 9, 311-319.
38. Ania, C.O.; Cabal, B.; Pevida, C.; Arenillas, A.; Parra, J.B.; Rubiera, F.; Pis, J.J. *Applied Surface Science* **2007**, 253, 5741-5746.
39. Yang, K.; Wang, X.L.; Zhu, L.Z.; Xing, B.S. *Environmental Science & Technology* **2006**, 40, 5804-5810.
40. Guo, L.; Lee, H.K. *Journal of Chromatography A* **2011**, 1218, 9321-9327.
41. Ismail, I.M.K.; Rodgers, S.L. *Carbon* **1992**, 30, 229-239.
42. Schwarzenbach, R.P.; Gschwend, P.M.; Imboden, D.M. *Environmental Organic Chemistry;* John Wiley and Sons: Hoboken, NJ, U.S.A., 2003.
43. Jonker, M.T.O.; Koelmans, A.A. *Environmental Science & Technology* **2002**, 36, 3725-3734.
44. Yang, K.; Wu, W.H.; Jing, Q.F.; Zhu, L.Z. *Environmental Science & Technology* **2008**, 42, 7931-7936.
45. Abraham, M.H.; Chadha, H.S.; Whiting, G.S.; Mitchell, R.C. *Journal of Pharmaceutical Sciences* **1994**, 83, 1085-1100.
46. Goss, K.U.; Schwarzenbach, R.P. *Environmental Science & Technology* **2001**, 35, 1-9.
47. Chen, W.; Duan, L.; Zhu, D.Q. *Environmental Science & Technology* **2007**, 41, 8295-8300.
48. Endo, S.; Grathwohl, P.; Haderlein, S.B.; Schmidt, T.C. *Environmental Science & Technology* **2008**, 42, 5897-5903.

3.6 Appendix A3

Further details on the POM-SPE method

The development of a solid-phase extraction (SPE) method using plastic polyoxymethylene (POM) was in details presented by Jonker and Koelmans [1]. Briefly, sorption experiments of hydrophobic organic compounds (HOC) on POM showed linear isotherms over several orders of magnitude. Sorption kinetic studies suggested that 28 d equilibration time are sufficient for PAH partitioning between POM and the aqueous phase. An application of the POM-SPE method to determine the distribution of HOC to sediments and soot indicated a high reproducibility of the method.

Since its first introduction, the POM-SPE method has been applied for the determination of HOC in aqueous environmental samples down to pictogram per liter concentrations [2] and the investigation of sorption of HOC to various sorbents (e.g., soil [3], particulate organic matter [4] and multi-walled carbon nanotubes [5]).

Table A 3-1: Selected properties of the sorbates studied.

Sorbate	Log S_i[a]	Log K_{ow} Literature[b]	Log K_{ow} EPI[c]	Log K_{ow} SPARC[d]	MV[e] [cm^3]	Polarizability[f] [10^{-23} cm^3]	A[g]	B[h]
Pyr	-2.35	4.88	4.93	5.25	161.98	2.87	0.00	0.29
Phen	-1.64	4.46	4.35	4.74	157.67	2.46	0.00	0.26
B[a]P	-4.21	6.13	6.11	5.85	196.09	3.58	0.00	0.44
B[a]A	-3.21	5.76	5.81	6.54	191.78	3.16	0.00	0.33

[a]logS_i: subcooled liquid solubility from [6]; log K_{ow}: octanol-water partition constant: [b]From [7], [c]derived by EPI Suite [8], and [d]derived by SPARC [9]. [e]MV: Molar volume taken from Chemspider database [10]. [f]Predicted by ACD Lab prediction software and available in the Chemspider database [10]; [g]A and B: ppLFER solute descriptors representing H-bond acidity and H-bond basicity obtained from [11].

Table A 3-2: Equations used to derive concentrations of PAH on nC60 dispersions.

Scenario	Equation
Mass balance for distribution of total amount of sorbate between 3 phases: water (w), POM, and nC60	$m_T = C_w V_w + C_{POM} M_{POM} + C_{nC60} M_{nC60}$
PAH concentration in solution	$C_W = C_{POM} / K_{POM}$
PAH concentration on nC60 calculated from system characteristics and K_{POM}	$C_{nC60} = \frac{m_T - C_{POM} V_W / K_{POM} - C_{POM} M_{POM}}{M_{nC60}}$

m_T: total mass of sorbate [µg]. C_{nC60} and C_{POM}: sorbate concentration in nC60 and POM, respectively [µg kg^{-1}]. M_{nC60} and M_{POM}: mass of nC60 and POM, respectively [kg]. C_W: freely dissolved PAH concentration in water [µg L^{-1}]. V_W: volume of solution [L]. K_{POM}: sorption coefficient of PAH by POM [L kg^{-1}]. K_{POM} values for PAH measured by Jonker and Koelmans [1] were applied in this study.

Table A 3-3: Nonlinear sorption models used to fit isotherms.

Model	Equation	Fitting parameters	p[b]
Freundlich (FM)	$C_s = K_F C_w^n$	K_F: Freundlich coefficient [(µg kg^{-1})/(µg L^{-1})$^{1/n}$] n: Freundlich exponent [-]	2
Langmuir (LM)	$C_s = \frac{Q_{max} K_L C_w}{1 + K_L C_w}$	Q_{max}: maximum sorption capacity [µg kg^{-1}] K_L: Langmuir affinity coefficient [µg L^{-1}]	2
Dubinin-Ashtakhov (DAM)	$\log C_s = \log Q_{max} + (\varepsilon_{sw} / E')^b$	Q_{max}: maximum sorption capacity [µg kg^{-1}] E': correlating divisor [J mol^{-1}] b: fitting parameter	3

C_s: sorbed sorbate concentration [µg kg^{-1}]; C_w: aqueous concentration [µg L^{-1}]; $\varepsilon_{sw} = -RT \ln(C_w/S_w)$ [kJ mol^{-1}]: effective sorption potential; R [8.314•10^{-3} kJ mol^{-1}K^{-1}]: universal gas constant; T [K]: absolute temperature; S_w: aqueous solubility. [b] p: number of fitting parameters.

Comment:

Calculation of model parameters were performed using Cs = f(Cw) for all sorption models investigated.

Table A 3-4: Fitting parameters ± standard error, mean weighted square error, and Akaike's Information Criterion (AIC) for three sorption model fits to the isotherms of pyrene by different C60 dispersions.

Freundlich Model (FM)						
Sample	**K_F**	**n**	**R^2**	**MWSE[a]**	**AIC**	**N[b]**
nC60-OH	1.93E+04 ± 1.79E+03	0.89 ± 0.03	0.92	0.0767	-24.82	12
nC60-L_O	7.06E+04 ± 6.56E+03	0.81 ± 0.03	0.93	0.0538	-24.92	11
nC60-D_O	1.76E+05 ± 2.22E+04	0.88 ± 0.04	0.92	0.0668	-22.54	11
nC60-L_A	4.62E+05 ± 1.48E+05	1.08 ± 0.07	0.61	0.3878	-4.55	12
nC60-D_A	7.88E+05 ± 2.05E+05	1.09 ± 0.06	0.76	0.2443	-8.28	11
Langmuir Model (LM)						
Sample	**Q_{max}**	**K_L**	**R^2**	**MWSE[a]**	**AIC**	**N[b]**
nC60-OH	1.76E+05 ± 1.67E+04	5.97 ± 0.91	0.96	0.0440	-31.48	12
nC60-L_O	2.65E+05 ± 1.76E+04	2.08 ± 0.23	0.96	0.0299	-31.38	11
nC60-D_O	3.68E+05 ± 5.34E+04	1.23 ± 0.28	0.97	0.0293	-31.59	11
nC60-L_A	8.56E+05 ± 1.28E+05	1.06 ± 0.25	0.56	0.4383	-3.09	12
nC60-D_A	1.51E+06 ± 3.04E+05	1.58 ± 0.44	0.66	0.3454	-4.47	11
Dubinin-Ashtakhov Model (DAM)						
Sample	**$\log Q_{max}$**	**E'**	**b**	**R^2**	**MWSE[a]**	**AIC**	**N[b]**
nC60-OH	5.47 ± 0.16	1.14E+04 ± 1.22E+03	1.55 ± 0.17	0.97	0.0357	-31.79	12
nC60-L_O	5.74 ± 0.18	1.34E+04 ± 1.49E+03	1.66 ± 0.22	0.97	0.0256	-29.16	11
nC60-D_O	5.75 ± 0.14	1.61E+04 ± 1.14E+03	2.09 ± 0.22	0.98	0.0175	-33.33	11
nC60-L_A	5.96 ± 0.19	2.04E+04 ± 1.27E+03	3.65 ± 0.61	0.95	0.1201	-15.23	12
nC60-D_A	6.02 ± 0.12	1.81E+04 ± 7.85E+02	2.82 ± 0.23	0.98	0.0270	-28.58	11

[a]MWSE=$1/\nu\ \Sigma[(C_{s,measured}-C_{s,predicted})^2/C^2_{s,measured}]$: mean weighted square error with ν=N-p the degrees of freedom. [b] N: number of data points. Other notations are described in Table A 3-3.

Comment:

The model with smallest Akaike's Information Criterion (AIC) values is most likely the best. AIC was calculated following Motulsky and Christopoulos [12]:

$$AIC = N \cdot \ln\left(\frac{WSS_{res}}{N}\right) + 2p + \frac{2p \cdot (p+1)}{N-p-1}$$

WSS_{res} is the weighted sum of squares residual:

$$WSS_{res} = \sum \frac{\left(C_{s,measured} - C_{s,predited}\right)^2}{C^2_{s,measured}}$$

Model parameters and predicted C_s values were computed with SigmaPlot using reduced Chi-square and weighted regression with weighting to reciprocal y^2.

Table A 3-5: Probability and evidence ratio for pairs of models compared, based on Akaike's Information Criterion.

Probability for nC60-OH				**Evidence ratio for nC60-OH**			
	FM	LM	DAM		FM	LM	DAM
FM	0.50	0.97	0.97	FM	1.00	0.04	0.03
LM	0.03	0.50	0.54	LM	27.94	1.00	0.85
DAM	0.03	0.46	0.50	DAM	32.77	1.17	1.00

Probability for nC60-L_O				**Evidence ratio for nC60-L_O**			
	FM	LM	DAM		FM	LM	DAM
FM	0.50	0.96	0.89	FM	1.00	0.04	0.12
LM	0.04	0.50	0.25	LM	25.38	1.00	3.04
DAM	0.11	0.75	0.50	DAM	8.36	0.33	1.00

Probability for nC60-D_O				**Evidence ratio for nC60-D_O**			
	FM	LM	DAM		FM	LM	DAM
FM	0.50	0.99	1.00	FM	1.00	0.01	0.00
LM	0.01	0.50	0.70	LM	92.61	1.00	0.42
DAM	0.00	0.30	0.50	DAM	220.08	2.38	1.00

Probability for nC60-L_A				**Evidence ratio for nC60-L_A**			
	FM	LM	DAM		FM	LM	DAM
FM	0.50	0.32	1.00	FM	1.00	2.08	0.00
LM	0.68	0.50	1.00	LM	0.48	1.00	0.00
DAM	0.00	0.00	0.50	DAM	208.09	433.44	1.00

Probability for nC60-D_A				**Evidence ratio for nC60-D_A**			
	FM	LM	DAM		FM	LM	DAM
FM	0.50	0.13	1.00	FM	1.00	6.72	0.00
LM	0.87	0.50	1.00	LM	0.15	1.00	0.00
DAM	0.00	0.00	0.50	DAM	25551.55	171742.97	1.00

Comment:

The probability and evidence ratio were calculated based on the difference of AIC (ΔAIC; as described below Table S4) with the following equations:

$$\text{probability} = \frac{e^{-0.5\Delta AIC}}{1+e^{-0.5\Delta AIC}}$$

The probability is based on differences between AIC values.

$$\text{evidence ratio} = \frac{1}{e^{-0.5\Delta AIC}}$$

The evidence ratio is based on absolute difference of AIC values rather than relative difference.

For further information, see Motulsky and Christopoulos [12].

Table A 3-6: Sorption coefficients (log K_{nC60}) of pyrene by C60 dispersions, measured in single and multiple sorbate experiments.

Sample	Log K_{nC60} Pyr[a] [L kg^{-1}]	Log K_{nC60} Pyr[b] [L kg^{-1}]	Log K_{nC60} Phen[b] [L kg^{-1}]	Log K_{nC60} BaA[b] [L kg^{-1}]	Log K_{nC60} BaP[b] [L kg^{-1}]	C_w [µg L^{-1}]
nC60-D_A	5.74	5.82 ± 0.05	4.55 ± 0.06	6.86 ± 0.05	7.03 ± 0.05	0.005
nC60-L_A	5.73	5.69 ± 0.09	4.66 ± 0.19	6.88 ± 0.03	7.05 ± 0.02	0.003
nC60-D_O	5.45	5.41 ± 0.08	4.23 ± 0.13	6.36 ± 0.10	6.49 ± 0.09	0.005
nC60-L_O	5.17	5.15 ± 0.03	3.97 ± 0.04	6.05 ± 0.02	6.17 ± 0.11	0.013
nC60-OH	4.44	4.41 ± 0.07	3.45 ± 0.02	5.58 ± 0.07	5.45 ± 0.21	0.024

[a]single sorbate [b] multiple sorbate experiments ± standard errors (n=3).

Table A 3-7: Correlations between (a) log K_{nC60} and log K_{ow}, log S_i, and MV and (b) K_{nC60}/K_{ow} and polarizability and H-bond basicity of PAHs for five C60 dispersion scenarios (n=4 for all correlations). The values presented for each pair of variables are the correlation coefficient and associated p value.

(a)	**Log K_{nC60} (L_O)**	**Log K_{nC60} (D_O)**	**Log K_{nC60} (L_A)**	**Log K_{nC60} (D_A)**	**Log K_{nC60} (OH)**
Log K_{ow}	0.991	0.986	0.996	0.994	0.981
Schwarzenbach	0.009	0.014	0.004	0.006	0.019
Log S_i	-0.936	-0.931	-0.946	-0.942	-0.902
	0.064	0.069	0.054	0.058	0.098
MV	0.940	0.926	0.956	0.946	0.941
	0.060	0.074	0.044	0.054	0.059

(b)	**K_{nC60}/K_{ow} (L_O)**	**K_{nC60}/K_{ow} (D_O)**	**K_{nC60}/K_{ow} (L_A)**	**K_{nC60}/K_{ow} (D_A)**	**K_{nC60}/K_{ow} (OH)**
Polarizability	0.841	0.792	0.876	0.862	0.772
	0.159	0.208	0.124	0.138	0.228
H-bond basicity	0.649	0.585	0.701	0.679	0.563
	0.351	0.415	0.299	0.321	0.437

Figure A 3-1: Microscope image of POM surface before (left) and after (right) wiping with a wet tissue, indicating the removal of sorbent prior to extraction.

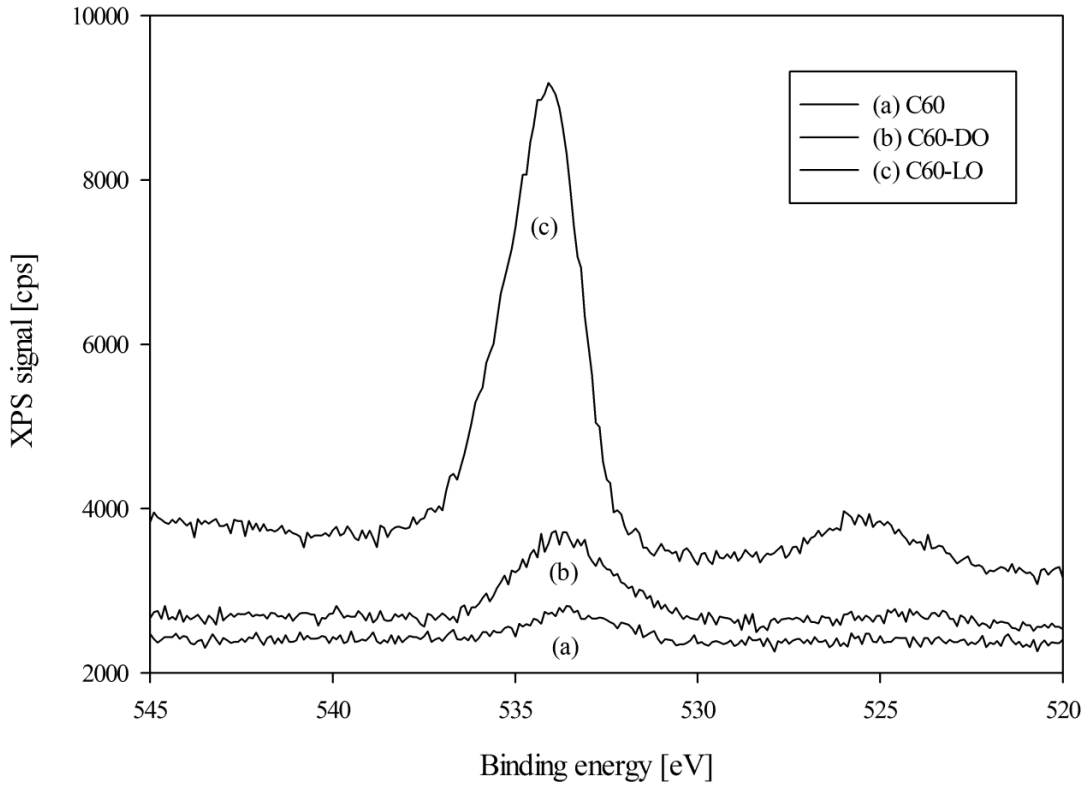

Figure A 3-2: XPS spectral envelopes of the O(1s) region for (a) as received C60, sorbent materials under aerobic conditions (b) in the dark (nC60-D_O), and (c) irradiated with UV light (nC60-L_O).

For scanning electron microscopy (SEM, Fei Quanta 3D FEG), copper grids (400 mesh) with Formvar thin carbon film were used. Particular attention was paid to maintain the structure of the aggregates as they occurred in the sorption test (e.g., no use of organic solvent for the sample preparation). The grids were dipped into the dispersions to collect sorbent particles and dried at room temperature in a clean bench at least overnight (Figure A 3-3). Samples of bulk C60 and C60-OH were imaged by adding little of sorbent material onto a sticky tape, which was then inserted into the microscope (Figure A 3-4).

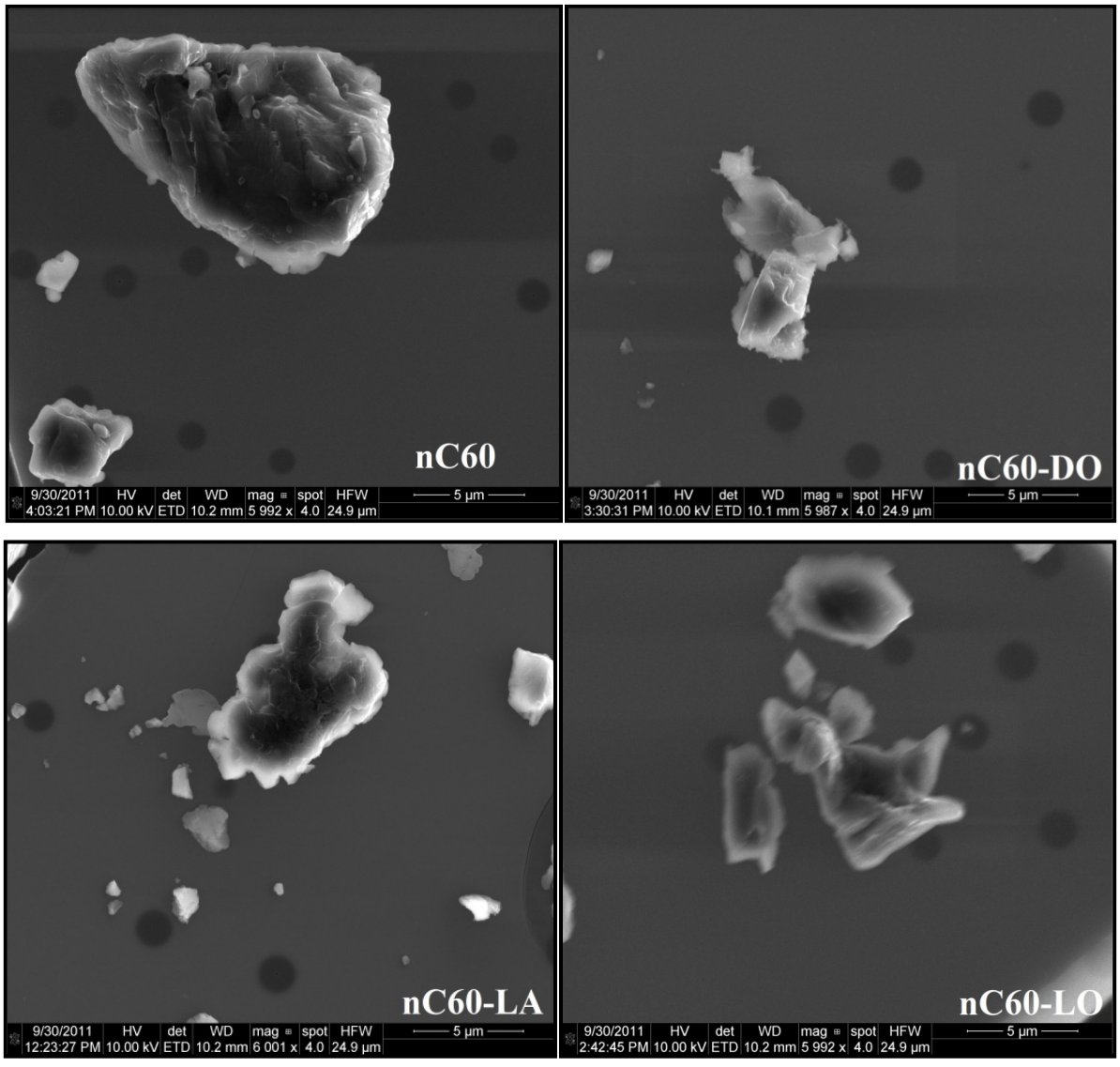

Figure A 3-3: SEM images of dried dispersions of unaged C60 (nC60, top-left), nC60-D_O (top-right), nC60-L_A (bottom-left), and nC60-L_O (bottom-right).

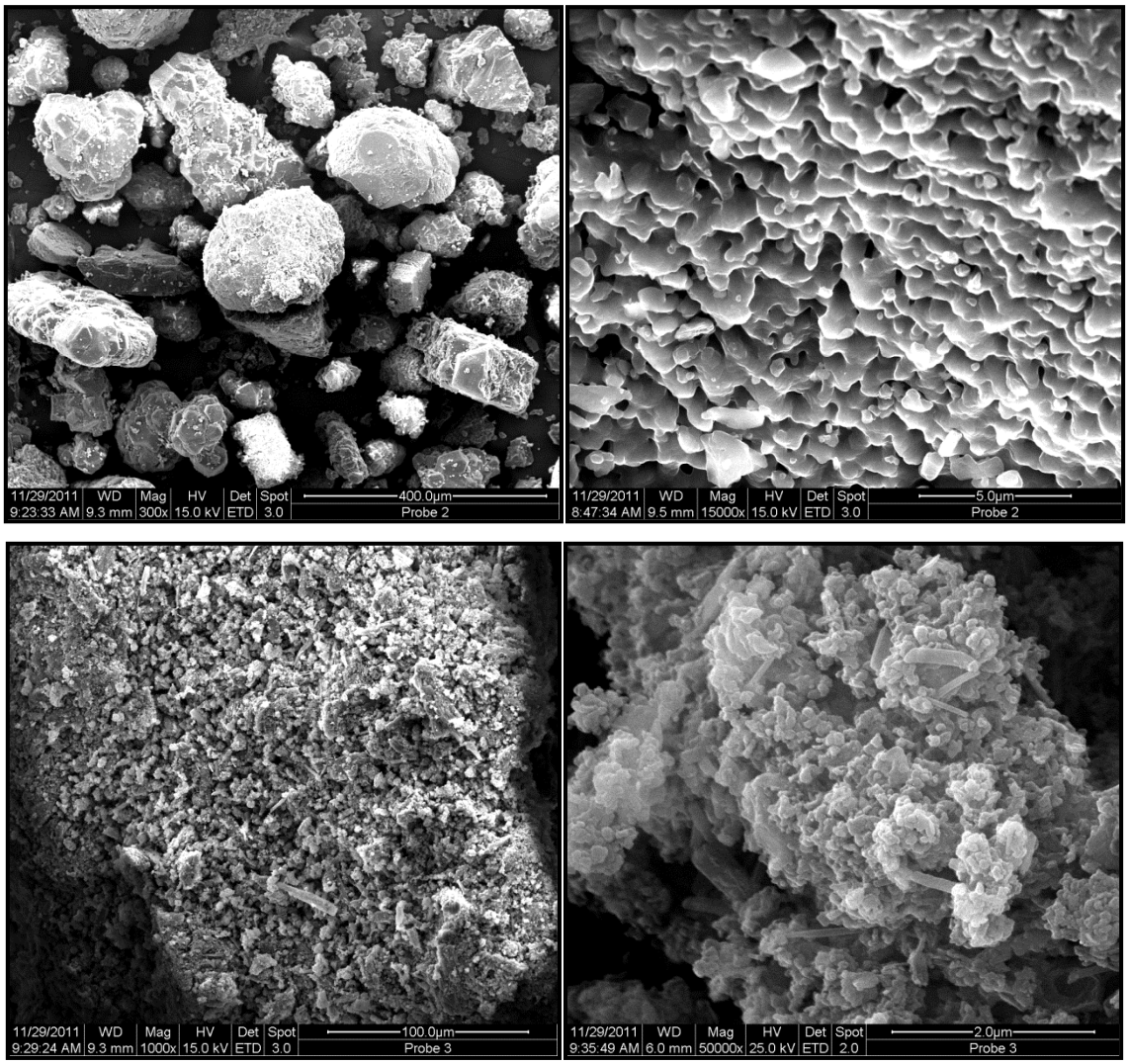

Figure A 3-4: SEM images of bulk materials: C60 (top) and C60-OH (bottom).

References for Appendix A3

1. Jonker, M.T.O.; Koelmans, A.A. *Environmental Science & Technology* **2001**, 35, 3742-3748.
2. Hawthorne, S.B.; Jonker, M.T.O.; van der Heijden, S.A.; Grabanski, C.B.; Azzolina, N.A.; Miller, D.J. *Analytical Chemistry* **2011**, 83, 6754-6761.
3. Hong, L.; Luthy, R.G. *Chemosphere* **2008**, 72, 272-281.
4. Kuivikko, M.; Sorsa, K.; Kukkonen, J.V.K.; Akkanen, J.; Kotiaho, T.; Vahatalo, A.V. *Environmental Toxicology and Chemistry* **2010**, 29, 2443-2449.
5. Zhang, X.; Kah, M.; Jonker, M.T.O.; Hofmann, T. *Environmental Science & Technology* **2012**, 46, 7166-7173.
6. van Noort, P.C.M. *Chemosphere* **2009**, 74, 1018-1023.
7. Schwarzenbach, R.P.; Gschwend, P.M.; Imboden, D.M. *Environmental Organic Chemistry;* John Wiley and Sons: Hoboken, NJ, U.S.A., 2003.
8. US-EPA, EPI Suite Package. Estimation Program Interface from the U.S. Environmental Protection Agency. Available at http://epa.gov/oppt/exposure/pubs/episuitedl.htm. Last accessed Feb., 2012.
9. Georgia, U. o. SPARC online calculator. http:sparc.chem.uga.edu/sparc/. Last accessed Feb., 2012.
10. Chemistry, T. R. S. o. Chemspider database. http://www.chemspider.com. Last accessed Feb., 2012.
11. Abraham, M.H.; Chadha, H.S.; Whiting, G.S.; Mitchell, R.C. *Journal of Pharmaceutical Sciences* **1994**, 83, 1085-1100.
12. Motulsky, H.J.; Christopoulos, A. *Fitting models to biological data using linear and nonlinear regression. A pracitcal guide to curve fitting;* GraphPad Software Inc.: San Diego, CA, U.S.A., 2003.

Chapter 4 Characterization of the Sorption Mode by Carbon Nanotubes in the Presence of Natural Organic Matter

Adapted from: Hüffer, T.; Schroth, S.; Schmidt, T.C. Is the Sorption Mode of Carbon nanotubes affected by Natural Organic Matter?. Submitted to *Environmental Science & Technology* **2013**.

4.1 Abstract

The presence of humic substances (HS) has previously been shown to alter sorption properties of multi-walled carbon nanotubes (MWCNTs), but the mechanisms behind this effect remain poorly understood. To systematically study this process, three alkane pairs were selected as molecular probe sorbates. The influence of four different HS on sorption affinity, sorption linearity, and the dominant sorption mode (i.e., *ad*- or *ab*sorption) by MWCNTs was investigated. All sorption isotherms of alkanes were determined at environmentally relevant concentrations over a range of at least three orders of magnitude. Isotherms of all sorbent scenarios were well fit with the Freundlich model. Sorption of *n*-alkanes by MWCNTs was generally stronger than of their cyclic homologues. The addition of HS led to a continuous decrease in sorption affinity and an increase in sorption linearity with increasing HS addition. Furthermore, the comparison of distribution coefficients of *n*- and cycloalkanes showed that the dominant sorption mode remains to be *ad*sorption regardless of the presence of HS on MWCNT surface. From this, it can be concluded that instead of a change in sorption mode to *ab*sorption of sorbates into HS-coated MWCNT, HS blocks high-energy sorption sites for subsequently added sorbates and that sorbates continuously sorb on the MWCNT surface.

4.2 Introduction

Since the discovery of carbon-based nanomaterials (CNM) in the early 1990s [1], the research and development of CNM have grown steadily due to their unique physicochemical properties. Together with an expected growth in production, the question of the environmental impact of CNM has become a controversial discussed issue among researchers. To date, most data on the environmental concentrations of CNM are based on modeling [2]. The predicted low concentrations are expected to increase in the future [3], which, among others, raises the question of the impact of CNM of the fate of other pollutants, e.g., hydrophobic organic compounds (HOC). Various environmentally relevant parameters have been shown to influence the sorption behavior by CNM, such as the presence of oxygen and sunlight [4] or natural organic matter (NOM) [5-7].

Generally, two mechanisms have been proposed on how natural organic matter (NOM) reduces HOC sorption by CNM. Firstly, NOM directly competes with HOC for sorption sites on CNM surface. This seems especially relevant as commonly low sorbate and high NOM concentrations have been combined [6], which represents a realistic environmental scenario. Secondly, sorption of HOC is reduced by large NOM molecules that block the entrances of CNM pores that may otherwise be available for HOC sorption [5, 8]. Recent investigations on the influence of NOM addition on HOC sorption have shown inconsistent effects on sorption strength of multi-walled carbon nanotubes (MWCNTs). A decrease in sorption strength of NOM-coated MWCNTs compared to the pristine tubes was assigned to an offset between "creating" new sorption sites due to increased dispersity and the reduced accessibility of polar moieties [6]. In contrast, the contribution of an increase in sorption due to higher MWCNT dispersion was very recently shown to overcome the observed decreased sorption due to NOM coating [9]. In addition, sorption became more linear after NOM addition. This was principally related to the presence of a co-solute, which reduces sorption of the primary solute (i.e., HOC) and thus increases sorption linearity [5]. For example, Zhang et al. studied the effect of NOM addition on sorption of phenanthrene, biphenyl, and phenylphenol by various carbon nanotubes (CNTs). From experimental data, sorption became more linear after NOM addition, while the largest change in linearity ($\Delta n = 0.1$-0.3) was obtained for preloaded CNTs [5]. Such changes in sorption linearity could indicate a potential change in sorption mode.

An important question in the phase transfer of HOC is to clarify the dominant sorption mode. Here, generally two sorption modes are discussed: one is the *ad*sorption on the surface of a sorbent, the other is *ab*sorption, which is the distribution between two condensed phases. To clarify the sorption mode, Endo et al. proposed an approach to differentiate between *ad*- and *ab*sorption, in which the distribution coefficients of linear alkanes (K_n) and their cyclic homologues (K_c) were compared as follows [10]:

$$K_n/K_c = \left(K_d/K_{aw} \text{ of n-alkane}\right)/\left(K_d/K_{aw} \text{ of cyclo-alkane}\right) \qquad \text{(Eq. 4-1)}$$

where K_d is the distribution coefficient and K_{aw} is the air-water partitioning constant. This comparison of the distribution coefficients of n- and cyclo-alkanes is based on the fact that linear alkanes preferably *ad*sorb on a surface, while the distribution (i.e., *ab*sorption) from air into a bulk phase of cyclo-alkanes is stronger than of their linear homologues [11]. Note that K_n and K_c cannot be directly compared as experimentally derived K_d values additionally include molecular interactions with water, and for the characterization of the dominant sorption mode by a given sorbent, only the molecular interactions in/on the sorbent are of interest. Given equation 4-1, K_n/K_c ratios < 1 indicate *ab*sorption as the dominant sorption mode. K_n/K_c ratio ~ 1 suggest *ad*sorption if steric effects are negligible, while for $K_n/K_c > 1$ steric hindrance, e.g., from size exclusion effects, has to be considered [12].

Endo et al. observed that for soot, commonly regarded as an *ad*sorber, the predominant sorption mode changed from *ab*sorption to *ad*sorption accompanied by an increase in sorption non-linearity following the removal of extractable organic matter [13]. A similar but reverse effect could explain the decrease in sorption non-linearity by CNM following NOM addition. To this end, the here presented study investigated the dominant sorption mode by MWCNTs influenced by the presence of various types and concentrations of humic substances (HS).

4.3 Experimental Section

4.3.1 Materials

Multi-walled carbon nanotubes (C150HP) were purchased from Bayer Material Science (Leverkusen, Germany). Properties of MWCNTs are given in Table A 4-1. Amorphous carbon was removed by heating the MWCNTs to 350 °C for 1 h [14]. Four *humic substances* (HS) were selected (Table 4-1 lists HS and selected properties). Stock solutions were prepared by dissolving 0.25-1 g HS in 100 mL 0.1 mol NaOH overnight. After filtration through a 0.45 µm cellulose membrane (Whatman), the solution was diluted to 1 L and the pH was adjusted to neutral with 0.1 mol NaCl. The concentration of the thereby obtained HS stock solutions was determined by total organic carbon (TOC; Shimadzu TOC-5000, Duisburg, Germany). HS stock solutions were kept at 4 °C in the dark no longer than six weeks and TOC concentration were regularly monitored. Working standard HS solutions were obtained by diluting stock solutions accordingly to concentration of 1 and 10 mg L^{-1}.

Three pairs of *n*- and *cycloalkanes* (C6-C8) were selected as molecular probe compounds (all purchased from Sigma-Aldrich with >99% purity). Stock solutions of alkanes were freshly prepared in methanol (HPLC grade, Fisher Scientific, UK) every week. Selected physico-chemical properties of sorbates are displayed in Table A 4-2.

4.3.2 Sorption batch experiments

Sorption isotherms were determined in a multi-phase system. 2-5 mg of MWCNTs were weighted into 20-mL amber vials, and 10 or 15 mL of background solution were added containing either 10 mmol $CaCl_2$ to regulate the ionic strength or the HS solution in concentrations as given in Table 4-1. The samples were then horizontally shaken for 24 h to allow the MWCNTs to be coated with HS. The samples were spiked with methanolic stock solutions resulting in 12 different sorbate concentrations ranging over 3-4 orders of magnitude. The methanol content did not exceed 0.5% (v/v) in water to minimize co-solvent effects. The samples were shaken for at least 24 h for equilibration at 25 °C in a temperature-controlled room. Equilibration times were pre-determined (data not shown). Subsequently, the vials were removed from the shaker and the analyte concentrations in the headspace of the vials were determined after 1 h air-water equilibration using an external calibration.

Table 4-1: Humic substances and their physical properties as given by the supplier.

Humic Substance	Abb.	Concentrations [mg L^{-1}]	Ash	C	H	O	N	Carbonyl C	Carboxyl C	Aromatic C	Aliphatic C
Humic Acid[a]	HA	1, 10	n.d.	n.d.	n.d.	n.d.	n.d.	n.d.	n.d.	n.d.	n.d.
Pahokee Peat Humic Acid Standard[b]	PPHAS	10	1.12	56.37	3.82	37.34	3.69	5	20	47	19
Leonardite Humic Acid Standard[b]	LHAS	10	2.58	63.81	3.70	31.27	1.23	8	15	58	14
Waskish Peat Humic Acid Reference[b]	WPHAR	10	1.60	54.72	4.04	38.54	1.47	8	18	42	18

[a]purchased from Fluka (Buchs, Switzerland); [b]purchased from International Humic Substances Society (IHSS; St. Paul, MN, USA); n.d: not determined.

The calibration vials were prepared one day prior to analysis and contained the according background solutions. For quantification, a gas chromatography-mass spectrometry system (TraceGC Ultra/DSQ, Thermo Finnigan) equipped with a PAL Combi-xt autosampler (CTC Analytics) was used. An HP-5 capillary column (30 m x 0.32 mm x 0.25 µm, J&W Scientific) and oven temperatures between 70 and 150 °C were used depending on the analyte retention times.

Sorbed concentrations could be determined by mass balance using air-water partitioning constants of the individual analytes (see Table A 4-2). Loss of analytes during the experiments was monitored and corrections were made in the mass balance. Sorption of alkanes by HS was pre-determined and incorporated into the calculations. Highest equilibrium aqueous concentrations of sorbates were 20 times below their aqueous solubility

4.3.3 Determination of sorption mode

The Freundlich model (FM) was used to fit the experimental isotherm data.

$$C_s = K_F (C_w)^n \qquad \text{(Eq. 4-2)}$$

where C_s is the sorbed sorbate concentration by MWCNTs [µg kg^{-1}], C_w is the aqueous concentration [µg L^{-1}], and K_F and n are the Freundlich coefficient [(µg kg^{-1})/(µg L^{-1})^n] and the Freundlich exponent [-], respectively. Sigma Plot 12.0 for Windows was used for statistical analyses and model fits. Computation of model parameters and their standard errors was performed with reduced Chi-square and weighted regression with weighting to reciprocal y^2.

Single point distribution coefficients ($K_d = C_s / C_w$; [L kg^{-1}]) were determined by interpolation at given sorbate air concentration. All determined isotherms were non-linear; thus, K_d and K_n/K_c ratios may vary with concentration. As pointed out by Endo et al., calculating K_n/K_c ratios with K_d values occurring at the same C_{air} as reference concentration, may be the most appropriate [12]. K_d values were hence calculated for an air-phase concentration of 10 µg L^{-1}.

4.4 Results and Discussion

4.4.1 Sorption isotherms

Sorption isotherms of alkanes by MWCNTs following various kinds and concentrations of humic substances are shown in Figure 4-1. In general, sorption isotherms of *n*- and cycloalkanes by all sorbent scenarios were parallel with an increase in sorption with increasing number of carbon atoms (i.e., C6 < C7 < C8). This observation is reflected by a corresponding increase of sorbate hydrophobicity parameters, such as an increase in the hexadecane-air partitioning constant (L) as displayed in Table A 4-2. However, it must be stressed that L refer to *ab*sorption processes, which limits its comparability to the *ad*sorption by CNM. Furthermore, by comparing sorption of *n*-alkanes with their cyclic homologous, it can be seen that sorption of *n*-alkanes was stronger by up to one order of magnitude. The sorbate morphology, such as the molecular size and shape, plays a major role with respect to availability of sorption sites on CNM surface. Stronger sorption was previously explained by a better contact of linear and planar compounds with the CNM surface [15]. Similar conclusions have been drawn for alkane sorption by flat surfaces, where linear *n*-hexane can interact with its six carbon atoms with the sorbent surface, while non-planar cyclohexane can only do so with three or four carbon atoms due to its non-planar shape [16, 17]. These differences in number of carbon contact atoms are also likely to be the case for *n*- and cyclooctane [18].

Isotherm data were well fitted with the Freundlich model ($R^2 > 0.95$). It has been previously discussed that other, more complex, non-linear sorption models are more suitable for a robust interpretation of sorption isotherm data especially if large concentration ranges are considered [19]. However, the aim of this study was to investigate how the presence of NOM affects sorption by MWCNTs in terms of sorption affinity and sorption linearity; therefore, only the Freundlich model was taken into account for isotherm data fitting. The results of Freundlich model fits are summarized in Table 4-2 (for standard errors and R^2 values, see Table A 4-3).

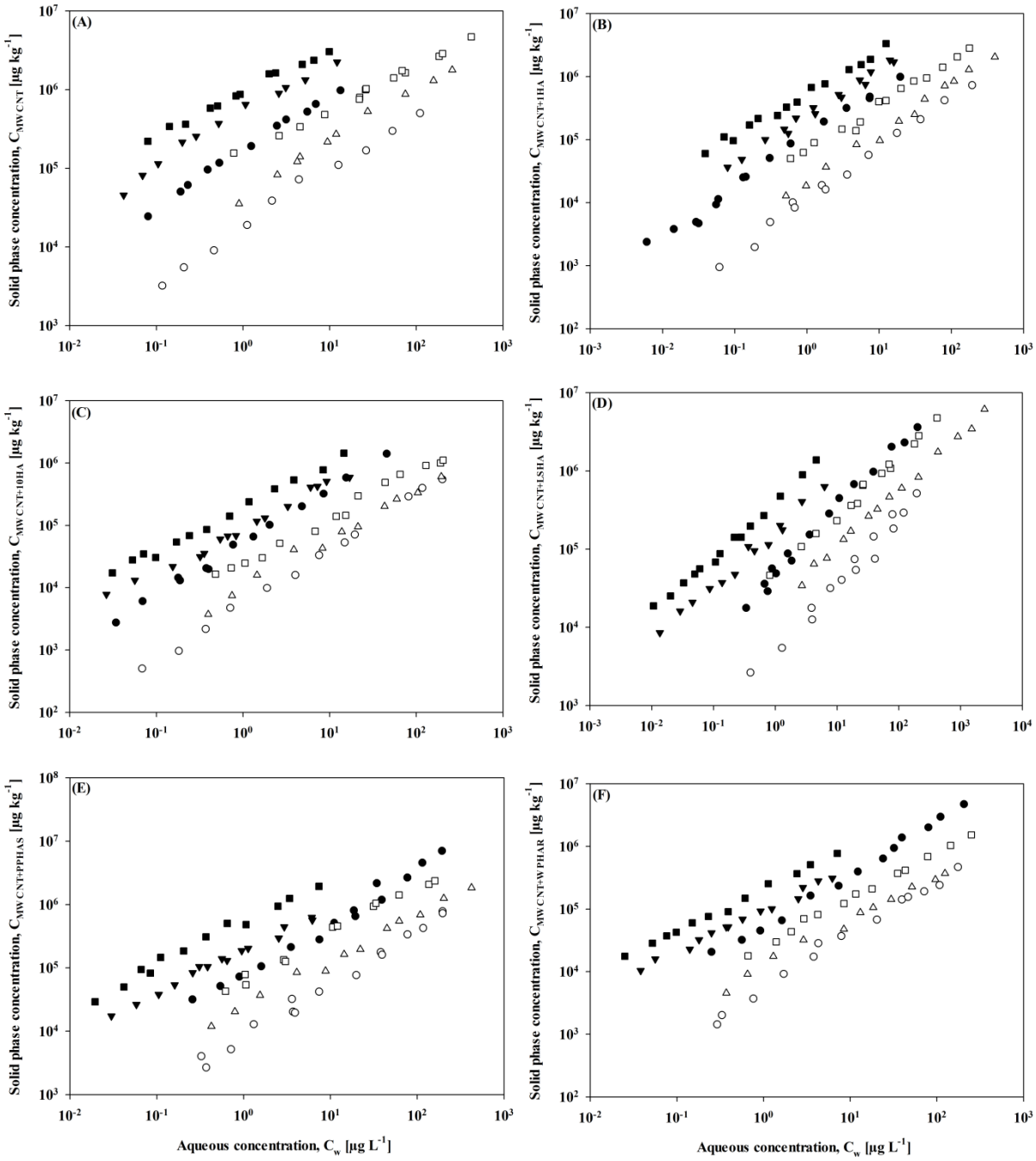

Figure 4-1: Sorption isotherms of (●) nHex, (○) cHex, (▼) nHep, (Δ) cHep, (■) nOct, and (□) cOct by MWCNTs (A), MWCNTs+1HA (B), MWCNTs+10HA (C), MWCNTs+LSHA (D), MWCNTs-PPHAS (E), and MWCNTs+WPHAR (F), respectively.

4.4.2 HS effect on sorption affinity

The sorption affinity (log K_F in Table 4-2) was reduced by the addition of HS in general, while there is a consistent trend of decreasing sorption affinity with increasing concentration of HA, i.e., K_F (MWCNT) > K_F (MWCNT-1HA) > K_F (MWCNT-10HA). Overall, the addition of 10 mg L^{-1} HA led to a decrease in sorption affinity ranging between 0.5 log units for nHex and 0.8 log units for cOct. Zhang et al. observed a clear linear decrease in sorption affinity of MWCNTs for pyrene following Suwannee River humic acid addition ranging from 0 to 200 mg L^{-1}; however, the obtained decrease in K_F was smaller than the almost one order of magnitude effect observed here [7].

Overall, the addition of NOM has led to a stabilization of CNT aggregates in combination with a reduction in sorption affinity due to the occupation of sorption sites by NOM [7, 8, 20]. This seems to be the case for the here investigated sorption scenarios, where sorption by MWCNTs was always reduced following the addition of HS. Furthermore, a decrease in sorption affinity for HOC may be explained by a decrease in hydrophobicity of CNT due to the introduction of polar moieties to CNT surface from NOM addition. This facilitates the formation of water clusters and as a consequence reduces the interaction with HOC due to a decrease in hydrophobicity of CNT surface [21]. In contrast, an increase in sorption due to a concomitant increase in available sorption sites following NOM addition, which has also been reported [6, 22], seems to result from a destabilization of CNM aggregates due to additional effects, resulting for example from sonication [9].

Previous investigations have shown that the strength of interaction between CNTs and HOC depends also on sorbent structural properties. While the effect of nanoscale curvature has been discussed for sorption of polycyclic aromatic hydrocarbons (PAHs) by single-walled carbon nanotubes (SWCNTs) [15], this effect is expected to play a minor role here as the investigated alkane sorbates are comparably small. Differences in decrease of sorption by MWCNTs and graphite have been explained by structural differences in the sorbent material. The interstitial and groove areas of CNT aggregates may not be available for sorption of large humic substance molecules [23], while these sites remain available for sorption of comparably small alkane molecules after HS addition.

Table 4-2: Summary of Freundlich parameters of sorption data of alkane pairs by various sorbents.

Sorbent	nHex		cHex		nHep		cHep		nOct		cOct	
	Log K_F	n	Log K_F	n	Log K_F	n	Log K_F	n	Log K_F	n	Log K_F	n
MWCNT	5.22	0.71	4.24	0.73	5.70	0.66	4.66	0.68	5.96	0.55	5.20	0.55
MWCNT+1HA	5.03	0.79	4.04	0.83	5.38	0.73	4.32	0.78	5.73	0.66	4.83	0.71
MWCNT+10HA	4.73	0.86	3.72	0.89	4.95	0.72	3.99	0.79	5.29	0.71	4.39	0.74
MWCNT+LSHA	4.70	0.83	3.69	0.86	5.22	0.69	4.31	0.72	5.61	0.71	4.70	0.74
MWCNT+PPHAS	4.89	0.82	3.90	0.85	5.28	0.67	4.38	0.73	5.73	0.70	4.81	0.74
MWCNT+WPHAR	4.71	0.84	3.73	0.87	4.99	0.66	4.09	0.72	5.32	0.68	4.41	0.74

Interestingly, the here obtained data for sorption affinity of alkanes by MWCNTs are well comparable with those previously obtained for hydrophobic organic compounds [24]. This is notable because so far specific electron donor-acceptor interactions have been discussed to be mainly responsible for the strong interaction between HOC and CNM [14, 20, 25]. However, since alkanes undergo only non-specifc van-der-Waals interactions, the influence of specific interactions can be excluded. Chen et al. investigated sorption of polar and non-polar organic compounds by CNM and found stronger sorption affinity of SWCNTs for aliphatic cyclohexane than for aromatic benzene [14]. It must be stressed that K_F values across different studies may only be comparable to some extent due to, among others, variation in reference points. However, these results emphasize the need for a more comprehensive investigation of sorption properties by CNM to quantitatively determine the contribution of individual interactions to overall sorption; e.g., by poly-parameter linear free-energy relationships. Very recently, such an approach was firstly published by Apul et al.; however the investigated probe compound set was limited to aromatic compounds [26]. The systematic investigation of a more comprehensive probe compound set, including also aliphatic compounds of various polarities, is currently underway in our laboratory and will be reported elsewhere.

The addition of reference HS material leads to comparable K_F values as the non-standardized material (see Table 4-2) with the exception of sorption of nHep, cHep, nOct, and cOct by MWCNT+WPHAR. These alkanes had sorption affinities similar to MWCNTs+10HA. This is interesting as overall all reference materials had similar properties regarding their elemental composition and carbon distribution (Table 4-1). A correlation between suppression of sorption affinity of alkanes by MWCNTs and properties of HS, such as aliphatic or aromatic carbon content cannot be observed for the data obtained here.

4.4.3 HS effect on sorption linearity

Non-linear sorption (n = 0.55-0.79) was observed for all sorbates by MWCNTs without NOM addition. This is generally consistent with recent investigations of sorption of non-ionic organic compounds [19, 24]. Commonly non-linear sorption by CNM is explained by a heterogeneous distribution of free-energy of sorption sites caused by e.g., surface defects or interstitial and groove areas of CNT aggregates [27]. Moreover, aggregation of CNTs may

lead to a heterogeneous distribution of sorption site energies [28]. The addition of 1 and 10 mg L^{-1} HA led to an increase in sorption linearity with Δn ranging between 0.08 and 0.19 for sorption of nHep and cOct, respectively. Previous studies reported similar results regarding the impact of NOM on sorption linearity of HOC by CNTs [5, 21]. However, an increase in sorption linearity has not been consistently reported in literature as in some studies no change in sorption linearity was observed following the addition of NOM [6, 20].

Furthermore, it must again be stressed at this point that comparisons of fitting parameters of non-linear sorption data across different studies have to be done with great caution for the following reasons: Firstly, they greatly depend on the investigated concentration range. This is in particular relevant for sorption linearity, which was previously shown for sorption of PAHs by MWCNTs, where sorption isotherms in the low concentration range were linear, while non-linear sorption was observed in higher concentration ranges [7]. Secondly, sorption of NOM by MWCNTs and furthermore their influence on sorption of co-sorbates by MWCNTs depends on surface properties of the sorbent [8].

The increase of sorption linearity in general suggests a more homogeneous distribution of available sorption sites. Endo et al. investigated sorption properties by carbonaceous materials. They found that for diesel soot commonly regarded as an adsorbing material sorption of *n*- and cyclooctane was linear [12]. In a further investigation they found that the extraction of extractable organic material from reference diesel soot material, sorption linearity significantly decreased to n = 0.75 and 0.85 for *n*- and cyclooctane, respectively [13]. The here observed decrease in sorption affinity (K_F) together with increasing sorption linearity (n) implies that strong sorption sites on MWCNTs surface are occupied by HS, which i) makes them no longer available for interaction and ii) results in a more homogeneous distribution of sorption site energies and thus more linear sorption. The latter could also result from a change of sorption mode to *ab*sorption of alkanes into HS-coated on MWCNTs surface, which will be discussed in the next section.

4.4.4 K_n/K_c ratios for sorption by MWCNT

K_n/K_c ratios for sorption of C6-C8 alkane pairs by MWCNTs under varying NOM addition conditions are given in Table 4-3. For sorption by MWCNTs, a K_n/K_c ratio for the C6-alkane pair of 2.01 was obtained. This is generally in accordance with previous reports for graphitized or activated carbons, where K_n/K_c values of 1.12 and 1.02 were reported for carbon nanotubes and carbon nanofibers, respectively [10]. From literature data for sorption of organic vapors by single-walled carbon nanotubes, a C6-K_n/K_c ratio of 1.08 can be calculated [29]. K_n/K_c values of C6 in Table 4-3 consistently decreased to 1.72 and 1.55 following 1 and 10 mg L^{-1} HA addition, respectively. Overall, a decrease in K_n/K_c ratios was observed for all alkane pairs following HS addition. However, K_n/K_c ratios of C6 and C7 alkane pairs for all sorbent scenarios remain larger than 1, which suggests *ad*sorption to be the dominant sorption mode regardless of HS addition.

Table 4-3: K_n/K_c ratios of C6-C8 alkane pairs for the investigated sorbents.

Sorbent	C6	C7	C8
MWCNT	2.01	1.73	0.96
MWCNT+1HA	1.72	1.43	0.84
MWCNT+10HA	1.55	1.17	0.72
MWCNT+LSHA	1.62	1.17	0.74
MWCNT+PPHAS	1.62	1.16	0.78
MWCNT+WPHAR	1.55	1.18	0.79

K_n/K_c ratios of the reference materials were similar to those obtained for non-certified material, suggesting that the effect of HS on sorption by MWCNTs is independent from the properties of HS. This implies that despite HS addition the dominant sorbent responsible for sorption remains MWCNTs. This is further supported by the fact that sorption of alkanes by HS was not found to be significant in pre-experiments (data not shown), which corresponds well with previous reports where sorption by HS was orders of magnitude lower than sorption by MWCNTs [7].

In order to further investigate a potential change in sorption mode following NOM addition, C8-K_n/K_c ratios were plotted against varying sorbate air-phase concentrations for all sorbents scenarios (see Figure 4-2). Sorption of *n*- and cyclooctane by MWCNTs shows K_n/K_c ~1 over the whole concentration range, which has also been observed for other rigid carbonaceous

materials, such as charcoal and activated carbon [12]. This suggests that adsorption is the dominant sorption mode regardless of sorbate concentration. However, the addition of HS in general led to a decrease in K_n/K_c with increasing sorbate concentration. This was similarly observed for carbonaceous geosorbents containing native organic matter, e.g., soot [12], for which in a further study sorption was explained by a combination of *ad*- and *ab*sorption [13]. However, it must be stressed at this point that this effect was far more pronounced than the here observed effect, where K_n/K_c ratios decreased from 1 to ~0.3 or lower for soils [12]. Thus the contribution of *ab*sorption by MWCNTs following HS addition does not seem to be of major importance.

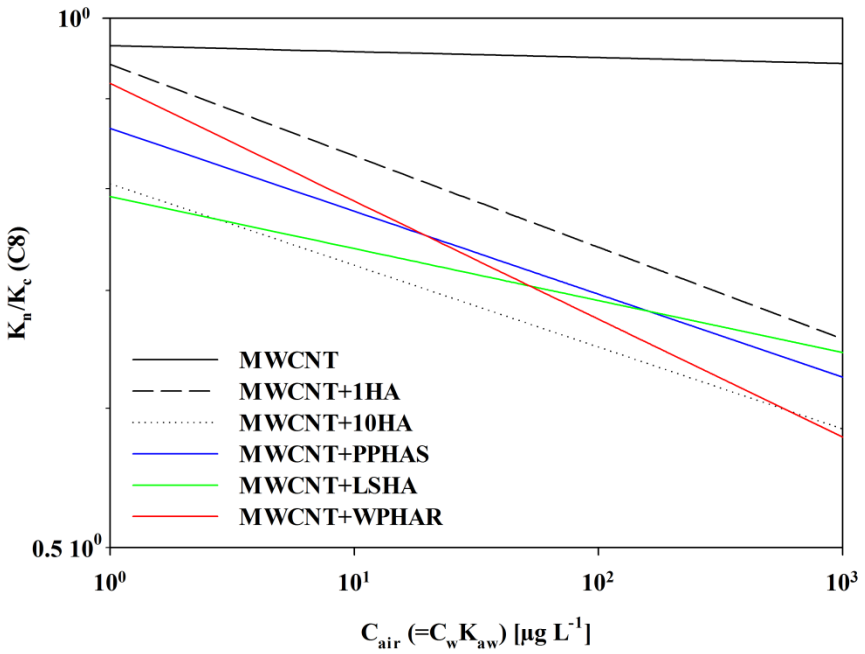

Figure 4-2: Plots of C8-K_n/K_c ratios against equilibrium air-phase concentration (C_{air}). Since sorption isotherms were conducted in sorbent-water system, C_{air} was calculated using air-water partitioning constants (K_{aw}).

In Table 4-3, a clear trend of decreasing K_n/K_c ratios with increasing number of sorbate carbon atoms can be seen. This has been observed previously but it has not led to contradicting results in terms of distinguishing the dominant sorption mode. However, the here observed changes are the highest observed so far for the K_n/K_c-concept. Despite the fact that the lowest K_n/K_c values were obtained for sorption of *n*- and cyclooctane by MWCNT+10HA, *ad*sorption can still be assumed to be the dominant sorption mode as K_n/K_c

of 0.72 is still above values obtained for typical *ab*sorbers, such as bulky liquids (e.g., C8-K_n/K_c of 0.23 for 1-octanol) or organic polymers (e.g., C8-K_n/K_c of 0.33 for polypropylene) [10].

Overall, the observed effects of HS addition on K_n/K_c were not as significant as in previous reports, where the removal of extractable organic matter from a standard reference material of diesel soot clearly resulted in a change in sorption mode from *ab*- to *ad*sorption [13]. In fact, K_n/K_c values for sorption of *n*- and cyclooctane by the untreated material ranged between 0.46-0.66, while sorption by the extracted material showed K_n/K_c values between 0.83 and 1.72. The here observed changes in K_n/K_c support the argument that sorption by HS-coated MWCNTs is still *ad*sorption by the nanotubes rather than *ab*sorption into the attached organic matter. HS is likely to interact with the strong sorption sites of MWCNTs [21]; therefore, these sites are subsequently blocked for sorbates. Such strong interaction sites are generally less available for bulky cycloalkanes compared to their linear homologous [12]. Thus, the influence of NOM addition is less pronounced for cycloalkanes, which results in a decrease in K_n/K_c.

Besides sorption onto the surface, pore-filling has been discussed as one of the major sorption mechanisms by CNM [4, 19, 27], which was especially relevant for low sorbate concentrations because of the high energetic sorption sites in the micropores of CNTs [6]. From this, the authors concluded that the observed decrease in sorption of HOC was a result of blocking of the micropores, whereas the strength of the blocking depended on the molecular size of HS. Meanwhile, it was suggested by Wang et al. that fractionation of HS components by MWCNTs occurs dependent on the molecular weight and composition of HS and on the porosity of MWCNTs [30]. Furthermore, it has previously been discussed that steric effects may have to be considered as the sorption capacity of PAHs by MWCNTs was, among others, negatively related to the sorbates' molecular size [31]. Commonly, the inner pores of nanotubes are not available for sorption [27], so any discussion on the impact of pore size on sorption is restricted to potential pores of CNT aggregates. Microporous materials may exhibit size exclusion effects as pores may not be available for sorbates that have larger sizes than the pore. This has led to C6-K_n/K_c ratios of up to 1500 for graphitized or activated carbons [10]. The volume of micro- and mesopores of MWCNTs applied in this study is given in Table A 4-1. Since K_n/K_c ratios for the here investigated sorbent scenarios were by

far smaller, the occurrence of size exclusion effects may be neglected. From this, we conclude that the addition of HS has the following impact on sorption behavior by MWCNTs: i) adsorption remains to be the dominant sorption mode regardless of HS addition, ii) size exclusion effects from pore blockage by HS may be neglected. This is further supported by the fact that C8-K_n/K_c ratios shown in Figure 4-2 remain constantly ~1. In contrast, K_n/K_c ratios decreased from >1 to ~1 with increasing sorbate concentration for lignite coke and activated carbon, where steric effects at low sorbate concentration were explained by higher availability of strong interaction sites for *n*- than for cyclooctane [12].

Nevertheless, it should be mentioned that for K_n/K_c values ~ 1 a clear conclusion of the dominant sorption mode may be difficult to draw, especially if sorbent mixtures are investigated. Thus, future projects may focus on an improvement of the K_n/K_c concept. Note that for sorption from aqueous phases in principle the cavity formation of vicinal water is necessary, which may result in thermodynamically an *ad*sorption mode. This could lead to inaccurate interpretation regarding the dominant sorption mode. However, this did not seem to be relevant here as for all alkane pairs K_n/K_c values were clearly greater than for typical *ab*sorbers.

4.5 References

1. Iijima, S. *Nature* **1991**, 354, 56-58.
2. Gottschalk, F.; Sonderer, T.; Scholz, R.W.; Nowack, B. *Environmental Science & Technology* **2009**, 43, 9216-9222.
3. Gottschalk, F.; Sun, T.; Nowack, B. *Environmental pollution* **2013**, 181, 287-300.
4. Hüffer, T.; Kah, M.; Hofmann, T.; Schmidt, T.C. *Environmental Science & Technology* **2013**, 47, 6935-6942.
5. Zhang, S.J.; Zhang, S.J.; Shao, T.; Karanfil, T. *Water Research* **2011**, 45, 1378-1386.
6. Wang, X.L.; Lu, J.L.; Xing, B.S. *Environmental Science & Technology* **2008**, 42, 3207-3212.
7. Zhang, X.; Kah, M.; Jonker, M.T.O.; Hofmann, T. *Environmental Science & Technology* **2012**, 46, 7166-7173.
8. Wang, X.L.; Tao, S.; Xing, B.S. *Environmental Science & Technology* **2009**, 43, 6214-6219.
9. Pan, P.; Zhang, D.; Li, H.; Wu, M.; Wang, Z.; Xing, B.S. *Environmental Science & Technology* **2013**, 47, 7722-7728.
10. Endo, S.; Grathwohl, P.; Schmidt, T.C. *Environmental Science & Technology* **2008**, 42, 3989-3995.
11. Goss, K.U. *Critical Reviews in Environmental Science and Technology* **2004**, 34, 339-389.
12. Endo, S.; Grathwohl, P.; Handerlein, S.B.; Schmidt, T.C. *Environmental Science & Technology* **2009**, 43, 393-400.
13. Endo, S.; Grathwohl, P.; Haderlein, S.B.; Schmidt, T. C. *Environmental Science & Technology* **2009**, 43, 3187-3193.
14. Chen, W.; Duan, L.; Zhu, D.Q. *Environmental Science & Technology* **2007**, 41, 8295-8300.
15. Gotovac, S.; Honda, H.; Hattori, Y.; Takahashi, K.; Kanoh, H.; Kaneko, K. *Nano Letters* **2007**, 7, 583-587.
16. Onjia, A.E.; Milonjic, S.K.; Rajakovic, L.V. *Journal of the Serbian Chemical Society* **2001**, 66, 259-271.
17. Smiciklas, I.D.; Milonjic, S.K.; Zec, S. *Journal of Materials Science* **2000**, 35, 2825-2828.
18. Dorofeeva, O.V.; Mastryukov, V.S.; Allinger, N.L.; Almenningen, A. *Journal of Physical Chemistry* **1985**, 89, 252-257.
19. Kah, M.; Zhang, X.; Jonker, M.T.O.; Hofmann, T. *Environmental Science & Technology* **2011**, 45, 6011-6017.
20. Chen, J.Y.; Chen, W.; Zhu, D. *Environmental Science & Technology* **2008**, 42, 7225-7230.
21. Sun, H.W.; Song, Q.; Luo, P.; Wu, W.L.; Wu, J.Z. *Environmental Science-Processes & Impacts* **2013**, 15, 307-314.
22. Gai, K.; Shi, B.; Yan, X.; Wang, D. *Environmental Science & Technology* **2011**, 45, 5959-5965.

23. Ji, L.L.; Chen, W.; Zheng, S.R.; Xu, Z.Y.; Zhu, D.Q. *Langmuir* **2009**, 25, 11608-11613.
24. Yang, K.; Wang, X.L.; Zhu, L.Z.; Xing, B.S. *Environmental Science & Technology* **2006**, 40, 5804-5810.
25. Pan, B.; Lin, D.H.; Mashayekhi, H.; Xing, B.S. *Environmental Science & Technology* **2008**, 42, 5480-5485.
26. Apul, O.G.; Wang, Q.; Shao, T.; Rieck, J.R.; Karanfil, T. *Environmental Science & Technology* **2013**, 47, 2295-2303.
27. Pan, B.; Xing, B.S. *Environmental Science & Technology* **2008**, 42, 9005-9013.
28. Zhang, S.; Shao, T.; Bekaroglu, S.S.K.; Karanfil, T. *Environmental Science & Technology* **2009**, 43, 5719-5725.
29. Agnihotri, S.; Rood, M.J.; Rostam-Abadi, M. *Carbon* **2005**, 43, 2379-2388.
30. Wang, X.; Shu, L.; Wang, Y.; Xu, B.; Bai, Y.; Tao, S.; Xing, B.S. *Environmental Science & Technology* **2011**, 45, 9276-9283.
31. Yang, K.; Zhu, L.Z.; Xing, B.S. *Environmental Science & Technology* **2006**, 40, 1855-1861.

4.6 Appendix A4

Table A 4-1: Properties of the multi-walled carbon nanotubes.

Property	Value	Unit	Method
C-Purity[a]	> 98	%	Elemental analysis[a]
Number of walls[b]	3-15	-	TEM[b]
Outer mean diameter[b]	13-26	nm	TEM[b]
Inner diameter distribution[b]	2-6	nm	TEM
Length[b]	>1	µm	SEM
Bulk density[b]	140-230	kg m^{-3}	EN ISO 60
BET surface area[a]	211	m^2 g^{-1}	BET
Total pore volume[a]	1.05	mL g^{-1}	BET
V_{micro}[a]	0.0425	mL g^{-1}	BET
V_{meso}[a]	0.706	mL g^{-1}	BET

[a]own data; [b] data given by supplier.

Table A 4-2: Alkane sorbates and their physico-chemical properties.

Sorbate	MW [g mol^{-1}]	ρ [g mL^{-1}]	MV [cm^3 mol^{-1}]	S_w [mg L^{-1}]	Log K_{ow}	Log K_{aw}	L
n-Hexane (nHex)	86.18	0.66	95.40	9.50	3.90	1.73	2.67
n-Heptane (nHep)	100.21	0.68	109.49	2.88	4.66	1.84	3.17
n-Octane (nOct)	114.23	0.70	123.58	0.66	5.18	1.95	3.68
c-Hexane (cHex)	84.16	0.78	84.54	55	3.44	0.78	2.96
c-Heptane (cHep)	98.19	0.81	98.63	30	4.00	0.63	3.70
c-Octane (cOct)	112.22	0.83	112.70	7.90	4.45	0.51	4.33

MW: molecular weight; ρ: density; MV: molar volume from [1]; S_w: aqueous solubility obtained from [2]; K_{ow}: octanol-water partitioning constant from Schwarzenbach [3]; K_{aw}: air-water partitioning constant (20 °C) from [4]; L: hexadecane-water partitioning constant from [5].

Table A 4-3: Fitting parameters ± standard errors, R^2, standard error of estimates (SE) for Freundlich model fitting the isotherms of C6-C8 alkanes pairs by MWCNTs following HS addition (N: number of data points).

		MWCNTs			
Sorbate	**K_F**	**n**	**R^2**	**SE**	**N**
nHex	1.69E+05 ± 4.48E+03	0.71 ± 0.02	0.9951	0.09	11
cHex	1.77E+04 ± 9.14E+02	0.73 ± 0.02	0.9720	0.15	10
nHep	5.03E+05 ± 2.65E+04	0.66 ± 0.03	0.9828	0.17	11
cHep	4.57E+04 ± 2.89E+03	0.68 ± 0.02	0.9922	0.12	10
nOct	9.20E+05 ± 2.11E+04	0.55 ± 0.02	0.9914	0.08	12
cOct	1.57E+05 ± 7.21E+03	0.55 ± 0.01	0.9941	0.08	14
		MWCNTs + 1HA			
Sorbate	**K_F**	**n**	**R^2**	**SE**	**N**
nHex	1.08E+05 ± 6.17E+03	0.79 ± 0.03	0.9508	0.20	15
cHex	1.09E+04 ± 5.53E+02	0.83 ± 0.02	0.9732	0.17	13
nHep	2.38E+05 ± 8.30E+03	0.73 ± 0.02	0.9793	0.13	15
cHep	2.07E+04 ± 1.50E+03	0.78 ± 0.03	0.9734	0.15	12
nOct	5.34E+05 ± 1.72E+04	0.66 ± 0.02	0.9908	0.12	14
cOct	6.71E+04 ± 4.86E+03	0.71 ± 0.03	0.9688	0.16	14
		MWCNTs + 10HA			
Sorbate	**K_F**	**n**	**R^2**	**SE**	**N**
nHex	5.39E+04 ± 1.60E+03	0.86 ± 0.01	0.9969	0.11	13
cHex	5.26E+03 ± 1.97E+02	0.89 ± 0.01	0.9979	0.11	12
nHep	8.98E+04 ± 3.28E+03	0.72 ± 0.02	0.9794	0.14	15
cHep	9.78E+03 ± 7.44E+02	0.79 ± 0.03	0.9783	0.17	11
nOct	1.96E+05 ± 6.94E+03	0.71 ± 0.02	0.9835	0.12	13
cOct	2.45E+04 ± 1.69E+03	0.74 ± 0.02	0.9888	0.17	14
		MWCNTs + LSHA			
Sorbate	**K_F**	**n**	**R^2**	**SE**	**N**
nHex	5.01E+04 ± 2.70E+03	0.83 ± 0.02	0.9914	0.17	15
cHex	4.94E+03 ± 5.85E+02	0.86 ± 0.04	0.9513	0.23	14
nHep	1.69E+05 ± 8.43E+03	0.69 ± 0.03	0.9741	0.15	13
cHep	2.03E+04 ± 1.24E+03	0.72 ± 0.01	0.9861	0.11	14
nOct	4.04E+05 ± 1.61E+04	0.71 ± 0.02	0.9841	0.10	14
cOct	4.98E+04 ± 3.87E+03	0.74 ± 0.02	0.9813	0.13	14

MWCNTs + PPHAS					
Sorbate	**K_F**	**n**	**R^2**	**SE**	**N**
nHex	7.78E+04 ± 7.35E+03	0.82 ± 0.03	0.9533	0.22	14
cHex	7.88E+03 ± 5.33E+02	0.85 ± 0.02	0.9698	0.19	15
nHep	1.89E+05 ± 5.31E+03	0.67 ± 0.02	0.9812	0.10	15
cHep	2.41E+04 ± 1.62E+03	0.73 ± 0.03	0.9728	0.15	12
nOct	5.37E+05 ± 2.79E+04	0.70 ± 0.02	0.9628	0.16	12
cOct	6.50E+04 ± 4.37E+03	0.74 ± 0.03	0.9692	0.16	12
MWCNTs + WPHAR					
Sorbate	**K_F**	**n**	**R^2**	**SE**	**N**
nHex	5.24E+04 ± 2.88E+03	0.84 ± 0.02	0.9847	0.13	13
cHex	5.34E+03 ± 3.35E+02	0.87 ± 0.03	0.9716	0.17	13
nHep	9.67E+04 ± 2.87E+03	0.66 ± 0.01	0.9912	0.10	14
cHep	1.22E+04 ± 8.20E+02	0.72 ± 0.02	0.9798	0.16	11
nOct	2.09E+05 ± 5.51E+03	0.68 ± 0.01	0.9965	0.08	12
cOct	2.60E+04 ± 9.55E+02	0.74 ± 0.01	0.9968	0.07	13

References for Appendix A4

1. Abraham, M.H.; McGowan, J.C. *Chromatographia* **1987***,* 23, 243-246.
2. Corporation, S. R. Interactive PhysProp Database Demo. http://www.syrres.com/esc/physdemo.htm Last accessed Feb., 2013.
3. Schwarzenbach, R.P.; Gschwend, P.M.; Imboden, D.M. *Environmental Organic Chemistry;* John Wiley and Sons: Hoboken, NJ, U.S.A., 2003.
4. Endo, S.; Grathwohl, P.; Schmidt, T.C. *Environmental Science & Technology* **2008**, 42, 3989-3995.
5. Abraham, M.H.; Ibrahim, A.; Acree, W.E.Jr. *Fluid Phase Equilibria* **2007**, 251, 93-109.

Chapter 5 Characterization of sorption properties of MWCNTs using poly-parameter linear free-energy relationships

5.1 Abstract

Sorption of organic compounds by carbon-based nanomaterials has been discussed to influence the mobility of contaminants in the environment. Thus, the accurate prediction of distribution coefficients is of major importance for the understanding of environmental processes and a risk assessment of the impact of released carbon-based nanomaterials. Poly-parameter linear free-energy relationships (ppLFER) have previously been shown to offer such an accurate prediction of sorption processes. The aim of this study was to indentify and quantify the contribution of individual molecular interactions to overall sorption by multi-walled carbon nanotubes (MWCNTs). To this end, sorption isotherms of 16 aliphatic and 12 aromatic compounds covering various relevant molecular interactions by MWCNTs were experimentally determined. This extends previous reports on ppLFER development to sorption of aliphatic compounds by MWCNTs, which have not yet been included. Thereby, a large sorption data set for diverse compounds covering wide concentration ranges was provided. The correlation of measured distribution coefficients to those derived by ppLFER equations were clearly better compared to commonly correlated hydrophobicity parameters. It could be shown that non-specific interactions represented by molar volume (V) were the most important for sorption by MWCNTs, whereas the sorbates polarity/polarizability (S) was shown to influence sorption linearity by MWCNTs .

5.2 Introduction

In recent years, research on the environmental behavior of carbon-based nanomaterials (CNM) has received growing attention, while, among others, the impact of CNM on the fate and transport of organic contaminants has been in the focus of researchers. In general, CNM are characterized by strong interactions with organic compounds [1]; however, the influences of molecular structure on overall sorption are yet poorly understood. For example, specific electron donor-acceptor interactions have been discussed to be responsible for the strong interaction [2-4], while sorption of cyclohexane, which can only undergo non-specific interactions, was found to be stronger than of aromatic benzene [4]. These contradictory observations emphasize the need for a more comprehensive approach to investigate sorption by CNM.

Furthermore, in contrast to the so far available reports on sorption of organic compounds by CNM, which deal mainly with the analysis of an single type of intermolecular interaction, there have been only very few attempts for the quantitative and qualitative determination of the contribution of multiple types of interactions to overall sorption by CNM [5, 6]. However, such an approach would be required for *a priori* prediction of sorption of organic compounds by CNM. Poly-parameter linear free-energy relationships (ppLFER) present such a promising approach as they offer the opportunity to take all relevant molecular interactions that influence distribution into account in a single equation. Thus, they have much more predictive power than commonly used one-parameter LFER (opLFER) based, e.g., on the octanol-water partitioning constant (K_{ow}) [7]. Abraham's ppLFER equation consists of terms describing the individual contribution of molecular interactions for both the properties of the sorbate (solute descriptors) and the sorbent (phase descriptors) [8, 9], which is given by:

$$\log K_{i,a/b} = e_{12}E_i + s_{12}S_i + a_{12}A_i + b_{12}B_i + v_{12}V_i + c_{12} \qquad \text{(Eq. 5-1)}$$

where $\log K_{i,a/b}$ represents the logarithmic distribution coefficient of a given sorbate i between phases a and b. The uppercase letters denote the solute descriptors representing the individual types of interactions: E, the excess molar refraction; S, the dipolarity/polarizability; A, the solute hydrogen (H)-bond acidity; B, the solute H-bond basicity; and V, the molar volume. The corresponding lowercase letters denote the phase descriptors and are derived by multiple

regression analysis (MRA), whereas c denotes the regression constant. E and V are descriptors representing non-specific interactions, such as the cavity formation energy and dispersive van-der-Waals interactions. The experimental determination of solute descriptors has been the subject of many studies [9]; thus, they have been tabulated for a large number of compounds with very good accuracy. Sorption mechanisms have successfully been determined by ppLFER, for example, for the distribution of non-ionic organic compounds from the gas phase to snow [10], from the aqueous phase to activated carbon [11], to solid-phase microextraction fibers [12], and to natural organic matter in soils and sediment [13, 14].

Most recently, Apul et al. developed a ppLFER model for the prediction of sorption of aromatic compounds by multi-walled carbon nanotubes (MWCNTs) [5]. However, their presented ppLFER equation has certain drawbacks. Firstly, only aromatic compounds have been used for the model development. This may lead to inaccurate description of sorption properties of MWCNTs resulting from the use of a biased probe sorbate set that does not include aliphatic compounds. Secondly, the ppLFER equation did not contain the term for excess molar refraction, which accounts for the contribution of non-specific interactions [15]; however, a comprehensive discussion of the relevant type of interaction may not be possible without taking all descriptors into account. Finally, for some of the probe compounds used for the ppLFER, only a single-point distribution coefficient was obtained from literature data, which may have to be considered with caution as the energy of sorption sites available on CNM is heterogeneously distributed and thus sorption is a non-linear process [1]. As a consequence, there is still improvement necessary for a comprehensive development of ppLFER for sorption by MWCNTs.

Thus, the aim of the here presented study was to derive a ppLFER for sorption by MWCNTs in order to investigate the contribution of individual intermolecular interactions to overall sorption and, furthermore, to characterize the sorption properties of MWCNTs. For ppLFER modeling, a probe set of 30 compounds was selected including aliphatic and aromatic compounds featuring various functionalities.

5.3 Experimental Section

5.3.1 Materials

MWCNTs (C150HP) were purchased from Bayer Material Science (Leverkusen, Germany). Properties of MWCNTs are given in Table A 4-1 in the appendix of Chapter 4. Amorphous carbon was removed by heating the MWCNTs to 350 °C for 1 h [4]. 30 sorbates were selected based on previous publications [13, 16] covering a broad range of various substance classes including the following: apolar aliphatics (alkanes), monopolar aliphatics (ethers and halogenated alkenes), bipolar aliphatics (alcohols), non-polar aromatics (polycyclic aromatic hydrocarbons), monopolar aromatics (e.g., anisole), and bipolar aromatics (phenols). The used probe compound set did not cover very large hydrophobic compounds or multifunctional polar compound (e.g., pesticides or polyfluorinated chemicals). The sorption isotherm data for phenanthrene and pyrene were not determined experimentally but taken from literature [17], where sorption experiments were performed with the same kind of sorbent with comparable experimental conditions. The basic physico-chemical properties of sorbates and their ppLFER descriptors are given in Table A 5-1 and Table 5-1, respectively. Stock solutions of sorbates were prepared weekly in methanol by dissolving the pure compound and kept at 4 °C in the dark.

5.3.2 Sorption batch experiments

2-5 mg of MWCNTs were weighted into 20-mL amber headspace screw vials. 10-20 mL of 10 mM $CaCl_2$ as background solution were added into the vials, which were then closed with screw caps with butyl/PTFE-lined septa. After the vials were shaken for 24 h to wet the sorbent, samples were spiked with methanolic sorbate standard solutions resulting in concentrations ranging over 3-4 orders of magnitude. The amount of sorbent was adjusted to achieve 30-90% of sorbate sorbed at equilibrium. The methanol content did not exceed 0.25% (v/v) in water to minimize co-solvent effects. Duplicate measurements were performed for each sorbate and each concentration. Samples were shaken for equilibration at 25 °C in a temperature-controlled room for no longer than 5 days. Equilibration times of probe sorbates were pre-determined. Subsequently, the vials were removed from the shaker and the sorbate concentration in the aqueous phase was determined.

For volatile sorbates (indicated with HS in Table A 5-1), batch sorption experiments were conducted in a three-phase system (gaseous, liquid, and solid), where vials contained 10-15 mL of the background solution. Note that a clear discrimination based on log K_{aw} was not feasible; however, sorbates analyzed by this method had a log K_{aw} of -1.54. After equilibration, vials were placed in the tray of the autosampler at least two hours prior to analysis in order to reach equilibrium between liquid and gaseous phase. Concentrations of sorbates in the gas phase were then determined by direct injection of 1000 µL of the vials headspace into GC-MS by the autosampler using an external calibration for quantification. After each measurement, the syringe was flushed with nitrogen for 4 min for cleaning.

For less volatile sorbates (indicated with ITEX2 in Table A 5-1, sorbates with log $K_{aw} \leq$ -0.80), vials contained 20 mL of the background solution leaving minimal headspace. After equilibration, samples were centrifuged at 2500 rpm for 20 min. Subsequently, 10 mL of the supernatant were transferred to clean vials and the headspace concentration of analytes in the samples was analyzed after 2 h air-water equilibration using in-tube microextraction (ITEX2). The ITEX2 option for the CombiPal autosampler was received from CTC Analytics (Zwingen, Switzerland) and consisted of a heated syringe holder, a trap heater, a 1.3 mL Hamilton syringe with side port (Hamilton, Bonaduz, Switzerland), and a single magnet mixer (SMM, Chromtech, Idstein, Germany). Tenax GR (BGB Analytik AG, Schlossboeckelheim, Germany) was used as trap material. The ITEX2 extraction procedure was generally adapted from Laaks et al. [18]. For extraction, samples were transferred to the SMM, where the samples were heated to 40-70 °C and stirred at 500 rpm for 10 min. 30-50 extraction strokes with an aspiration and dispensing volume of 1 mL at a flow of 50 µL s^{-1} were performed. The temperatures of the trap and the syringe were 40 and 70 °C, respectively, to avoid condensation of water in the syringe. After the extraction, 500 µL helium were aspirated as desorption gas from the injector. The trap was then heated for desorption to 280-300 °C and the aspired desorption gas was injected into the GC injector at 50 µL s^{-1}. To avoid cross contamination, the trap was heated to 330 °C for 10 min and flushed with nitrogen at 5 mL min^{-1} after injection.

For all samples, quantification was achieved using an external calibration. 12-16 calibration standards were prepared in 10 mL background solution one day prior to analysis. All analyses were conducted using a Trace GC Ultra (Thermo Electron Corporation, Austin (Texas), USA)

coupled to a DSQ single quadrupole mass spectrometer (Thermo Electron Corporation, Austin (Texas), USA) equipped with a split/splitless injector (SSL) and a CombiPAL autosampler (CTC Analytics, Zwingen, Switzerland). An HP-5 capillary column (30 m x 0.32 mm x 0.25 µm, J&W Scientific) and isothermal oven temperatures between 70 and 150 °C were used depending on the analyte retention. Helium was used as carrier gas at a flow of 1.5 mL min^{-1}.

The temperature of the SSL was set to 200-250 °C. The temperatures of the transfer line and the ion source of the mass spectrometer were set to 250 and 220 °C, respectively. The mass spectrometer was operated in electron ionization mode with ionization energy of 70 eV. Quantification of analytes was done in scan-mode.

5.3.3 Data analysis

The sorbed concentrations by MWCNTs were calculated by mass balance. Loss of analytes during the experimental procedure was monitored by preparing spiked samples without sorbent. The loss of analytes was incorporated in the calculations.

The calculated sorbed concentration and the aqueous concentration were log-converted, plotted, and then fitted to the log-converted Freundlich model equation:

$$\log C_s = n \log C_w + K_F \qquad \text{(Eq. 5-2)}$$

where, C_s [µg kg^{-1}] and C_w [µg L^{-1}] denote the sorbed sorbate and the aqueous concentrations, respectively, and K_F [[(µg kg^{-1})/(µg L^{-1})]$^{1/n}$]and n [-] are the Freundlich coefficient and exponent, respectively. Model fits were performed with Sigma Plot 12.0 for Windows. The distribution coefficient K_d [L kg^{-1}] was then calculated at concentrations of 10^{-2} and 10^{-5} of the sorbates aqueous solubility:

$$K_d = C_s / C_w = K_F C_w^{n-1} \qquad \text{(Eq. 5-3)}$$

For ppLFER development, the calculated K_d values were then regressed against corresponding solute descriptors according to equation 5-1. Solute descriptors used for MRA are summarized in Table 5-1. MRA was performed with Microsoft Excel 2010.

Table 5-1: Solute descriptors of probe compounds used for ppLFER development.

	E	S	A	B	V	L	Ref.
alkanes							
n-Hexane	0.000	0.00	0.00	0.00	0.954	2.688	[19]
n-Octane	0.000	0.00	0.00	0.00	1.095	3.173	[19]
Cyclohexane	0.305	0.10	0.00	0.00	0.845	2.964	[19]
Cyclooctane	0.413	0.10	0.00	0.00	1.127	4.329	[20]
Isohexane	0.000	0.00	0.00	0.00	0.954	2.503	[19]
halo-aliphatics							
Tetrachloromethane	0.458	0.38	0.00	0.00	0.739	2.823	[19]
Trichloroethylene	0.524	0.37	0.08	0.03	0.715	2.997	[19]
Tetrachloroethylene	0.639	0.44	0.00	0.00	0.837	3.584	[19]
monopolar aliphatics							
Di-*n*-propyl ether	0.008	0.22	0.00	0.45	1.013	2.803	[19]
Di-*n*-butyl ether	-0.008	0.24	0.00	0.45	1.295	3.324	[19]
Methyl tert-butyl ether	0.024	0.28	0.00	0.54	0.872	2.270	[21]
2-Octanone	0.108	0.68	0.00	0.51	1.252	4.257	[19]
bipolar aliphatics							
1-Octanol	0.199	0.42	0.37	0.48	1.295	4.619	[19]
2,6-Dimethyl-2-heptanol	0.131	0.27	0.31	0.60	1.435	4.469	[16]
4-Methyl-4-nonanol	0.167	0.30	0.31	0.60	1.576	5.219	[16]
3-Ethyl-3-hexanol	0.203	0.30	0.31	0.60	1.295	4.189	[16]
nonpolar aromatics							
Benzene	0.610	0.52	0.00	0.14	0.716	2.786	[19]
n-Propylbenzene	0.604	0.50	0.00	0.15	1.139	4.230	[19]
Chlorobenzene	0.718	0.65	0.00	0.07	0.839	4.230	[19]
1,2-Dichlorobenzene	0.872	0.78	0.00	0.04	0.961	4.518	[19]
Naphthalene	1.340	0.92	0.00	0.20	1.085	5.161	[19]
Phenanthrene	2.055	1.29	0.00	0.26	1.454	7.632	[19]
Pyrene	2.808	1.71	0.00	0.29	1.585	8.833	[19]
Benzofurane	0.888	0.83	0.00	0.15	0.905	4.355	[22, 23]
monopolar aromatics							
Anisole	0.708	0.74	0.00	0.29	0.916	3.890	[19]
Ethylbenzoate	0.689	0.85	0.00	0.46	1.214	5.075	[19]
4-Nitrotoluene	0.870	1.11	0.00	0.28	1.032	5.154	[22, 23]
bipolar aromatics							
4-Ethylphenol	0.800	0.90	0.55	0.36	1.057	4.737	[19]
2-Chlorophenol	0.853	0.88	0.32	0.31	0.898	4.178	[19]
Indole	1.200	1.12	0.44	0.22	0.946	5.505	[22, 23]

5.4 Results and Discussion

5.4.1 Sorption isotherms

The measured isotherms of the probe compounds are shown in Figure 5-1, whereas the results of Freundlich model fits and calculated log K_d values are shown Table A 5-2. Most of the sorbate isotherms were well fit with the Freundlich Model ($R^2 > 0.97$). However, the goodness of fit for sorption of TeCM, 2OCT, 4M4H, pBenz, and ANIS was lower, where R^2 ranged between 0.93 and 0.97. For these compounds, a sensitivity analysis of the influence of differences in obtained Freundlich parameters on the calculation of logarithmic distribution coefficients (log K_d) and consequently on ppLFER development was evaluate. An error of 0.1 log-units for K_F and 0.03 for n did not significantly result in changes in phase descriptor obtained by ppLFER (data not shown). From the isotherm data fit, it can be observed that with some exceptions sorption linearity of aliphatic compounds tends to higher, while sorption of aromatic compounds seems to be more non-linear. Furthermore, the sorption isotherms of n-Oct, MTBE, and TeCM were almost linear (n = 0.9-1), which was not observed for other sorbates within the same compound class. Thus, experimental data of these compounds for the following discussion is included with caution as the observed irregularities may be a result of experimental error despite the fact that all sorption experiments were performed at least twice. Overall, a large consistent data set for sorption of diverse compounds by MWNCTs covering wide sorbate concentration ranges is provided.

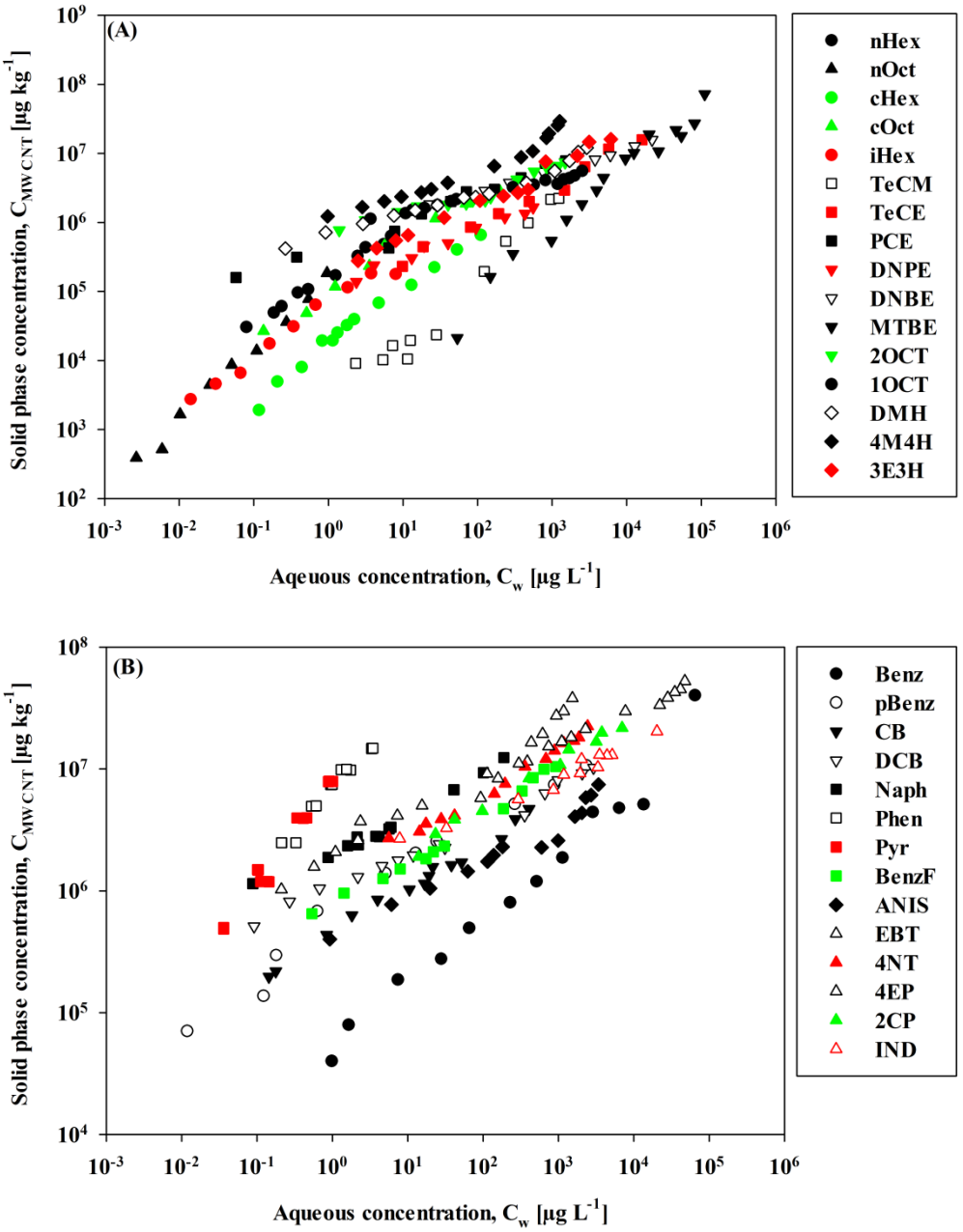

Figure 5-1: Sorption isotherms of aliphatic (A) and aromatic (B) probe compounds by MWCNTs. Sorbate abbreviations are given in Table A 5-1.

5.4.2 Development of the ppLFER

The calculated log K_d values for sorption of all sorbates by MWCNTs at concentrations of 10^{-2} and 10^{-5} of the sorbates aqueous solubility (S_w) were fitted to equation 5-1. The calculated and measured log K_d values for both concentration levels are compared in Figure 5-2. For 26 out of 30 probe sorbates at the higher concentration, the deviation between calculated and experimentally measured log K_d was below 0.3 log-unit, which shows the good fitting of the ppLFER model. However, at the lower concentration level, only 20 out of 30 compounds were below the 0.3 log-unit deviation range. Interestingly, the outliers cannot be assigned to a certain compound class. Overall, the increasing differences in fitting quality may be assigned to heterogeneous sorption by MWCNTs as sorption linearity of some probe sorbates were higher than that of the rest of the probe sorbate set (e.g., nOct and MTBE). Since at high concentration levels all high-energy sorption sites are already occupied by sorbates, the contribution of heterogeneity is less significant [16].

Most commonly, distribution coefficients are correlated in opLFER with solubility or hydrophobicity parameters of sorbates, such as the octanol-water partitioning constant (K_{ow}) [24]. However, such correlations have to be considered with caution since for example K_{ow} refers to *ab*sorption between two bulk phases, whereas sorption by MWCNTs was shown to be an *ad*sorption process (Chapter 4). In addition, it has previously been discussed that the prediction of sorption of organic compounds by various sorbents may not be accurate by K_{ow} [1, 4], especially at environmentally relevant low concentrations [16]. To emphasize the advantage of ppLFER for an accurate prediction of sorption, calculated distribution coefficients at both concentration levels were correlated to log K_{ow}. As can be seen in Figure 5-3, the correlation with log K_{ow} was by far worse with $R^2 = 0.73$ at 10^{-2} S_w and 0.46 at 10^{-5} S_w. Especially in the low concentration range, which represents environmentally relevant concentrations, the ability of ppLFER to predict sorption coefficients clearly exceeds that of K_{ow} correlation. In order to ensure that the increased goodness of sorption prediction by ppLFER is not a result of the higher degrees of freedom, AIC was calculated for opLFER and ppLFER at high and at low concentration levels (for details of AIC calculation see appendix of Chapter 3). AIC values were -142.00 and -123.52 for ppLFER and -123.07 and -106.75 for opLFER at high and at low concentration, respectively. Therefore, it can be concluded that the improved prediction of sorption with ppLFER is not due to overparameterization. From

the derived linear regression shown in Figure 5-3, it is apparent that K_{ow} underestimated measured K_d values by one order of magnitude at high concentration, while this discrepancy increases to almost three orders of magnitude at low concentrations. Kah et al. established a log K_d-log K_{ow} correlation for sorption of 13 PAHs by the same kind of MWCNTs used in this study and obtained a fairly well linear regression ($R^2 = 0.90$) with a slope of 0.36 and y-intercept of 5.72 [17]. The slopes of the here obtained log K_d-log K_{ow} correlations are clearly higher and closer to 1, and are well comparable to the relationships derived by Xia et al. for sorption of aromatic compounds covering various polarities [6]. As previously pointed out by Endo et al., care must be taken when extrapolating from the commonly stated class-specific agreement of K_{ow} correlation to class-comprehensive conclusions since a clear distinction between interaction properties requires quantitative indicators [16]. It must be stressed at this point that a consistent correlation of K_d values to K_{ow} is further complicated by the fact that K_{ow} values reported in literature vary to some extent. Overall, the comparison between opLFER with K_{ow} and ppLFER emphasizes the advantage of ppLFER for a comprehensive discussion of sorption properties.

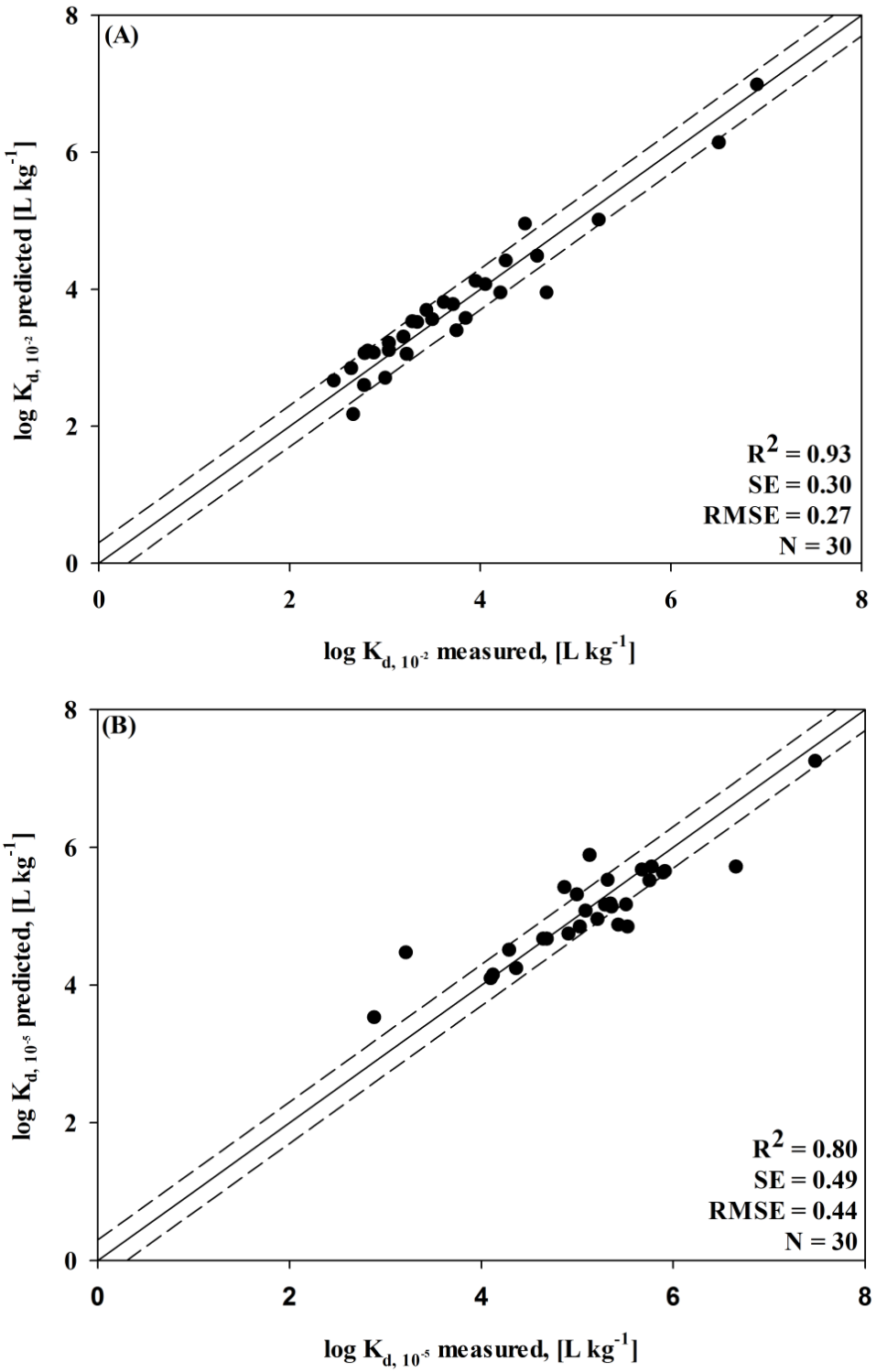

Figure 5-2: Comparison between predicted and measured log K_d values for sorption by MWCNTs at 10^{-2} (A) and 10^{-5} (B) of sorbates aqueous solubility. Solid lines represent 1:1 fits, and dashed lines indicate 0.3 log-unit deviations from measured values. R^2: regression coefficient; SE: standard error of estimates; RMSE: root mean squared error; N: number of data points.

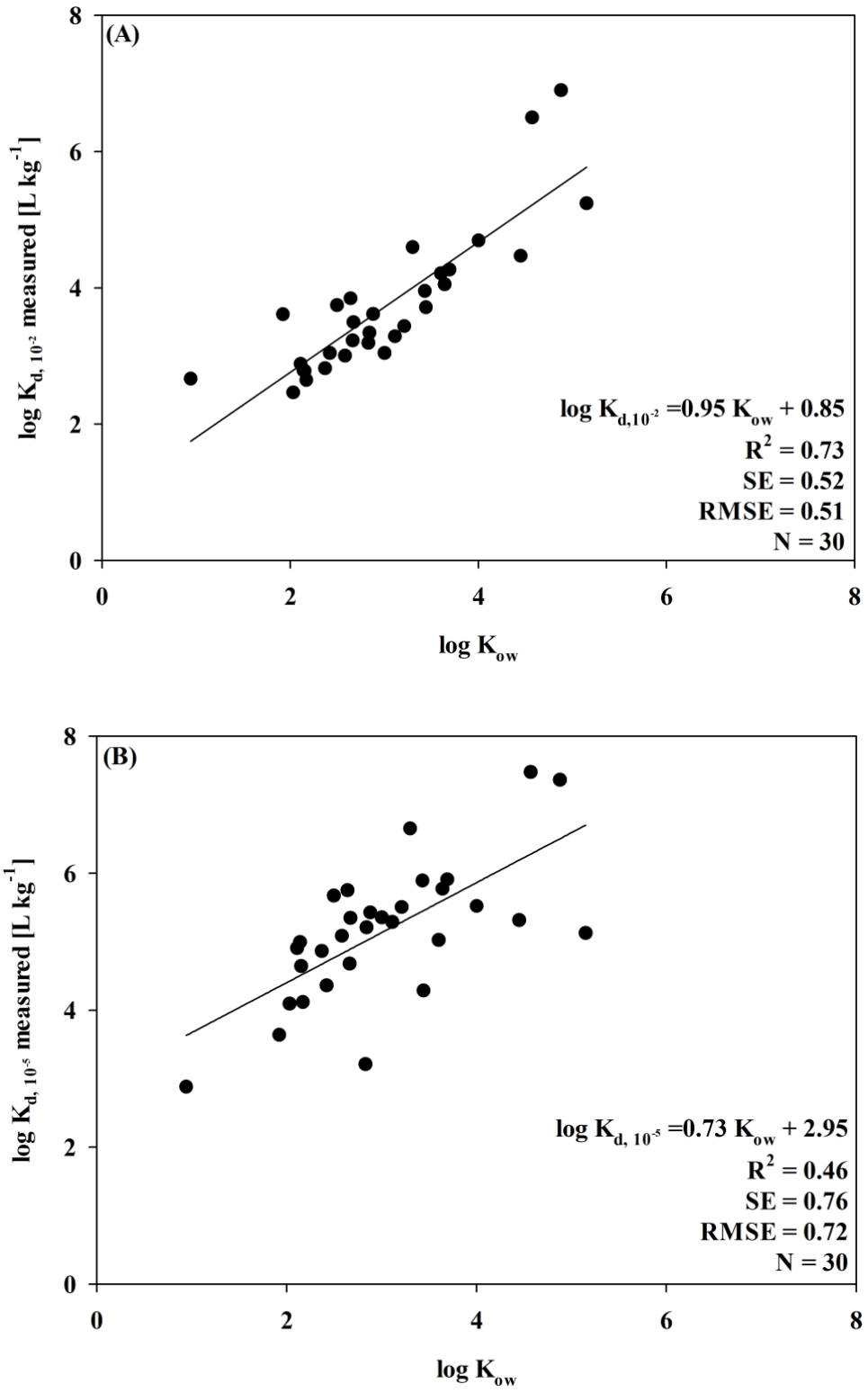

Figure 5-3: Correlations between experimentally determined log K_d values at 10^{-2} (A) 10^{-5} S_w (B) and log K_{ow}. R^2: regression coefficient; SE: standard error of estimates; RMSE: root mean squared error; N: number of data points.

The ppLFER phase descriptors for MWCNTs obtained from MRA are shown in Table 5-2. Statistical details of the regression analyses are given in Table A 5-3 to Table A 5-6. Recently, ppLFER models were derived for sorption of aromatic compounds by MWCNTs [5, 6]. As can be seen from Table 5-2, the v phase descriptor was the highest positive descriptor with v = 3.77 and 3.69 for high and low concentration levels, respectively. This is qualitatively in agreement with previously publications [5, 6], for which obtained phase descriptors are also shown in Table 5-2. However, the here obtained values for v are lower than in previous reports, which may be assigned to different ranges of v values of the probe sorbates. In order to ensure comparability of the here developed ppLFER with previous reports, the ranges of solute descriptors used for ppLFER development are compared in Figure A 5-1. Note that e values for the probe compound set used by Apul et al. were collected from literature as the authors did not take the eE-term into account, which is further discussed below. In both reports it was concluded that hydrophobicity and non-specific interactions significantly contribute to sorption by MWCNTs [5, 6]. However, the eE-term represents the excess molar refraction, which also includes non-specific interactions involving induction of dipoles within the solute [9, 25]. A comprehensive discussion of the contribution of individual interactions may be difficult without taking all descriptors into account.

Table 5-2: ppLFER for sorption by MWCNTs at two concentrations developed in the present study and obtained from previous reports.

	e	s	a	b	v	c	R^2	N
$\log K_{d,10^{-2}}$	+1.06	-0.85	-1.19	-2.96	+3.77	0.36	0.93	30
SE	0.30	0.42	0.39	0.51	0.36	0.33		
$\log K_{d,10^{-2}}$ (Apul et al.)[a]	-	+0.67	-1.31	-2.86	+4.41	-3.81	0.85	20
SE		0.47	0.56	1.22	0.70	0.78		
$\log K_{d,10^{-5}}$	-0.24	+1.39	-0.34	-2.83	+3.69	1.33	0.80	30
SE	0.48	0.68	0.63	0.82	0.58	0.53		
$\log K_{d,10^{\infty}}$ (Apul et al.)[a]	-	+0.61	+0.05	-0.48	+4.55	-4.34	0.83	29
SE		0.34	0.32	0.86	0.56	0.56		
$\log K_d$ (Xia et al.)[b]	0.04	+1.75	-0.37	-2.78	+4.18	-1.33	0.93	28

[a]taken from Ref [5]. Note that $K_{d,10}^{\infty}$ refers to *infinite dilution* conditions at an average of 0.2% of the sorbate aqueous solubility. [b]taken from Ref [6]. K_d values were determined at an average of 10^{-4} of the sorbates aqueous solubility. SE: standard errors of coefficients; R2: regression coefficient; N: number of compounds.

The contribution of non-specific interactions ($\Delta\log K_{non\text{-}specific}$) to overall sorption in this study was calculated as:

$$\Delta \log K_{non-specific} = \log K_d - c - aA - bB - sS \qquad \text{(Eq. 5-4)}$$

$\Delta\log K_{non\text{-}specific}$ was then correlated with V and E descriptors of sorbates. It must be stressed that a clear discrimination of interactions based on the ppLFER descriptors is not necessarily straight forward as cross effects may have to be considered. For example, the sS-term, representing dipolarity/polarizability, may include cross effects of eE, even though this effect was shown to be small [26]. In this study, no significant correlation was observed when plotting $\Delta\log K_{non\text{-}specific}$ vs. E (not shown), whereas a clear relationship was found between $\Delta\log K_{non\text{-}specific}$ and V (Figure 5-4). As can be seen the quality of linear regression decreased from 0.70 to 0.78 from high to low concentration; however, at both concentration the correlation of $\Delta\log K_{non\text{-}specific}$ and V was highly significant ($p < 0.0001$). This substantiates that non-specific interactions by MWCNTs are of major importance.

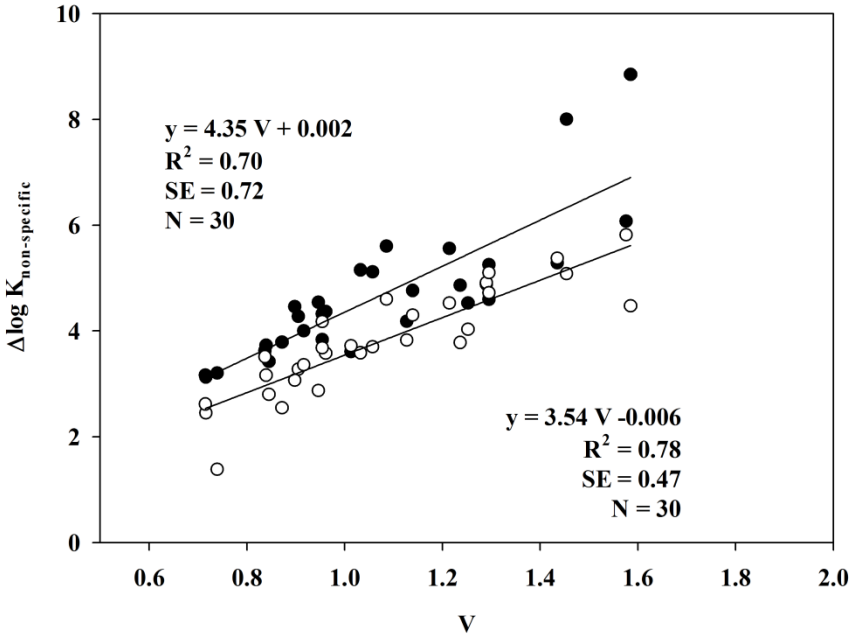

Figure 5-4: Contributions of non-specific interaction vs the molar volume (V) at 10^{-2} (●) and 10^{-5} (○) S_w concentration levels.

From Table 5-2, it can be seen that the b phase descriptor for MWCNTs changed only slightly for the investigated concentration range. Furthermore, a negative correlation of b with sorption of the probe sorbates from water by MWCNTs indicates that the H-bond donating capability of MWCNT to the probe compounds is lower than that of water [6], which is generally plausible since there are no potential H-bond donating functional groups on the sorbent surface. A comparison of b-terms of pristine MWCNTs with that of surface modified MWCNTs (e.g., hydroxyl- or carboxyl-MWCNTs), which was beyond the scope of this study, should yield further information on the H-bond donor-acceptor ability of MWNCTs. As pointed out by Apul et al., a discrimination of ppLFER between H-bond and π-H-bond is not possible; thus, the b phase descriptors may include interactions between H-bond accepting functionalities of sorbates and π electrons on MWCNTs surface. Furthermore, Apul et al. observed a concentration dependence of b, indicating that b significantly contributed to overall sorption only at higher concentration but not at lower concentration. Such an effect cannot be confirmed in the present study (Table 5-2), which includes more diverse compounds than Apul et al. (Figure A 5-1).

In contrast to molar volume (v) and H-bond basicity (b), a concentration-dependence at various concentration levels was observed for the s and a phase descriptors, which varied from -0.85 to 1.39 for s and from -1.19 and -0.34 for a at high and low concentration, respectively. Xia et al. obtained an even higher positive contribution of dipolarity/polarizability to overall sorption (s = 1.75) [6]. By an extrapolation of phase descriptors over a probe sorbate concentration approaching infinite dilution, a similar trend for the concentration dependence of s was observed by those authors. In order to further assess the concentration dependence of dipolarity/polarizability, sorption non-linearity (i.e., the Freundlich coefficient n) and S of sorbates were plotted (Figure A 5-2). Previously, a significant relationship was reported for S and non-linear sorption by soil-organic carbon [13, 16]. In general, a significant negative correlation ($p < 0.01$) was obtained between S and n for the experimentally determined sorbates; i.e., with increasing dipolarity/polarizability of a sorbate sorption non-linearity by MWCNTs also increased. However, sorption linearity of some compounds (nOct, MTBE, TeCM, Phen, and Pyr) did not fit into this scheme since the sorption linearities of these compounds were higher (Figure A 5-2). The S descriptors for Phen and Pyr were higher than those of the other compounds; thus, they could be considered

to be outside the calibration range for S (shown in Table 5-1 and Figure A 5-1). This indicates that additional factors may have to be considered for these compounds.

In order to further compare the data of the present study with previous publications, a ppLFER model was developed using only aromatic compounds from the probe set shown in Table 5-1. By taking only aromatic compounds into account for ppLFER development, phase descriptors were obtained that were very similar to those obtained in previous reports. The results of ppLFER development for aromatic probe sorbates (shown in Table A 5-7) indicate that the aforementioned differences in obtained phase descriptors for MWCNTs can be assigned to the fact that the probe compound set here used is extended to aliphatic compounds, which certainly allows a more comprehensive discussion of the relevant interactions by MWCNTs.

As previously mentioned, Apul et al. did not take the eE-term into account for ppLFER. By definition, the eE-term also incorporates non-specific interactions [15], which have previously been discussed to be relevant for CNM interaction, even though its contribution was generally of minor importance [6]. A re-calculation of the data given by the authors with a ppLFER that does take eE into account (as shown in Table A 5-7) indicates the significance of the contribution of eE was concentration dependent. In fact, the contribution of eE was found to be insignificant for *infinite dilution*, while an e descriptor of 1.20 was calculated to significantly ($p < 0.05$) contribute in the ppLFER at a concentration level of 10^{-2} S_w. To assure that this comparison is correct, the data set was additionally re-calculated without eE, which lead to almost the same phase descriptors and statistical analyses as given by Apul et al. From the discussion above it becomes apparent that generally all descriptors should be taken into account for a comprehensive discussion of the relevant molecular interactions.

5.4.3 Validation of the ppLFER

The developed ppLFER models were validated with an independent compound set as shown in Table A 5-15. The validation set consisted of seven compounds, one from each compound class as categorized in Table 5-1. The predicted log K_d values of the compounds used for validation were plotted against log K_d values experimentally determined (Figure A 5-3) The validation showed reasonable agreement between the predicted and the experimentally

determined log K_d values. However, it must be stressed that a probe set with more compounds would be necessary for better validation of the derived ppLFER equations.

The here derived ppLFER was further validated by a mutual comparison with literature, i.e., experimental data of this study were predicted by the ppLFER from Apul et al., and vice versa. For this comparison all sorbates measured in the present study (i.e., from ppLFER development and validation) was taken into account. Figure 5-5A compares the measured log K_d values of this study with the prediction by Apul's ppLFER. The deviation between the predicted and measured log K_d values of aliphatic compounds is significantly lower for the ppLFER developed in this study (RMSE for aliphatic compounds of 0.31 for ppLFER of this study and of 0.63 for ppLFER by Apul et al.). Additionally, most data points are located below the 1:1 prediction line indicating an underestimation of the distribution coefficients by ppLFER from literature. Aromatic probe sorbates were also better predicted by ppLFER of this study (RMSE for aromatic compounds of 0.26 for ppLFER of this study and of 0.47 for ppLFER by Apul et al.). Again, Apul's ppLFER mostly underestimates log K_d values of aromatic compounds.

The comparison between log K_d collected by Apul et al. and predictions by the ppLFER calibrated on log K_d experimentally measured in this study is shown in Figure 5-5B. The results show that log K_d of most sorbates used by Apul et al. could well be predicted with our ppLFER (RMSE = 0.60). However, the predictions of Apul's log K_d with their derived ppLFER were indeed better (RMSE = 0.47). Most of the compounds that were not well predicted with ppLFER derived in this study were phenols and heterocyclic compounds with sorbate descriptors that were outside the calibration range used in this study. Thus, further experimental data is necessary, especially with regard to sorbates with a broader range in A and B descriptors. This would also give useful insights into the contribution of H-bond interactions of MWCNTs.

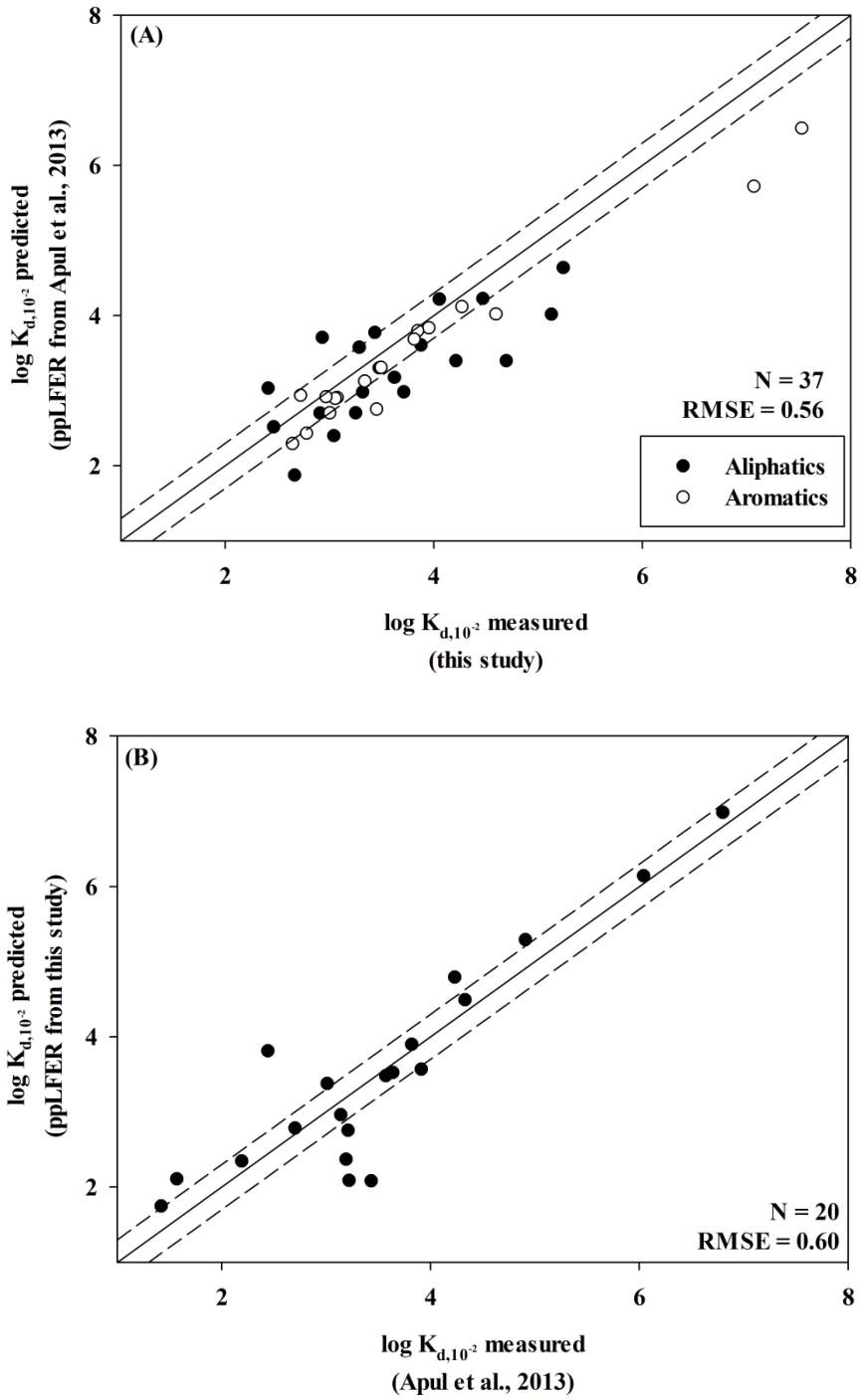

Figure 5-5: Comparison of the predicted and measured log K_d. (A) Prediction by the ppLFER from Ref [5] vs log K_d measured in this study. (B) Prediction by the ppLFER calibrated in this study vs. log K_d collected by Ref [5]. Solid lines represent the 1:1 agreement, and dashed lines indicate 0.3 log-unit deviations. N = number of data points; RMSE: root mean squared error.

5.4.4 Comparison of sorption properties of MWCNTs with activated carbon

In literature, sorption by CNM is often compared to that of other carbonaceous materials, such as activated carbon (AC) [28-30]. This is mainly due to the fact that CNM have been proposed as superior sorbents that, with increasing production rate and consequently decreasing cost, may become at least competitive to traditionally used activated carbon; for example, in water treatment processes [31, 32]. Observed differences in sorption affinity between CNM and AC were assigned to molecular sieving effects from pore-filling mechanisms for CNM [29, 30]. ppLFER should be able to qualitatively and quantitatively display the observed difference in interaction strength that were mainly assigned to non-specific van-der-Waals and specific electron donor-acceptor (EDA) interactions [30]. The ppLFER equations derived here were thus compared to previously reported ppLFER equations for sorption by AC. Shih and Gschwend used a ppLFER to investigate the contribution of individual interactions to overall sorption of organic compounds by granular AC at various levels of sorbate saturation [11]. For reason of comparability, only the ppLFER derived at a concentration level of 10^{-2} S_w is discussed here:

$$\log K_{d,10^{-2}} = 0.33 \pm 0.60E - 0.12 \pm 0.51S - 0.52 \pm 0.51A - 4.52 \pm 0.51B + 4.59 \pm 0.52V + 0.79 \pm 0.52$$

($R^2 = 0.97$, $N = 14$) (Eq. 5-5)

It becomes apparent that sorption of organic compounds by activated carbon is influenced by similar interactions since the descriptors in ppLFER equation 5-5 and those derived in the present study (Table 5-2) are qualitatively comparable, while ppLFER equations for both AC and MWCNTs substantially differ from those for example reported for sorption by natural organic matter [15]. However, there are quantitative differences in phase descriptors observable for AC and MWCNTs (i.e., v is higher and b is lower for AC). These differences were found be insignificant since standard errors of the individual descriptors tend to be rather large if a relatively small number of probe sorbates. The ppLFER equations currently available for sorption by AC and MWCNTs are therefore not able to display the aforementioned differences observed in sorption between the two sorbents. This indicates a potential disadvantage of ppLFER as this approach does not take structural properties, such as pore volume of the sorbent, into account. ppLFER were in principle derived to describe the

partitioning of a compound between two bulk phase; even though they were proposed to be applicable independent from the type of *ad*sorbent [7] and in practice they have successfully been used to describe sorption processes by typical *ad*sorbers [5, 6, 11].

5.5 References

1. Pan, B.; Xing, B.S. *Environmental Science & Technology* **2008**, 42, 9005-9013.
2. Pan, B.; Lin, D.H.; Mashayekhi, H.; Xing, B.S. *Environmental Science & Technology* **2008**, 42, 5480-5485.
3. Chen, J.Y.; Chen, W.; Zhu, D. *Environmental Science & Technology* **2008**, 42, 7225-7230.
4. Chen, W.; Duan, L.; Zhu, D.Q. *Environmental Science & Technology* **2007**, 41, 8295-8300.
5. Apul, O.G.; Wang, Q.; Shao, T.; Rieck, J.R.; Karanfil, T. *Environmental Science & Technology* **2013**, 47, 2295-2303.
6. Xia, X.R.; Monteiro-Riviere, N.A.; Riviere, J.E. *Nature Nanotechnology* **2010**, 5, 671-675.
7. Goss, K.U.; Schwarzenbach, R.P. *Environmental Science & Technology* **2001**, 35, 1-9.
8. Abraham, M.H. *Chemical Society Reviews* **1993**, 22, 73-83.
9. Abraham, M.H.; Ibrahim, A.; Zissimos, A.M. *Journal of Chromatography A* **2004**, 1037, 29-47.
10. Roth, C.M.; Goss, K.U.; Schwarzenbach, R.P. *Environmental Science & Technology* **2004**, 38, 4078-4084.
11. Shih, Y.H.; Gschwend, P.M. *Environmental Science & Technology* **2009**, 43, 851-857.
12. Endo, S.; Droge, S.T.J.; Goss, K.U. *Analytical Chemistry* **2011**, 83, 1394-1400.
13. Endo, S.; Grathwohl, P.; Haderlein, S.B.; Schmidt, T.C. *Environmental Science & Technology* **2008**, 42, 5897-5903.
14. Bronner, G.; Goss, K.U. *Environmental Science & Technology* **2011**, 45, 1307-1312.
15. Nguyen, T.H.; Goss, K.U.; Ball, W.P. *Environmental Science & Technology* **2005**, 39, 913-924.
16. Endo, S.; Grathwohl, P.; Haderlein, S.B.; Schmidt, T.C. *Environmental Science & Technology* **2009**, 43, 3094-3100.
17. Kah, M.; Zhang, X.; Jonker, M.T.O.; Hofmann, T. *Environmental Science & Technology* **2011**, 45, 6011-6017.
18. Laaks, J.; Jochmann, M.A.; Schilling, B.; Schmidt, T.C. *Analytical Chemistry* **2010**, 82, 7641-7648.
19. Abraham, M.H.; Andonianhaftvan, J.; Whiting, G.S.; Leo, A.; Taft, R.S. *Journal of the Chemical Society-Perkin Transactions 2* **1994**, 8, 1777-1791.
20. Abraham, M.H.; Ibrahim, A.; Acree, W.E. *Fluid Phase Equilibria* **2007**, 251, 93-109.
21. Endo, S.; Schmidt, T.C. *Fluid Phase Equilibria* **2006**, 246, 143-152.
22. Abraham, M.H. *Journal of Chromatography* **1993**, 644, 95-139.
23. Abraham, M.H.; Chadha, H.S.; Whiting, G.S.; Mitchell, R.C. *Journal of Pharmaceutical Sciences* **1994**, 83, 1085-1100.
24. Schwarzenbach, R.P.; Gschwend, P.M.; Imboden, D.M. *Environmental Organic Chemistry;* John Wiley and Sons: Hoboken, NJ, U.S.A., 2003.
25. Abraham, M.H.; Poole, C.F.; Poole, S.K. *Journal of Chromatography A* **1999**, 842, 79-114.

26. Arey, S. J. *Environmental Screening of Future Gasoline Additives: Computational tools to estimate chemical partitioning and forecast widespread groundwater contamination*. Ph.D. Thesis, Massachusetts Institute of Technology 2004.
27. Goss, K.U. *Fluid Phase Equilibria* **2005**, 233, 19-22.
28. Kim, P.; Agnihotri, S. *Journal of Colloid and Interface Science* **2008**, 325, 64-73.
29. Ji, L.L.; Chen, W.; Duan, L.; Zhu, D.Q. *Environmental Science & Technology* **2009**, 43, 2322-2327.
30. Zhang, S.J.; Shao, T.; Kose, H.S.; Karanfil, T. *Environmental Science & Technology* **2010**, 44, 6377-6383.
31. Mauter, M.S.; Elimelech, M. *Environmental Science & Technology* **2008**, 42, 5843-5859.
32. Upadhyayula, V.K.K.; Deng, S.G.; Mitchell, M.C.; Smith, G.B. *Science of the Total Environment* **2009**, 408, 1-13.

5.6 Appendix A5

Appendix A5-1: Probe sorbate properties

Table A 5-1: List of all sorbates used in this study, their physico-chemical properties, and their analytical methodology.

	Abb.	log S_w	log K_{aw}	log K_{ow}	Method of determination
alkanes					
n-Hexane	nHex	0.98	1.73	3.90	HS
n-Heptane	nHep	0.46	1.84	4.66	HS
n-Octane	nOct	-0.18	1.95	5.18	HS
Cyclohexane	cHex	1.74	0.78	3.44	HS
Cycloheptane	cHep	1.48	0.63	4.00	HS
Cyclooctane	cOct	0.90	0.51	4.45	HS
Isohexane	iHex	1.15	1.75	3.21	HS
halo-aliphatics					
Tetrachloromethane	TeCM	2.90	-0.02	2.83	HS
Trichloroethylene	TeCE	3.11	-0.50	2.42	HS
Tetrachloroethylene	PCE	2.31	-0.27	2.88	HS
monopolar aliphatics					
Di-*n*-propyl ether	DNPE	3.69	-0.97	2.03	HS
Di-*n*-butyl ether	DNBE	2.48	-0.69	3.21	HS
Methyl tert. butyl ether	MTBE	4.71	-1.54	0.94	HS
2-Octanone	2OCT	2.95	-1.98[a]	2.37	ITEX2
Hexanenitrile	HXNT	3.39	-2.30[a]	1.66	ITEX2
bipolar aliphatics					
1-Heptanol	1HEP	3.22	-3.21[a]	2.62	ITEX2
1-Octanol	1OCT	2.73	-3.24[a]	3.00	ITEX2
2,6-Dimethyl-2-heptanol	DMH	2.76	-2.30[a]	3.11	ITEX2
4-Methyl-4-nonanol	4M4H	2.34[b]	-2.52[a]	3.64[b]	ITEX2
3-Ethyl-3-hexanol	3E3H	3.17	-2.40[a]	2.69	ITEX2
nonpolar aromatics					
Benzene	Benz	3.25	-0.65	2.17	HS
Toluene	Tol	2.72	-0.60	2.69	HS
n-Propylbenzene	pBenz	1.72	-0.40	3.69	HS
Chlorobenzene	CB	2.70	-0.80	2.84	ITEX2
1,2-Dichlorobenzene	DCB	2.19	-1.04	3.43	ITEX2
Naphthalene	Naph	1.49	-1.74	3.33	ITEX2

Phenanthrene	Phen	0.06	-2.85	4.66	[1]
Pyrene	Pyr	-0.87	-3.32	4.88	[1]
Benzofurane	BenzF	2.83	-2.07[a]	2.67	ITEX2
monopolar aromatics					
Anisol	ANIS	3.02	-1.92	2.11	ITEX2
Acetophenone	ACET	3.79	-3.37	1.58	ITEX2
Ethylbenzoate	EBT	2.86	-2.38	2.67	ITEX2
4-Nitrotoluene	4NT	2.65	-2.76	2.37	ITEX2
bipolar aromatics					
4-Ethylphenol	4EP	3.69	-4.40	2.58	ITEX2
2,6-Dimethylphenol	DMP	3.78	-3.70	2.36	ITEX2
2-Chlorphenol	2CP	4.05	-3.24	2.15	ITEX2
Indole	IND	3.55	-3.93[a]	2.14	ITEX2

S_w: aqueous solubility [mg L^{-1}] at 25 °C from Ref [2]; K_{aw}: air-water partitioning constant [-] from Ref [3] unless otherwise noted. K_{ow}: octanol-water partitioning constant [-] from Ref [2].

[a]calculated using a combination of equations 6-15 and 6-17 from Ref [3]:

$$K_{aw} = \frac{p_i\,[atm]}{S_W\,[mol\,L^{-1}]} \cdot \frac{1}{T\,[K] \cdot R[atm\ L\ mol^{-1}\ K^{-1}]}.$$

[b] taken from SciFinder database [4]

Appendix A5-2: Results of the Freundlich Model fit of isotherm data and thereby calculated log K_d values

Table A 5-2: Freundlich parameters from isotherm fits for all sorbates and their calculated distribution coefficients.

Sorbate	log K_F	n	R^2	N	log K_d at 10^{-2} S_w	log K_d at 10^{-5} S_w
n-Hexane	5.24	0.7245	0.9866	12	4.70	5.52
n-Heptane	5.70	0.6573	0.9828	12	5.13	6.16
n-Octane	5.21	1.0382	0.9897	10	5.24	5.13
Cyclohexane	4.24	0.8082	0.9874	13	3.71	4.29
Cycloheptane	4.66	0.6803	0.9922	11	3.88	4.84
Cyclooctane	5.00	0.7184	0.9887	10	4.47	5.31
Isohexane	4.79	0.7289	0.9784	10	4.21	5.03
Tetrachloromethane	3.26	0.9982	0.9642	11	3.25	3.25
Trichloroethylene	4.85	0.5592	0.9784	10	3.04	4.36
Tetrachloroethylene	5.66	0.3851	0.9889	11	3.62	5.47
Di-*n*-propyl ether	5.02	0.4557	0.9749	11	2.46	4.10
Di-*n*-butyl ether	5.84	0.3095	0.9909	10	3.43	5.51
Methyl tert. butyl ether	3.07	0.9285	0.9731	15	2.67	2.88
2-Octanone	5.81	0.3129	0.9269	14	2.81	4.87
Hexanenitrile	5.13	0.3820	0.9740	9	2.41	4.26
1-Heptanol	5.41	0.4096	0.9874	10	2.91	4.69
1-Octanol	5.92	0.2286	0.9850	14	3.04	5.36
2,6-Dimethyl-2-heptanol	5.79	0.3324	0.9715	14	3.29	5.29
4-Methyl-4-nonanol	5.97	0.4260	0.9567	14	4.05	5.77
3-Ethyl-3-hexanol	5.25	0.5151	0.9808	13	3.23	4.68
Benzene	4.74	0.5080	0.9864	12	2.64	4.12
Toluene	5.47	0.3260	0.9889	11	2.97	4.99
Propylbenzene	5.76	0.4525	0.9657	11	4.27	5.91
Chlorobenzene	5.65	0.3761	0.9888	14	3.34	5.21
1,2-Dichlorobenzene	6.02	0.3528	0.9864	14	3.95	5.89
Naphthalene	6.30	0.3145	0.9756	12	4.60	6.65
Phenanthrene	6.85	0.6747	0.9721	15	6.50	7.48
Pyrene	6.92	0.8461	0.9758	15	6.90	7.36
Benzofuran	5.86	0.3831	0.9846	12	3.49	5.34
Anisol	5.59	0.3248	0.9548	14	2.88	4.91
Acetophenone	5.86	0.3443	0.9770	12	2.72	4.69
ethylbenzoate	6.29	0.3651	0.9752	14	3.85	5.75

4-Nitrotoluol	6.09	0.3583	0.9872	14	3.75	5.67
4-Ethylphenol	6.26	0.3052	0.9775	13	3.00	5.09
2,6-Dimethylphenol	7.16	0.2242	0.9801	12	3.45	5.78
2-Chlorphenol	5.92	0.3788	0.9878	12	2.78	4.64
Indole	6.14	0.2635	0.9732	12	2.79	4.99

Log K_F: logarithmic Freundlich coefficient; n: Freundlich exponent; R^2: regression coefficient; N: number of data points; log K_d: logarithmic distribution coefficient.

Appendix A5-3: Statistical analyses of ppLFER taking all probe sorbates into account

Table A 5-3: Parameters for ppLFER at 10^{-2} S_w.

	Coefficient	SE	p-value
c	0.36	0.33	0.2829
e	1.06	0.30	0.0016
s	-0.85	0.42	0.0486
a	-1.19	0.39	0.0055
b	-2.96	0.51	<0.0001
v	3.77	0.36	<0.0001

Table A 5-4: Parameters for ppLFER at 10^{-5} S_w.

	Coefficient	SE	p-value
c	1.33	0.53	0.0183
e	-0.24	0.48	0.6216
s	1.39	0.68	0.0535
a	-0.34	0.63	0.5984
b	-2.83	0.82	0.0021
v	3.69	0.58	<0.0001

Table A 5-5: ANOVA for ppLFER at 10^{-2} S_w.

	DF	SS	MS	F-value	F-critical
Model	5	30.53		65.83	3.19E-13
Residue	24	2.23	6.11		
Total	29	32.75	0.09		

Table A 5-6: ANOVA for ppLFER at 10^{-5} S_w.

	DF	SS	MS	F-value	F-critical
Model	5	22.48	4.50	18.63	1.45E-07
Residue	24	5.79	0.24		
Total	29	28.27			

Comments regarding Table A5-3 - Table A 5-6:

All parameters were calculated at a 95% confidence level.

SE: standard error of estimates

DF: degrees of freedom

SS: sum of squares

MS: mean square

Appendix A5-4: Comparison of sorbate descriptors

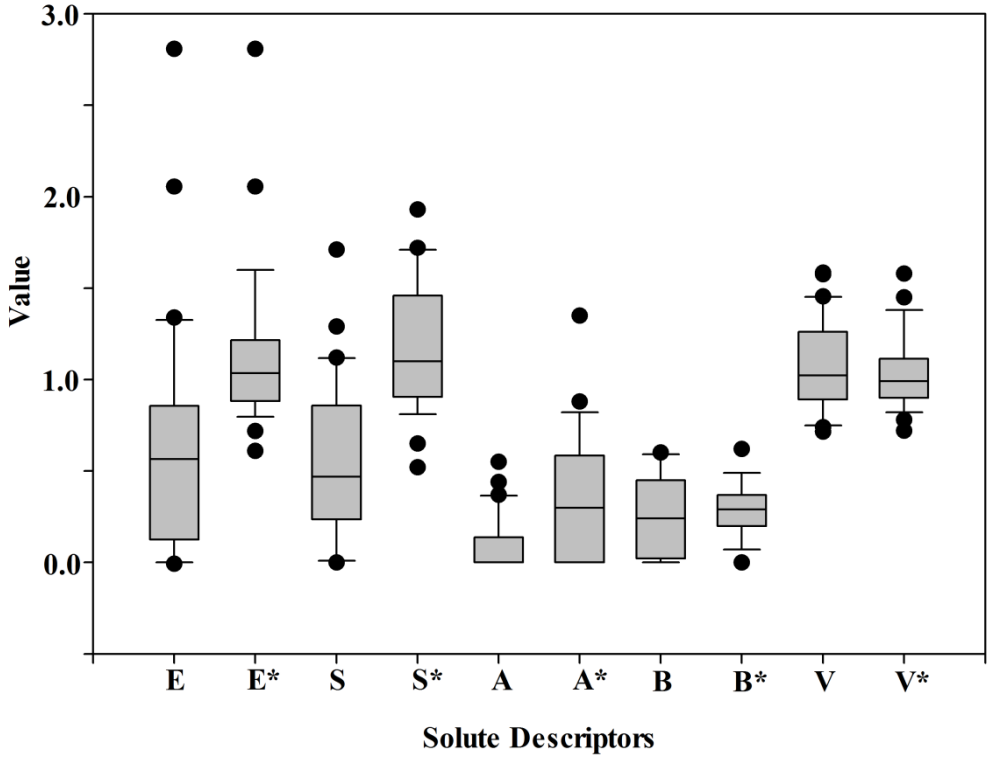

Figure A 5-1: Box plots for the ppLFER solute descriptors E, S, A, B, and V. The descriptors used by Apul et al. [5] are indicated with (*).

Appendix A5-5**: **Plot of Freundlich exponents vs. S descriptor

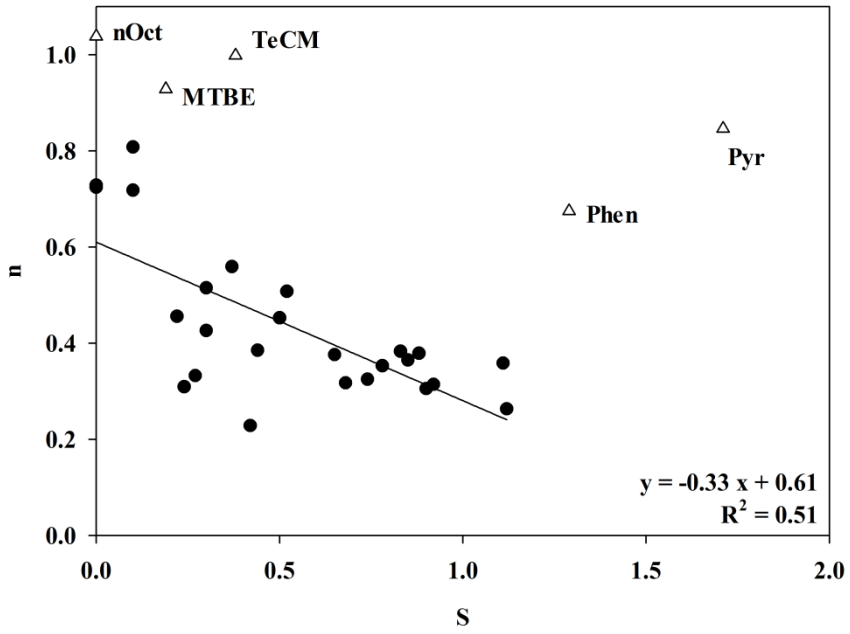

Figure A 5-2: Freundlich exponent (n) for sorption by MWCNTs vs. S descriptor of sorbates.

Appendix A5-6: ppLFER modeling for the aromatic probe sorbates used in this study

Table A 5-7: ppLFER derived for aromatic probe sorbates used in this study.

Descriptor	Coefficient at 10^{-2} S_w	SE
c	-0.36	0.43
e	0.73	0.33
s	-0.42	0.57
a	-1.24	0.37
b	-2.25	0.81
v	4.28	0.56

Statistics	
N	14
R^2	0.9844
RMSE	0.16

Comments regarding Table A 5-7:

All parameters were calculated at a 95% confidence level.

SE: standard error of estimates

N: Number of compound taken into account

SS: sum of squares

RMSE: root mean squared error

Appendix A5-7: Re-calculation of ppLFER equations for log K_d reported by Apul et al. (2013)

The ppLFER equations reported by Apul et al. [5] were re-calculated in this study using the data and descriptors given by the authors. All distribution data of sorbates considered and the descriptors are given in Table A 5-8. The re-calculation was done for two concentration levels (i.e., 10^{-2} and 10^{-5} of the sorbates aqueous solubility, S_w) taking the sE-term into account by multi regression analysis (MRA) of the given log K_d values against the descriptors given in the Table A 5-8. Note that the sorbate descriptors for E were additionally collected from the literature [6-12] since they were not considered by Apul et al.. Pyrogallol was removed for the data set as not value for E could be obtained from the data bases and no distribution coefficient was given for the higher concentration level. The results of MRA are given in Table A 5-9 to Table A 5-14.

Table A 5-8: List of sorbates from Apul et al. [5], their ppLFER descriptors, and calculated log K_d values.

Sorbate	E	S	A	B	V	log $K_{d,\infty}$	log $K_{d,0.01}$
Phenanthrene	2.06	1.29	0.00	0.26	1.45	3.29	3.04
Pyrene	2.81	1.71	0.00	0.29	1.59	4.01	3.80
Naphthalene	1.34	0.92	0.00	0.20	1.09	1.63	1.33
1-Naphthol	1.52	1.05	0.61	0.37	1.14	0.76	0.91
Biphenyl	1.36	0.99	0.00	0.22	1.32	2.05	1.91
2-Phenylphenol	1.55	1.40	0.56	0.49	1.38	1.63	0.82
Benzene	0.61	0.52	0.00	0.14	0.72	-0.45	-
Chlorobenzene	0.72	0.65	0.00	0.07	0.84	-0.33	0.64
1,2,4-Trichlorobenzene	0.98	0.81	0.00	0.00	1.08	1.17	1.23
Nitrobenzene	0.87	1.11	0.00	0.28	0.89	0.33	-
2,4-Dinitrotoluene	1.17	1.27	0,07	0.51	1.21	2.38	0.57
Phenol	0.81	0.89	0.60	0.31	0.78	-0.54	-1.58
Catechol	0.97	1.07	0.85	0.52	0.83	0.21	-
Pyrogallol	-	1.35	1.35	0.62	0.89	1.18	-
2,4,6-Trichlorophenol	1.01	1.14	0.42	0.15	1.14	1.43	-0.56
3-Nitrotoluene	0.87	1.1	0.00	0.25	1.03	1.03	-
4-Nitrophenol	1.07	1.72	0.82	0.26	0.95	0.77	-
Aniline	0.96	0.96	0.26	0.41	0.82	-0.77	-1.43
4-Chloroaniline	1.06	1.13	0.30	0.31	0.94	-0.66	-0.30
2-Nitroaniline	1.18	1.37	0.30	0.36	0.99	1.60	0.21
3-Nitroaniline	1.20	1.71	0.42	0.35	0.99	0.72	0.19
4-Nitroaniline	1.22	1.91	0.46	0.38	0.99	0.95	0.43
4-Methylphenol	0.82	0.87	0.57	0.31	0.92	0.06	-0.81
2-Chlorophenol	0.85	0.88	0.32	0.31	0.90	0.08	-
4-Chlorophenol	0.92	1.08	0.67	0.21	0.90	0.74	-
2,4-Dichlorophenol	0.96	0.82	0.54	0.17	1.02	0.96	0.01
2-Nitrophenol	1.02	1.05	0.05	0.37	0.95	0.56	0.14
3-Nitrophenol	1.05	1.57	0.79	0.23	0.95	0.92	0.22
1,3-Dinitrobenzene	1.15	1.60	0.00	0.47	1.06	1.46	-

Table A 5-9: Parameters for re-calculated ppLFER at 10^{-2} S_w without E.

Descriptor	Recalculated coefficients	SE	p-value	Coefficients derived by Apul et al. [5]	SE	p-value
c	-3.78	0.74	0.0001	-3.81	0.78	0.0002
s	0.90	0.45	0.0642	0.67	0.47	0.1734
a	-1.49	0.54	0.0156	-1.31	0.56	0.0321
b	-2.70	1.10	0.0264	-2.86	1.22	0.0335
v	4.16	0.69	<0.0001	4.41	0.70	<0.0001
Statistics						
N	20			20		
R^2	0.87			0.85		

Table A 5-10: Parameters for recalculated ppLFER at 10^{-2} S_w with E.

Descriptor	Recalculated coefficients	SE	p-value
c	-2.70	0.80	0.0044
e	1.20	0.52	0.0359
s	0.47	0.44	0.3006
a	-1.27	0.49	0.0213
b	-2.78	0.97	0.0122
v	2.21	1.03	0.0511

Table A 5-11: ANOVA for re-calculated ppLFER at 10^{-2} S_w with E.

	DF	SS	MS	F-value	F-critical
Model	5	29.86	5.97	26.79	1.06E-06
Residue	14	3.12	0.22		
Total	19	32.98			

Table A 5-12: Parameters for re-calculated ppLFER at 10^{-5} S_w without E.

Descriptor	Recalculated coefficients	SE	p-value	Coefficients derived by Apul et al. [5]	SE	p-value
c	-4.25	0.55	<0.0001	-4.30	0.55	<0.0001
s	0.54	0.34	0.1288	0.49	0.31	0.0883
a	-0.02	0.33	0.9488	0.05	0.32	0.7769
b	-0.20	0.82	0.8122	-0.48	0.86	0.5843
v	4.49	0.56	<0.0001	4.56	0.55	<0.0001
Statistics						
N	29			29		
R^2	0.82			0.82		

Table A 5-13: Parameters for recalculated ppLFER at 10^{-5} S_w with E.

Descriptor	Recalculated coefficients	SE	p-value
c	-3.96	0.66	<0.0001
e	0.11	0.46	0.8166
s	0.67	0.35	0.0665
a	-0.38	0.35	0.2791
b	-0.79	0.81	0.3390
v	4.20	0.94	0.0002

Table A 5-14: ANOVA for re-calculated ppLFER at 10^{-5} S_w with E.

	DF	SS	MS	F-value	F-critical
Model	5	29.32	5.86	26.77	1.16E-08
Residue	22	4.82	0.22		
Total	27	34.14			

Comment regarding Table A 5-9 - Table A 5-14:

All parameters were calculated at a 95% confidence level.

SE: standard error of estimates

DF: degrees of freedom

SS: sum of squares

MS: mean square

Appendix A5-8: Validation of the ppLFER

Table A 5-15: Solute descriptors of the probe compounds used for validation of the ppLFER model.

compound	E	S	A	B	V	L	Ref.
n-Heptane	0.000	0.00	0.00	0.00	0.954	2.668	[6]
Cycloheptane	0.350	0.10	0.00	0.00	0.986	3.704	[11]
Toluene	0.601	0.52	0.00	0.14	0.857	3.325	[6]
Hexanenitrile	0.166	0.90	0.00	0.36	0.968	3.513	[10, 13]
2,6-Dimethylphenol	0.860	0.79	0.39	0.39	1.057	4.480	[6]
1-Heptanol	0.211	0.42	0.37	0.48	1.154	4.115	[6]
Acetophenone	0.818	1.01	0.00	0.49	1.014	4.501	[6]

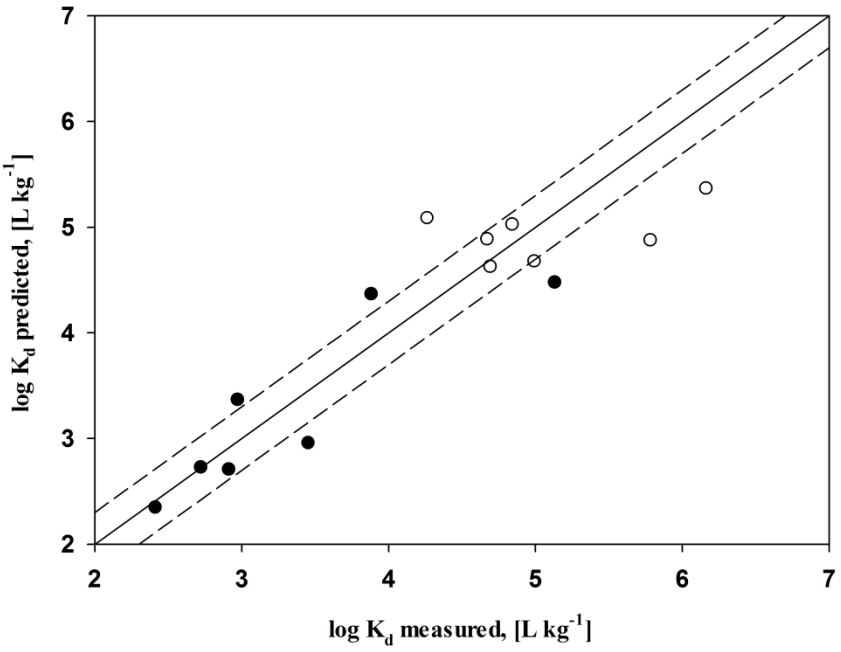

Figure A 5-3: Validation of ppLFER at 10^{-2} (●) and 10^{-5} (○) of the seven probe sorbates solubility. Solid line represents 1:1 fit and dashed lines indicate 0.3 log-unit deviations from measured values.

References for Appendix A5

1. Kah, M.; Zhang, X.; Jonker, M.T.O.; Hofmann, T. *Environmental Science & Technology* **2011**, 45, 6011-6017.
2. Corporation, S. R. Interactive PhysProp Database Demo. http://www.syrres.com/esc/physdemo.htm Last accessed Feb., 2013.
3. Schwarzenbach, R.P.; Gschwend, P.M.; Imboden, D.M. *Environmental Organic Chemistry;* John Wiley and Sons: Hoboken, NJ, U.S.A., 2003.
4. SciFinder, Chemical Abstract Service. https://www.cas.org/products/scifinder Last accessed Jun., 2013.
5. Apul, O.G.; Wang, Q.; Shao, T.; Rieck, J.R.; Karanfil, T. *Environmental Science & Technology* **2013**, 43, 2295-2303.
6. Abraham, M.H.; Andonianhaftvan, J.; Whiting, G.S.; Leo, A.; Taft, R.S. *Journal of the Chemical Society-Perkin Transactions 2* **1994**, 8, 1777-1791.
7. Abraham, M.H.; Poole, C.F.; Poole, S.K. *Journal of Chromatography A* **1999**, 842, 79-114.
8. Abraham, M.H.; Ibrahim, A.; Zissimos, A.M. *Journal of Chromatography A* **2004**, 1037, 29-47.
9. Abraham, M.H. *Journal of Chromatography* **1993**, 644, 95-139.
10. Abraham, M.H.; Chadha, H.S.; Whiting, G.S.; Mitchell, R.C. *Journal of Pharmaceutical Sciences* **1994**, 83, 1085-1100.
11. Abraham, M.H.; Ibrahim, A.; Acree, W.E. *Fluid Phase Equilibria* **2007**, 251, 93-109.
12. Abraham, M.H. *Chemical Society Reviews* **1993**, 22, 73-83.
13. Weckwerth, J.D.; Carr, P.W.; Vitha, M.F.; Nasehzadeh, A. *Analytical Chemistry* **1998**, 70, 3712-3716.

Chapter 6 Multi-walled carbon nanotubes as sorptive material for solventless in-tube microextraction (ITEX2) – A factorial design study

Adapted from: Hüffer, T.; Osorio, X.L.; Jochmann, M.A.; Schilling, B.; Schmidt, T.C. Multi-walled carbon nanotubes as sorptive material for solventless in-tube microextraction (ITEX2) – A factorial design study. *Analytical and Bioanalytical Chemistry* **2013**, 405, 8387-8395.

http://link.springer.com/article/10.1007/s00216-013-7249-7

6.1 Abstract

Multi-walled carbon nanotubes were evaluated as sorptive packing material for in-tube microextraction (ITEX2) in combination with GC-MS for the analysis of benzene, toluene, ethylbenzene, xylenes (BTEX), and naphthalene in aqueous samples. For method development, a 3-level full factorial design of experiment (DoE) was performed incorporating extraction temperature, number of extraction strokes, and extraction flow. The statistical analysis of method development showed that all considered extraction parameters significantly affected the extraction yield. Furthermore, it was shown that some factors significantly interacted with each other, which indicates the advantage of using DoE for method development. The thereby optimized ITEX2 protocol was validated regarding its linear dynamic range, method detection limit (MDL), and precision. The MDLs of investigated analytes ranged between 2 ng L^{-1} for naphthalene and 11 ng L^{-1} for *p*-xylene. The relatively low MDL obtained for naphthalene, despite its comparably low air-water partitioning, can be explained by its strong interaction with carbon nanotubes. All obtained MDLs are at least comparable to previous reports on microextraction techniques, emphasizing both the quality of ITEX2 and the highly promising sorbent characteristics of carbon nanotubes. Furthermore, the method was applied to three real samples, which indicated good recoveries of analytes from tap water, a bank filtrate, and an effluent from a waste water treatment plant.

6.2 Introduction

Since their first introduction in 1991 [1], carbon-based nanomaterials (CNM) have attracted more and more attention as a result of their unique mechanical, thermal, electronic, and chemical properties [2]. CNM are among others characterized by a large surface area to volume ratio and electron delocalization. As a result, CNM have been proposed and shown to be strong sorbents for the removal of organic pollutants in various sorptive separation techniques, such as purge & trap, solid phase extraction (SPE) or solid phase microextraction (SPME), in environmental science [3-5] and analytical chemistry [2, 6, 7].

Carbon nanotubes (CNTs), cylindrically rolled graphene sheets, have been shown to have excellent sorbent characteristics for micropreconcentration units due to their high sorption capacity and efficient sorbate removal during desorption [2, 8]. Furthermore, strong sorption due to high-energy sorption sites, e.g., from surface defects and interstitial as well as groove regions between CNT bundles, in combination with their hydrophobicity make CNTs highly promising sorbents for the extraction of non-polar organic compounds. Especially, electron donor-acceptor (EDA) interactions between the CNT sidewall and aromatic ring systems predetermine them as effective sorbent material for aromatic hydrocarbons, i.e., benzene, toluene, ethylbenzene, xylenes (BTEX) and polycyclic aromatic hydrocarbons (PAHs) [5, 9].

The application of CNTs in sample preparation mainly relies on protocols for SPE [10, 11] and SPME [5, 12-14]. For the latter, most often CNT-SPME coatings need to be prepared prior to usage, which may be time consuming, and especially fused silica fibers need to be handled with great care [15]. During the last decade, several needle based extraction techniques have been developed and applied for the extraction of volatile organic compounds (VOCs) [16-18]. Among these, the use of an in-tube microextraction device (ITEX2) has been shown to be a promising alternative to commonly used SPME or purge & trap systems [19]. ITEX2 consists of a sorbent-packed needle, which is surrounded by an external thermal desorption heater unit. Sample enrichment is carried out by aspirating and dispensing the syringe, so that the sample can pass the sorbent packing several times. After extraction, the analytes are thermodesorbed into the GC injector with a desorption gas. ITEX2 was applied for the analysis of volatile components from blood [20], odor [21], and aroma compounds in food [22] and beverages [23, 24]. Major advantages of ITEX2 are the reduced susceptibility

to contamination and reduced instrumental effort in combination with low method detection limits down to 1-10 ng L^{-1} for VOCs [19].

The extraction yield of BTEX determined with ITEX2 is influenced by sample and extraction related parameters. Sample related parameters are the air-water partitioning of the analytes, the variation of the phase ratio in the vial, the extraction temperature, the ionic strength, and the stirring of the sample. Extraction related parameters are the number of aspirating and dispensing cycles (extraction strokes), the volume and flow of each extraction stroke (extraction flow), the desorption temperature, the desorption gas volume, and the desorption flow during sample injection.

Commonly, method development studies are performed by the optimization of individual extraction parameters. For each parameter, the extraction yield, i.e., the optimal response, is determined. However, such approaches to method development are usually time and cost intensive. A highly efficient tool to investigate the influence of factors and their interactions are experimental designs (design of experiment, DoE); especially when the researcher is interested in which factors significantly affect the response of the extraction [25]. Furthermore, a classical "one-factor-at-a-time" approach can be significantly less efficient when the parameters interact, which may often be the case [26]. Recently, DoE has been used for optimization of determination of various analytes using solid phase dynamic extraction (SPDE) [27] or SPME [28, 29]. Overall, applying DoE for method development yields a lot of information for a relatively small number of experiments.

In this study we combine the advantages of the ITEX2 system with the promising properties of CNTs for the analysis of non-polar organic compounds in aqueous samples. On the basis of our previous studies, three factors affecting the maximum sensitivity of the extraction were selected. Furthermore, in order to reduce the number of experiments as well as to identify those parameters significantly affecting the extraction yield, a 3-level full factorial DoE was applied for method optimization.

6.3 Experimental Section

6.3.1 Materials

The ITEX2 needle was packed with 52 mg of multi-walled carbon nanotubes (MWCNTs; C150HP) purchased from Bayer Material Science (Leverkusen, Germany). Properties of MWCNTs are given in Table A 4-1 in the appendix of Chapter 4 and scanning electron microscopy images of MWCNTs are presented in Figure 6-1. The packed ITEX2 needle was used throughout this study without change of the sorbent.

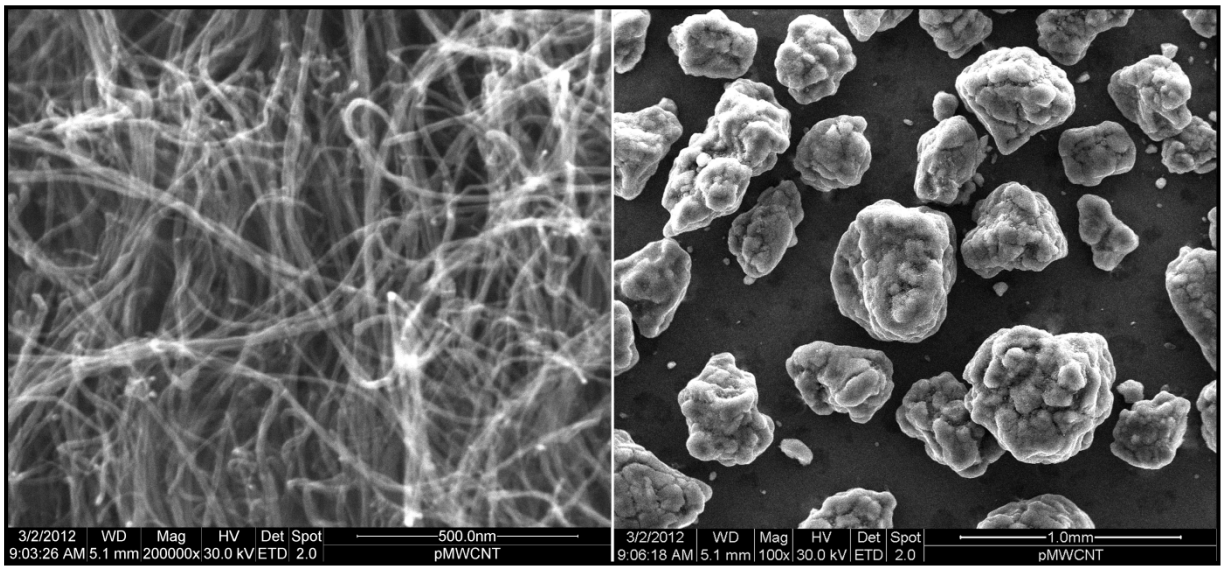

Figure 6-1: SEM images at two different magnifications of MWCNTs used for ITEX2 packing.

Benzene (Benz), toluene (Tol), ethylbenzene (eBenz), *o*-xylene (*o*Xyl), *p*-xylene (*p*Xyl), and naphthalene (Naph) were chosen as analytes and purchased at≥99.5% purity from Sigma - Aldrich (Steinheim, Germany); selected properties of analytes are given in Table 6-1.

Table 6-1: Analytes used in this study and their physico-chemical properties.

Compound	CAS No.	MW[a]	ρ[a]	Bp[a]	S_w[a]	A[b]	B[b]	K_{aw}[b]
Benzene	71-43-2	78.12	0.88	80.0	1790	5.053	1693	2.46
Toluene	108-88-3	92.14	0.87	110.6	526	5.271	1745	2.92
Ethylbenzene	100-41-4	106.17	0.86	136.1	169	6.541	2100	5.73
o-xylene	95-47-6	106.17	0.88	144.5	178	5.064	1719	2.14
p-xylene	106-42-3	106.17	0.86	138.3	162	4.900	1615	2.84
Naphthalene	91-20-3	128.18	1.06	217.9	31	6.059	2332	0.43

[a]obtained from [30]; [b]obtained from [31]; *MW*: molecular weight in g mol^{-1}; *ρ*: density in g mL^{-1}; *Bp*: boiling point in °C; S_w: aqueous solubility in mg L^{-1}; A & B: constants for temperature dependent air-water partitioning constants; K_{aw}: air-water partitioning constants calculated for 65 °C via a van't Hoff type equation log K_{aw} = A-B/T.

6.3.2 Standard and Sample Preparation

Stock solutions of BTEX were prepared by dissolving 10 µL of pure compounds in 100 mL methanol (Chromasolve, Sigma-Aldrich) in volumetric flasks using gas-tight microliter glass syringes (Hamilton™, Bonaduz, Switzerland) resulting in concentrations of the stock solutions between 86 and 88 mg L^{-1} for ethylbenzene and benzene, respectively. Naphthalene stock solution was prepared by diluting 15 mg of solid compound in 100 mL methanol in a volumetric flask. From stock solutions, a standard mix solution was prepared in methanol with 1 mL of individual stock solution resulting in concentrations of analytes in the standard mix ranging between 3.4 and 6 mg L^{-1} for ethylbenzene and naphthalene, respectively. All stock and standard solutions were stored at 4 °C. The standard mix was freshly prepared every two weeks, while the stock solution was kept for no longer than two months.

Sample vials were prepared by adding 10 mL deionized water to 20-mL amber headspace vials with rubber-PFTE septa (BGB Analytik, Rheinfelden, Germany). Subsequently, 8 x 3 mm PFTE coated magnetic stir bars (VWR International GmbH, Darmstadt, Germany) were placed into the vials and samples were spiked with 10 µL standard mix solution resulting in sample analyte concentrations between 3.4 and 6.0 µg L^{-1} for ethylbenzene and naphthalene, respectively. After sample preparation, vials were immediately closed, shaken by hand for 30 s to ensure complete analyte mixing, and placed on the GC autosampler tray for analysis.

6.3.3 GC-MS Instrument and Parameters

All samples were analyzed by GC-MS (Trace Ultra gas chromatograph coupled to a single quadrupole mass spectrometer model DSQ II (S+H Analytik, Mönchengladbach, Germany); Rxi-5ms column (30 m x 0.32 mm x 0.25 µm, Restek, Bad Homburg, Germany). The GC was equipped with a Combi-PAL autosampler (Axel Semrau, Sprockhövel, Germany), a split/splitless injector (SSL), and an Optic 3 programmed temperature vaporization injector with a cryofocusing unit (Axel Semrau), in which an uncoated, deactivated fused silica tubing with 0.53 mm i.d. (BGB Analytik) was used. The ITEX2 option for the Combi-PAL was obtained from CTC Analytics (Zwingen, Switzerland), consisting of a heatable syringe holder, a 1.3-mL syringe with a side port (Hamilton^{TM}), and a trap heater. Furthermore, the Combi-PAL was equipped with a Single Magnet Mixer (SMM, Chromtech, Idstein, Germany).

Instrument control, data acquisition, and evaluation were performed by Xcalibur 1.4 software (Thermo Scientific), while ITEX2 procedures were controlled by manufacturer supplied macros, customized in the PAL Cycle Composer (CTC Analytics).

The injector was used in splitless mode set at a temperature of 220 °C. The Optic 3 was set to 250 °C and the cryotrap temperature to -120 °C with a hold/transfer time of 60 s. After the transfer time, the split was opened at 10 mL min^{-1}, and the cryotrap was heated to 250 °C at a ramp rate of 30 °C s^{-1}. A constant column flow of 1.5 mL min^{-1} He 5.0 (Air Liquide, Oberhausen, Germany) was set. The oven program started at 35 °C for 1 min and was then ramped 4 °C min^{-1} to 130 °C, which was held for 2 min. The temperatures of MS transferline and ion source were 250 and 220 °C, respectively. The MS was set to electron ionization (EI) with an ionization energy of 70 eV in scan mode (m/z: 70-130, 7 scans s^{-1}).

6.3.4 ITEX2 method development by factorial design

After the samples were placed on the Combi-PAL, the vials were transported to the SMM, where the samples were heated and stirred at 500 rpm for 15 min. Extraction strokes were performed by aspirating and dispensing 1 mL of sample headspace volume. The temperatures of trap and syringe were set to 40 and 70 °C, respectively. Following the extraction, 500 µL of helium were aspirated as desorption gas from the SSL. Subsequently, thermal desorption

was performed into the Optic 3 with a desorption flow of 50 µL s^{-1} at a desorption temperature of 250 °C. To avoid analyte carry-over the trap was heated to 300 °C and flushed with nitrogen for 5 min.

Based on a previous study the following extraction parameters were selected for ITEX2 optimization [19]: extraction temperature, number of extraction strokes, and extraction flow. A 3-level full factorial design was used to study the effects of the extraction parameters and for the ITEX2 method development (Table 6-2). Despite the fact that the application of a central composite design or Box–Behnken design would have led to a decrease in experimental runs, a 3-level full factorial design was chosen as it certainly provides highest quality prediction, especially in cases where quadratic coefficients have to be considered [25]. Furthermore, the installation of automatized equipment significantly reduces the amount of work for the researcher as it allows over-night analyses. The application of a 3-level full factorial design with three factors resulted in 27 experiments (3^3). Three replicates of the DoE were run at a randomized order resulting in a total number of 81 experiments. The statistical analysis of the DoE was conducted with MiniTab16 software (ADDITIVE GmbH, Friedrichsdorf, Germany) and the regression analysis was performed with *R* 2.12.0 (R Development Core Team).

Table 6-2: Investigated factors and factor levels of the full factorial design.

Factor	Setting	Unit	Low (-)	Medium (0)	High (+)
T	Extraction temperature	°C	40	55	70
S	Extraction strokes	-	20	50	80
F	Extraction flow	µL s^{-1}	30	60	90

6.4 Results and Discussion

6.4.1 Extraction Parameters

In the following, we consider only the results of benzene and naphthalene as the trends and observations for all BTEX compounds were alike.

The effect of extraction parameters on the response, i.e., peak area, of both analytes in the chromatogram is given in Figure 6-2. Apparently, the effect of extraction strokes and extraction flow showed a similar trend on both compounds, whereas a difference in the effect of extraction temperature was observed. Generally, the response increased for all compounds when the extraction temperature was increased from 40 to 55 °C, which can be explained by higher partitioning of analytes from the aqueous to the gas phase in the vials (air-water partitioning constants given in Table 6-1). When the extraction temperature was further increased from 55 to 70 °C, the extraction yield of naphthalene further increased while for BTEX compounds the peak areas decreased. Similar observations have been made by previous studies not only using ITEX2 [19] and SPDE [32] extraction techniques, but also in SPME, where CNTs were utilized for fiber coating [13]. In general, a stagnation or decrease in extraction yield was previously explained by the fact that an increase in air-water phase transfer of these compounds is predominated by a simultaneous decrease in air-sorbent distribution of the analyte at elevated temperatures due to exothermic enthalpy in the sorption process. Diaz *et al.* found an enthalpy of adsorption of ΔH_{ads} = - 34.4 kJ mol^{-1} for benzene using CNTs in inverse gas chromatography [33]; however, there are only very limited thermodynamic data available for the air-CNTs phase transfer.

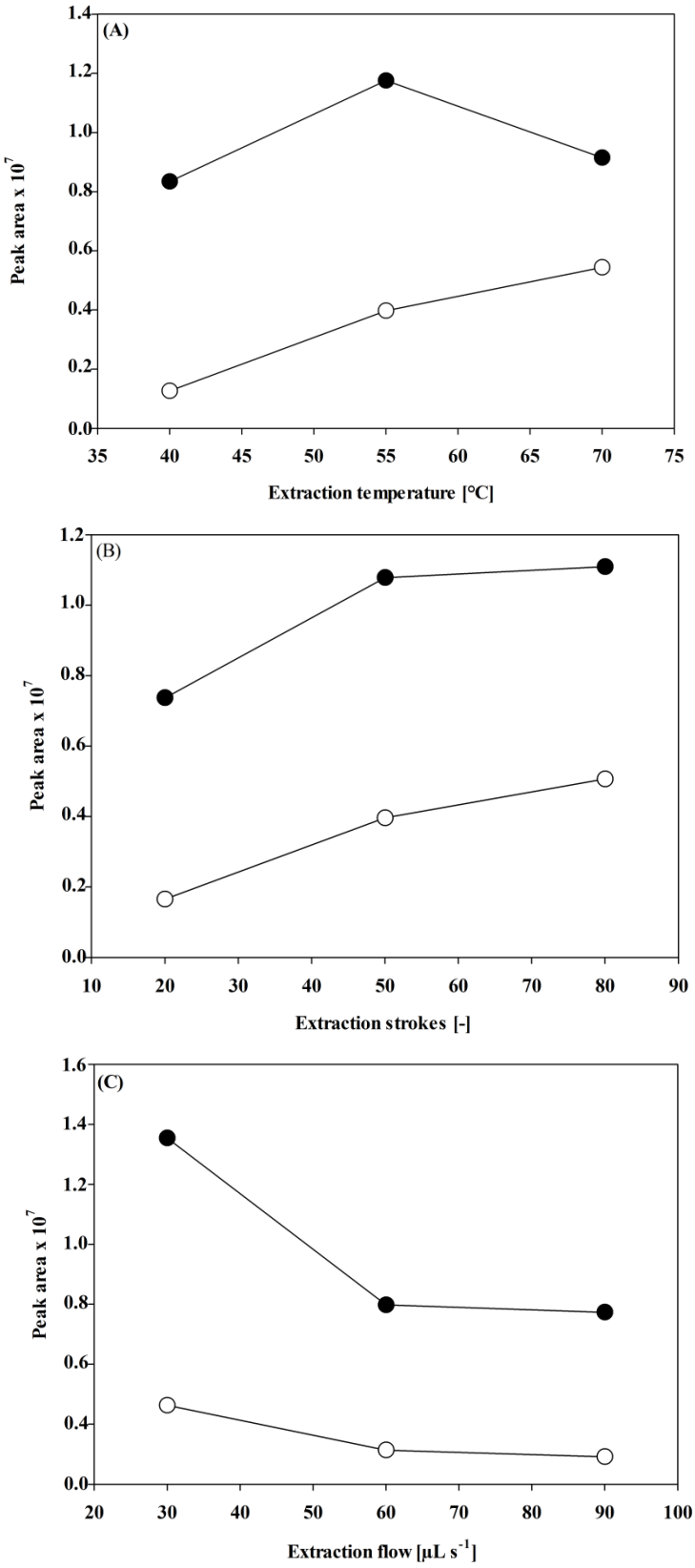

Figure 6-2: Obtained peak areas of Benz (●) and Naph (○) affected by extraction temperature (A), extraction strokes (B), and extraction flow (C).

Among the most critical parameters for ITEX2 is the extraction time [19, 34], which is determined by the number of extraction strokes and the extraction flow. Based on the settings for both parameters investigated in this study, the total extraction time ranged between 3.7 and 44.4 min. For all analytes the extraction yield was highest for an extraction flow of 30 µL s^{-1} followed by a 2-fold or higher decrease for an extraction flow of 60 µL s^{-1} (Figure 6-2), while there was no further decrease in peak area observed from 60 to 90 µL s^{-1}. A lower extraction flow results in a longer exposure of analytes to the sorbent material; thus, more analyte can be extracted. Meanwhile, increasing the number of extraction strokes from 20 to 50 resulted in an increase in extraction yield by factors of 1.5 and 2.4 for benzene and naphthalene, respectively. A continuous increase in extraction strokes resulted in no further increase in response for BTEX compounds, while extraction yield of naphthalene increased by a factor of 1.3.

In general, two major mechanisms may influence phase distribution in headspace microextraction techniques: air-water (K_{aw}) and sorbent-air (K_{CNT-a}) distribution [35]. A discussion of the influence of the latter process is not necessarily straightforward as (i) K_{CNT-a} data are not as abundant as for example sorbent-water (K_{CNT-w}) distribution data and (ii) the application of a thermodynamic cycle to derive K_{CNT-a} from K_{CNT-w} via K_{aw} is not feasible without some restrictions [36]. However, since the extractions were performed at 65 °C in a closed container, one can estimate the relative humidity in the system to be close to 100%. The CNT surface fully submerged in water (i.e., K_{CNT-w}) and its surface exposed to gaseous sample during the extraction procedure (i.e., K_{CNT-a}) should thus be characterized by similar properties. This should make the application of a thermodynamic cycle for a rough estimation of K_{CNT-a} data feasible. K_{CNT-a} values were thus estimated from sorbate isotherms obtained in aqueous solution (unpublished data) and range from 10^5 for benzene to 10^8 for naphthalene. These values correspond well with K_{CNT-a} data obtained by breakthrough curves [4]. As a consequence, one can conclude that the sorbate-sorbent interaction for naphthalene is by far stronger than the interaction of BTEX compounds with MWCNTs but may require much more time to reach equilibrium [35].

6.4.2 Significance and interaction of parameters

One of the major advantages of the application of DoE for method optimization is the fact that not only the effect of individual factors on the response can be examined, but also the interaction of two or more parameters, and the significance of their contribution to the extraction yield can easily be evaluated. For the data analysis of the DoE applied in this study, terms for each extraction parameter, the interaction of two parameters, as well as a term for the interaction of all three parameters was taken into account. Furthermore, for the derivation of the best model fit, not only linear regression coefficients were considered but also quadratic to reflect the occurrence of a local maximum in extraction yield as can be seen in Figure 6-2 for the effect of extraction temperature on the response for benzene.

The influence of individual parameters on the extraction yield varied among the investigated analytes. Apparently, there is no linear effect of the temperature on the extraction of benzene (Figure 6-2). Thus, a quadratic term for the extraction temperature was taken into account in the regression model, which increased the significance of *T* contribution to the response. Furthermore, there seemed to be a significant interaction between the extraction temperature and the number of extraction strokes (*T*S* in Table 6-3). Overall, the incorporation of a quadratic temperature term and the interaction of temperature and strokes, significantly improved the multiple response model for benzene derived from the factorial DoE ($p < 0.001$), which is therefore given by:

$$A_{Benz} = 1640247 \cdot T - 13234 \cdot T^2 - 4191 \cdot TS + 298098 \cdot S - 77648 \cdot F - 39396134 \quad \text{(Eq. 6-1)}$$

For the extraction yield of naphthalene, *T* had the strongest effect in the response, closely followed by *S*, while *F* had the lowest effect ($p < 0.01$). Meanwhile, all considered interactions did not seem to significantly improve the linear model, from which it can be concluded that there do not seem to be interactions between the parameters. In order to further improve the model, quadratic terms for each factor were considered but only the quadratic term for the extraction strokes (S^2) significantly contributed to the response (not shown). As can be seen from equation 6-2, the contribution of S^2 is rather low compared to the other coefficients. For confirmation, the two models (i.e., linear and linear + S^2) were compared and the second model showed a strong significant improvement ($p < 0.001$). Thus, the multiple response model for naphthalene derived from the factorial DoE is given by:

$$A_{Naph} = 141150 \cdot T + 299957 \cdot S - 2496 \cdot S^2 - 32885 \cdot F - 9511612 \quad \text{(Eq. 6-2)}$$

The statistical data of equations 6-1 and 6-2 are given in Table 6-3. Despite the fact that results of the lack of fit given in Table 6-3 is comparably high, which may be a result of the relatively high deviation of some experimental data due to the randomized order of the experiments, the regression of the obtained data by equations 6-1 and 6-2 were both highly significant ($p < 0.0001$) indicating a correlation between the obtained peak areas from the DoE and the regression models given in equations 6-1 and 6-2. The thereby derived model coefficients were used to predict the responses of benzene and naphthalene for the optimized extraction parameters (as given in the next section). A comparison between the predicted and the measured responses shows a fairly good correlation (shown in Figure A 6-1).

Table 6-3: Analyses of variance for a linear regression for the response to Benz and Naph.

Source[a]	Benzene				Source[a]	Naphthalene			
	DF	SS[c]	F-value	p-value		DF	SS[c]	F-value	p-Value
Model	5	8.10E+14	12.44	<0.0001	Model	4	5.09E+14	27.15	<0.0001
T	1	7.64E+12	0.59	0.4462	T	1	2.42E+14	51.67	<0.0001
T^2	1	1.60E+14	12.25	<0.0001	S	1	1.23E+14	26.33	<0.0001
T*S	1	1.28E+14	9.83	0.0025	S^2	1	9.08E+13	19.39	<0.0001
S	1	2.22E+14	17.06	<0.0001	F	1	5.26E+13	11.22	0.0001
F	1	2.93E+14	22.50	<0.0001					
Residual[d]	75	9.77E+14			Residual[d]	76	3.56E+14		
LoF[e]	21	9.28E+14	47.46	<0.0001	LoF[e]	22	3.26E+14	27.32	<0.0001
P.E.[f]	54	5.05E+13			P.E.[f]	54	2.93E+13		
Cor. total[g]	80	1.79E+15			Cor. total[g]	80	8.65E+14		

[a]Factor labels according to Table 6-2; [b]degree of freedom; [c]sum of squares; [e]Lack of Fit; [f]Pure error; [g]Corrected total sum of squares.

The statistical data in general confirm the observations made in the previous section, which are displayed in the main effect plots in Figure 6-2 and the observed tendencies are in accordance with earlier reports using ITEX2 with a mixed bed of commercially available trap materials [19].

6.4.3 Determination of method parameters

Based on the results of the factorial DoE, which are shown in Figure 6-2, 65 °C extraction temperature was chosen as optimum. This temperature empirically reflects to result in the highest extraction yields for all analytes. Furthermore, a high number of extraction strokes in combination with a low extraction flow lead to an increase in extraction yield. In order to keep the total extraction time as low as possible a combination of 60 extraction strokes with an extraction flow of 30 µL s^{-1} was chosen. A chromatogram obtained for optimized parameters with analyte concentrations as given in the previous section is shown in Figure A 6-2.

For the validation of the ITEX2 method, the linear dynamic range (LDR), method detection limits (MDLs), and precision were determined. For LDR, a nine-point calibration (each point in triplicate) was prepared. The method detection limits (MDLs) for the analytes were calculated according to a procedure used by the U.S. Environmental Protection Agency [37]. The MDLs were calculated by using Eq. (3):

$$MDL = t_{(\mathrm{N}-1,1-\alpha=0.99)} \times s_{rep} \qquad \text{(Eq. 6-3)}$$

For the calculation of the MDLs, seven replicates (s_{rep}) were measured for each compound, at a concentration level with a signal-to-noise ratio (S/N) of around five to one, or in case of chromatographic background or not totally blank free water the slope of the calibration curve exhibited a break nearing low analyte concentrations. All validation data are given in Table 6-4.

Table 6-4: Validation data for the presented ITEX2-GC-MS method.

Analyte	m/z	t_R in min	LDR in µg L^{-1}	R^2	MDL in ng L^{-1}	Precision low in %[a]	Precision high in %[b]	Recovery tab water[c]	Recovery bank filtrate[c]	Recovery WWTP effluent[c]	Spiking level in µg L^{-1}
Benzene	77, 78	2.16	0.005-5	0.9999	2	6.3	4.1	98 ± 3	93 ± 1	94 ± 2	0.88
Toluene	91, 92	3.47	0.004-4	0.9993	4	6.7	4.2	108 ± 2	106 ± 1	107 ± 6	0.87
Ethylbenzene	91, 106	5.54	0.014-35	0.9988	9	8.7	5.2	103 ± 3	100 ± 2	104 ± 1	0.86
o-xylene	91, 106	6.42	0.002-35	0.9979	2	3.6	5.8	92 ± 3	89 ± 1	93 ± 3	0.88
p-xylene	91, 106	5.78	0.015-35	0.9988	11	4.0	6.8	92 ± 2	85 ± 13	102 ± 2	0.86
Naphthalene	128	16.13	0.006-30	0.9997	2	3.5	3.8	93 ± 3	107 ± 1	93 ± 1	1.50

m/z: mass-to-charge ratio. t_R: retention time. LDR: linear dynamic range. MDL: method detection limit. [a]determined at MDL. [b]determined at concentrations two orders of magnitude higher than MDL ranging from 0.34 µg L^{-1} for *p*Xyl to 0.60 µg L^{-1} for Naph. [c]Recoveries in % ± RSD (n=3).

The linear ranges of all analytes covered at least three orders of magnitude, while the MDLs ranged from 2 ng L^{-1} for benzene, *o*-xylene, and naphthalene to 11 ng L^{-1} for *p*-xylene. Interestingly, the MDL of naphthalene is among the lowest despite the fact that its air-water partitioning is the lowest (Table 6-1). This can be explained by the strong sorption of naphthalene by MWCNTs. From a mechanistic perspective, organic compounds-CNTs interactions are predominately influenced by the capability of the sorbate-sorbent-system to undergo EDA interactions [38]. Furthermore, for gas sorption by hydrophobic sorbents van-der-Waals force is of major importance [39]. Since among all analytes naphthalene is the most hydrophobic and with the highest aromaticity, its interaction with the also hydrophobic MWCNTs is most likely to be stronger than for the other analytes. This is substantiated by the fact that solute descriptors used to describe specific and non-specific interactions in poly-parameter linear free-energy relationships (ppLFER) increases by the order Benz < Tol < eBenz < Xyl < Naph [40]. Despite the fact that up to date most mechanistic studies on the interactions between hydrophobic organic compounds (HOC) and CNTs are mainly limited to sorption from aqueous phases [41, 42], similar mechanisms should be of importance here even with the already mentioned thermodynamic restrictions. An extension of the analyte set to PAHs with more benzene rings (i.e., pyrene, chrysene, or others) should thus show a similar tendency. Furthermore, a consideration of analytes featuring various functionalities should yield further insights into relevant HOC-CNTs interactions.

The precision of the proposed extraction procedure was evaluated at two concentration levels (n=7); the lower concentration was approximately at the MDL, while the precision for the higher concentration was determined at concentrations two orders of magnitude higher than MDL ranging from 0.34 µg L^{-1} for *p*-xylene to 0.60 µg L^{-1} for naphthalene. As can be seen in Table 6-4, the precision of all analytes at both concentration levels ranged between 3.5 to 8.7%. The precision obtained for the ITEX2 method are well comparable to other methods using different sorptive packing material for ITEX2 [19] or SPDE [32].

A comparison of MDLs obtained for analytes in this study with various headspace microextraction techniques using identical analytes is given in Table 6-5. It should be mentioned that of course detection limits in general are only comparable to some extent as they certainly are method-biased. In fact, detection limits determined as a specified signal-to-noise ratio, tend to be lower than those determined by other protocols such as EPA or DIN

32645 method. Thus, detection limits were additionally determined by signal-to-noise ratio to enhance the comparability of our data. Overall, the detection limits of the here presented ITEX2 method using MWCNTs as sorptive packing material were well comparable to recently reported methods for BTEX analysis, which emphasizes the potential of MWCNTs for the preconcentration of analytes with stronger EDA interaction ability (e.g., PAHs).

Table 6-5: Comparison of detection limits (ng L^{-1}) obtained in this study with similar headspace microextraction works.

Analyte	ITEX2			Headspace SPME[a,b]	
	MWCNTs (this study)		Tenax GR/ Carbosieve S III[c] [19]	MWCNTs	Other coatings
	MDL[c]	S/N:3/1[b]			
Benzene	2	0.025	1	3 [13]	280[d] [28]
Toluene	4	0.041	5	2 [13]	190[d] [28]
Ethylbenzene	9	0.042	2	0.7 [13]	60[d] [28]
o-xylene	2	0.093	5	0.6 [13]	50[d] [28]
p-xylene	11	0.030	4	-	50[d] [28]
Naphthalene	2	0.290	-	60 [14]	200[e] [29]

[a]Headspace-SPME-GC-FID; [b]Signal-to-noise ratio 3:1; [c]MDL determined by EPA method (n=7); [d]100 µm PDMS; [e]85 µm PA.

Furthermore, the recovery was determined from three different water samples: tap water, a bank filtrate from the river Ruhr, and an effluent from a wastewater treatment plant. The spiking level ranged from 0.86 to 1.50 µg L^{-1} for *p*-xylene and naphthalene, respectively. The recovery was then calculated by the ratio between the average determined concentration of the samples and the initial spike concentration (Table 6-4). In addition, the water samples were analyzed unspiked to ensure no initial analyte concentrations. In case initial concentrations were obtained, those were subtracted from the measured concentration. The recoveries in principle ranged between 85 and 108% with RSDs below 10%, only the RSD for *p*-xylene in the bank filtrate was higher than 10%. The method was additionally applied to determine the concentrations of the target analytes in the real aqueous samples used for recovery determination. The results given in Table 6-6 show that the concentrations of benzene, ethylbenzene, and naphthalene were below MDL, while the concentrations of toluene and the xylenes were well below guideline or limit values (e.g., by the European Union [43].)

Table 6-6: Concentrations (in μg L^{-1}) of analytes in non-spiked real aqueous samples (n=3)[a].

Analyte	Tab water	RSD	Bank filtrate	RSD	WWTP Effluent	RSD
Benzene	(<0.002)		(<0.002)		(<0.002)	
Toluene	0.010	8%	0.034	4%	0.041	8%
Ethylbenzene	(<0.009)		(<0.009)		(<0.009)	
o-xylene	0.009	6%	0.008	12%	0.009	10%
p-xylene	0.019	7%	0.017	15%	0.012	6%
Naphthalene	(<0.002)		(<0.002)		(<0.002)	

[a]values below the MDL are indicated by (<MDL).

6.5 References

1. Iijima, S. *Nature* **1991**, 354, 56-58.
2. Valcarcel, M.; Cardenas, S.; Simonet, B.M.; Moliner-Martinez, Y.; Lucena, R. *TrAc, Trends in Analytical Chemistry* **2008**, 27, 34-43.
3. Mauter, M.S.; Elimelech, M. *Environmental Science & Technology* **2008**, 42, 5843-5859.
4. Li, Q.L.; Yuan, D.X.; Lin, Q.M. *Journal of Chromatography A* **2004**, 1026, 283-288.
5. Feng, X.; Tian, M.; Li, A.; Zhao, X.; Zhang, Y. *Analytical Letters* **2010**, 43, 2477-2486.
6. Merkoci, A. *Microchimica Acta* **2006**, 152, 157-174.
7. Perez-Lopez, B.; Merkoci, A. *Microchimica Acta* **2012**, 179, 1-16.
8. Hussain, C.M.; Mitra, S. *Analytical and Bioanalytical Chemistry* **2011**, 399, 75-89.
9. Saridara, C.; Brukh, R.; Iqbal, Z.; Mitra, S. *Analytical Chemistry* **2005**, 77, 1183-1187.
10. Cai, Y.Q.; Jiang, G.B.; Liu, J.F.; Zhou, Q.X. *Analytical Chemistry* **2003**, 75, 2517-2521.
11. Ravelo-Perez, L.M.; Herrera-Herrera, A.V.; Hernandez-Borges, J.; Rodriguez-Delgado, M.A. *Journal of Chromatography A* **2010**, 1217, 2618-2641.
12. Jiang, R.F.; Zhu, F.; Luan, T.G.; Tong, Y.X.; Liu, H.; Ouyang, G.F.; Pawliszyn, J. *Journal of Chromatography A* **2009**, 1216, 4641-4647.
13. Sarafraz-Yazdi, A.; Amiri, A.; Rounaghi, G.; Hosseini, H.E. *Journal of Chromatography A* **2011**, 1218, 5757-5764.
14. Maghsoudi, S.; Noroozian, E. *Chromatographia* **2012**, 75, 913-921.
15. Herrera-Herrera, A.V.; Angel Gonzalez-Curbelo, M.; Hernandez-Borges, J.; Angel Rodriguez-Delgado, M. *Analytica Chimica Acta* **2012**, 734, 1-30.
16. Berezkin, V.G.; Makarov, E.D.; Stolyarov, B.V. *Journal of Chromatography A* **2003**, 985, 63-65.
17. Saito, Y.; Ueta, I.; Kotera, K.; Ogawa, M.; Wada, H.; Jinno, K. *Journal of Chromatography A* **2006**, 1106, 190-195.
18. Eom, I.Y.; Niri, V.H.; Pawliszyn, J. *Journal of Chromatography A* **2008**, 1196, 10-14.
19. Laaks, J.; Jochmann, M.A.; Schilling, B.; Schmidt, T.C. *Analytical Chemistry* **2010**, 82, 7641-7648.
20. Viinamaki, J.; Rasanen, I.; Vuori, E.; Ojanpera, I. *Forensic Science International* **2011**, 208, 42-46.
21. Niu, L.Y.; Bao, J.F.; Zhao, L.; Zhang, Y. *Journal of Essential Oil Research* **2011**, 23, 1-6.
22. Socaci, S.A.; Socaciu, C.; Tofană, M.; Raţi, I.V.; Pintea, A. *Phytochemical Analysis* **2013**, 24, 319-328.
23. Zapata, J.; Mateo-Vivaracho, L.; Lopez, R.; Ferreira, V. *Journal of Chromatography A* **2012**, 1230, 1-7.
24. Zapata, J.; Lopez, R.; Herrero, P.; Ferreira, V. *Journal of Chromatography A* **2012**, 1266, 1-9.
25. Hibbert, D.B. *Journal of Chromatography B* **2012**, 910, 2-13.

26. Harvey, D. *Modern Analytical Chemistry;* McGraw-Hill, Columbus, U.S.A., 2000.
27. Kamphoff, M.; Thiele, T.; Kunz, B. *Journal of AOAC International* **2007**, 90, 1623-1627.
28. Gaujac, A.; Emidio, E.S.; Navickiene, S.; Costa Ferreira, S.L.; Dorea, H.S. *Journal of Chromatography A* **2008**, 1203, 99-104.
29. Zuazagoitia, D.; Millan, E.; Garcia, R. *Chromatographia* **2007**, 66, 773-777.
30. Corporation SR Interactive PhysProp Database Demo. http://www.syrres.com/esc/physdemo.htm. Accessed Jan., 2013.
31. Staudinger, J.; Roberts, P.V. *Chemosphere* **2001**, 44, 561-576.
32. Jochmann, M.A.; Yuan, X.; Schmidt, T.C. *Analytical and Bioanalytical Chemistry* **2007**, 387, 2163-2174.
33. Diaz, E.; Ordonez, S.; Vega, A. *Journal of Colloid and Interface Science* **2007**, 305, 7-16.
34. Jochmann, M.A.; Yuan, X.; Schilling, B.; Schmidt, T.C. *Journal of Chromatography A* **2008**, 1179, 96-105.
35. Zhang, Z.Y.; Pawliszyn, J. *Analytical Chemistry* **1993**, 65, 1843-1852.
36. Goss, K.U. *Environmental Science & Technology* **2004**, 38, 1622-1623.
37. Glaser, J.A.; Foerst, D.L.; Mckee, G.D.; Quave, S.A.; Budde, W.L. *Environmental Science & Technology* **1981**, 15, 1427-1435.
38. Pan, B.; Xing, B.S. *Environmental Science & Technology* **2008**, 42, 9005-9013.
39. Adamson, A.W. *Physical Chemistry of Surfaces*. John Wiley and Sons, New York, U.S.A., 1990.
40. Abraham, M.H.; Andonian-Haftvan, J.; Whiting, G.S.; Leo, A.; Taft, R.S. *Journal of the Chemical Society - Perkin Transactions 2* **1994**, 8, 1777-1791.
41. Kah, M.; Zhang, X.; Jonker, M.T.O.; Hofmann, T. *Environmental Science & Technology* **2011**, 45, 6011-6017.
42. Yang, K.; Zhu, L.Z.; Xing, B.S. *Environmental Science & Technology* **2006**, 40, 1855-1861.
43. The Council of the European Union *Official Journal of the European Communities* **1998**, 41, 32-54.

6.6 Appendix A6

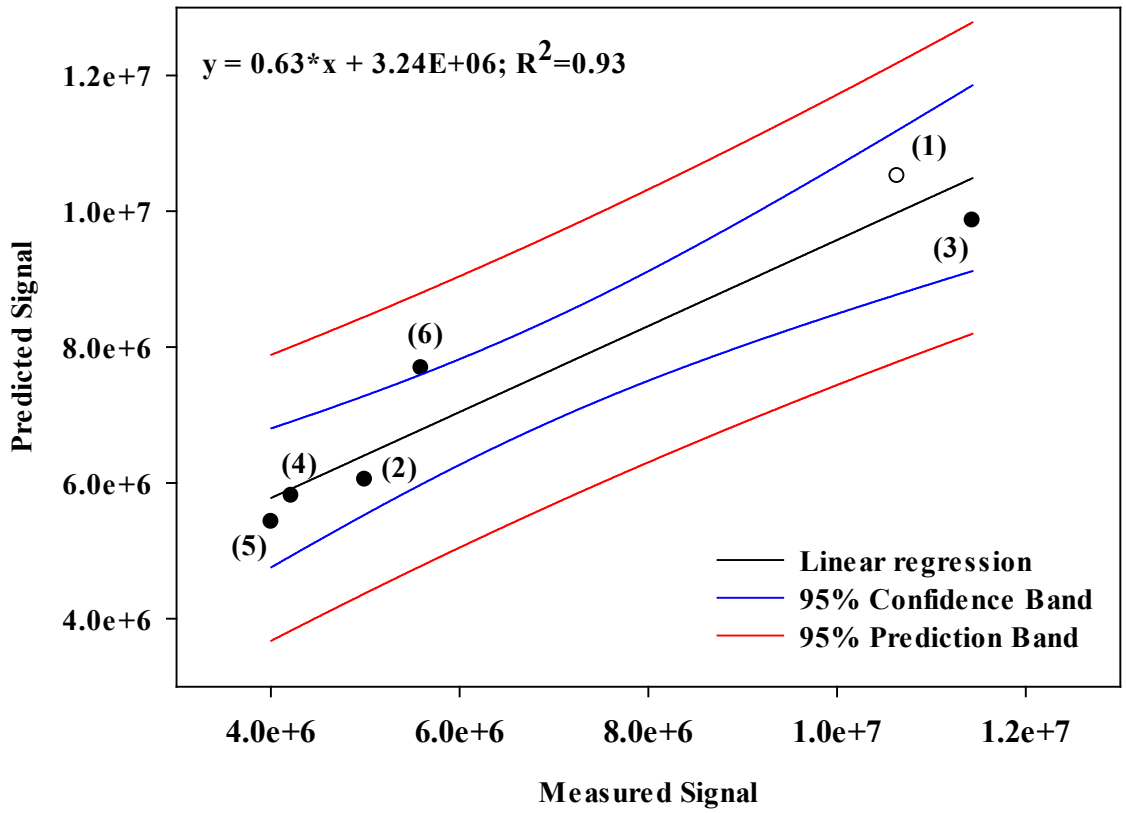

Figure A 6-1: Correlation of predicted response from multiple response models and experimentally obtained responses (n=3) for (1) Benz, (2) Tol, (3) eBenz, (4) *p*Xyl, (5) *o*Xyl, (6) Naph from optimized factor settings (Extraction temperature: 65 °C, extraction strokes: 60, and extraction flow 30 µL s^{-1}).

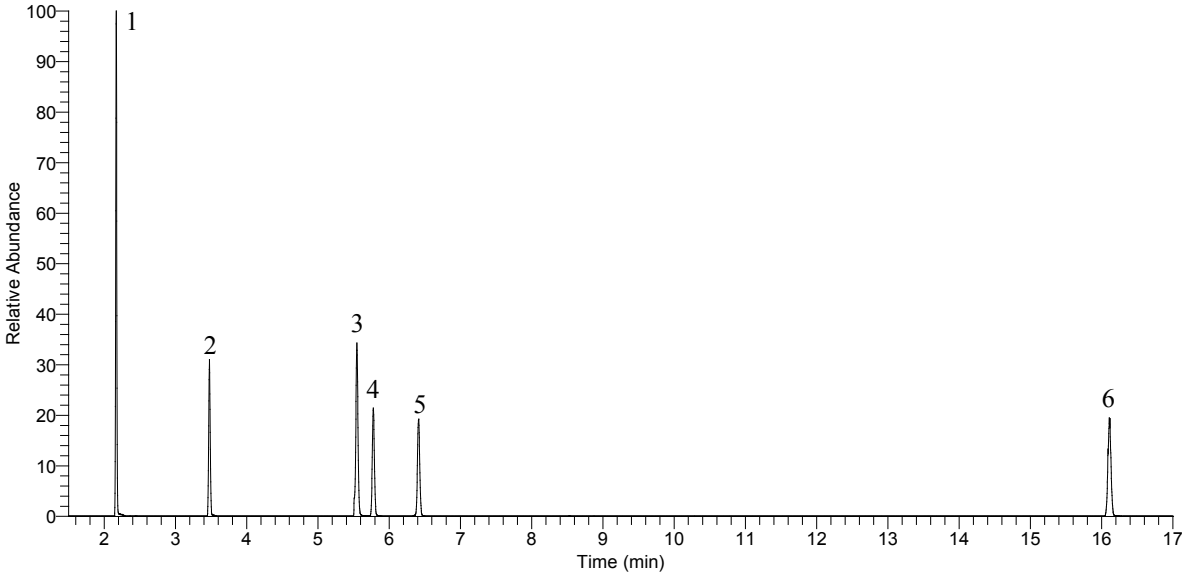

Figure A 6-2: Chromatogram obtained from GC-MS in full scan mode (m/z 70-130) for analytes extracted with optimized CNTs-ITEX2 parameters. Target analytes: (1) Benz, (2) Tol, (3) eBenz, (4) *p*Xyl, (5) *o*Xyl, (6) Naph. Analyte concentrations ranged between 3.4 and 6 µg L^{-1} for eBenz and Naph, respectively.

Chapter 7 General Conclusions and Outlook

Characterization of Sorption

In Chapters 3 and 4, the influence of environmental parameters on sorption by carbon-based nanomaterials (CNM) was systematically investigated. In **Chapter 3**, the change in redox conditions, resulting from the presence of oxygen, and irradiation were shown to significantly alter the surface properties of aqueous dispersed fullerenes (nC60). As a consequence, the sorption of polycyclic aromatic hydrocarbons (PAHs) by nC60 was suppressed. From the fit of isotherm data, it was concluded that *ad*sorption to nC60 surface and pore-filling seem to be the major sorption processes. The correlation of hydrophobicity-normalized distribution coefficients indicated that other interactions have to be additionally considered for the understanding of overall sorption. Thus, the ratio of sorption coefficients of *n*-alkanes to cycloalkanes (K_n/K_c) by multi-walled carbon nanotubes (MWCNTs) was determined in **Chapter 4** to investigate the dominant sorption mode (*ad*- vs. *ab*sorption). The results clearly indicated for *ad*sorption to be the dominant sorption mode by pristine MWCNTs since the derived K_n/K_c ratios were ~ 1. The addition of natural organic matter (NOM) resulted in a reduction of sorption. Meanwhile, the observed decrease in the non-linearity of sorption could not be connected to a potential change in sorption mode to *ab*sorption by NOM-coated MWCNTs since K_n/K_c remained ~1 regardless of NOM addition.

In summary, both investigated environmental factors significantly influenced the interaction of hydrophobic organic compounds (HOC) with nC60 and MWCNTs in terms of sorption capacity and affinity. From the observed decrease in sorption, it can be concluded that CNM, once released into the environment, may have a smaller impact on the fate and transport of HOC than pristine CNM. This seems especially relevant since the concentrations of other carbonaceous geosorbents, with supposed weaker interactions, exceed those of CNM by far. Future studies should focus on surface-modified CNM for an environmental risk assessment rather than or at least in addition to pristine CNM. Furthermore, CNM should be investigated as sorbates; for example, in column studies, in order to assess their transport in environmental matrices, which is yet problematic due to the limited number of analytical procedures for CNM.

Modeling of Sorption

The results of Chapters 3 and 4 have indicated that a single mechanism alone cannot fully explain sorption by CNM and that more systematic approaches are necessary for an accurate prediction and comprehensive understanding of sorption by these materials. Thus, in **Chapter 5**, a molecular probe set including 30 sorbates covering various compound classes was selected for sorption by MWCNTs. Poly-parameter linear free-energy relationships (ppLFER) were derived from the calculated distribution coefficients at various sorbate concentration levels to gain insights into the relevant molecular interactions and their contribution to overall sorption. Direct comparison between the prediction of distribution coefficients by one-parameter linear free-energy relationships (e.g., with the octanol-water partitioning constant) and by ppLFER indicated the advantage of using ppLFER. The improved prediction of sorption was especially pronounced in the low, environmentally relevant, concentration ranges. This can be assigned to the broad concentration range for which this ppLFER was calibrated. Furthermore, the ppLFER equations derived in this study were compared to previously reported ppLFER equations for sorption of aromatic compounds by MWCNTs. It was shown that the incorporation of aliphatic compounds in the probe set in this study significantly affected the derived phase descriptors for MWCNTs and consequently provided better prediction of sorption of organic compounds regardless of their compound class. In addition, previous conclusions on the significance of the contribution of individual descriptors to overall sorption were re-evaluated. By this, it was shown that for a comprehensive understanding of the relevant interaction, all phase descriptors of ppLFER should be considered. In conclusion, the here developed ppLFER, which was calibrated for a diverse set of probes, clearly improved previously reported equations.

Future studies should incorporate larger sorbates, for example, with higher polarities and a broader distribution of the hydrogen bond acidity (A) of Abraham in order to assess the contribution of H-bond to overall sorption. In this regard, it would be very interesting to incorporate also other kinds of CNM, for example, with surface functional groups. This would contribute to an a priori prediction of sorption by surface-modified CNM.

Application of Sorption

As a result of the generally strong interaction of HOC and CNM, MWCNTs were investigated as sorptive packing material for in-tube microextraction in **Chapter 6**. The application of a design of experiment for the method development process gave insights not only into significance of the effect of extraction parameters on the extraction yield, but also on the interaction of extraction parameters. This substantiated the general importance and advantage of such an approach in analytical method development. The results further emphasized the promising potential of the application of CNM as sorbents in analytical chemistry. Future work should on the one hand focus on a broader investigation with respect to analytes taken into account. Here, the indicated strong interaction of MWCNTs with PAHs could result in an improvement of the detection limits for these compounds in aqueous matrices, especially of PAHs with higher polycyclicity. Furthermore, a comparison of different CNM with various functionalities should explore the specific application of surface-modified CNM.

Overall, the studies carried out in this thesis emphasized the importance of systematic approaches for the characterization, modeling, and application of sorption of non-ionic organic compounds by CNM. Thereby, useful insights were given into the relevant interaction mechanisms, how they may be affected by environmental factors, their prediction, and their potential use for analytical applications.

Chapter 8 Appendix

8.1 List of Figures

8.2 List of Tables

8.3 List of Abbreviations and Symbols

A	Hydrogen bond acidity
AIK	Akaike's information criterion
ATR-FTIR	Attenuated total reflectance Fourier transform infrared spectroscopy
B	Hydrogen bond basicity
BaA	Benz[a]anthracene
BaP	Benz[a]pyrene
Benz	Benzene
eBenz	Ethylbenzene
Bp	Boiling point [°C]
BTEX	Benzene, toluene, ethylbenzene, and xylenes
C_{nC60}	Sorbate concentration on nC60 [µg kg^{-1}]
C_{POM}	Sorbate concentration on POM [µg kg^{-1}]
C_s	Sorbed sorbate concentration [µg kg^{-1}]
C_w	Aqeuous concentration [µg L^{-1}]
C60	Fullerenes
nC60	Aqueous dispersed fullerenes
nC60-DA	Aqueous dispersed fullerenes treated under dark anoxic conditions
nC60-DO	Aqueous dispersed fullerenes treated under dark oxic conditions
nC60-LA	Aqueous dispersed fullerenes treated under light anoxic conditions
nC60-LO	Aqueous dispersed fullerenes treated under light oxic conditions
C60-OH	Polyhydroxy fullerenes
CNM	Carbon-based nanomaterials
CNTs	Carbon nanotubes
DAM	Dubinin-Ashthakov model
DF	Degrees of freedom
DLS	Dynamic light scattering
DoE	Design of experiments
E	Excess molar refraction
E'	Correlating divisor [J mol^{-1}]
EDA	Electron donor-acceptor
EI	Electron ionization

ENM	Engineered nanomaterials
FM	Freundlich model
FT-IR	Fourier transform infrared spectroscopy
ΔG_{12}	Free-energy of transfer [kJ mol^{-1}]
GC	Gas chromatography
GC-MS	Gas chromatography-mass spectrometry
ΔH_{ads}	Enthalpy of adsorption [kJ mol^{-1}]
HA	Humic acid
cHep	Cycloheptane
nHep	n-Heptane
cHex	Cyclohexane
nHex	n-Hexane
HOC	Hydrophobic organic compounds
HS	Humic substances
ITEX2	In-tube microextraction
K_{aw}	Air-water partitioning constant [-]
K_c	Distribution coefficient of cyclic alkanes
K_{CNT-a}	CNT-air distribution coefficient [L kg^{-1}]
K_{CNT-w}	CNT-water distribution coefficient [L kg^{-1}]
K_d	Distribution coefficient
K_F	Freundlich coefficient $[(\mu g\ kg^{-1})/(\mu g\ L^{-1})]^{1/n}$
K_L	Langmuir affinity coefficient [$\mu g\ L^{-1}$]
K_n	Distribution coefficient of linear alkanes
K_{ow}	Octanol-water partitioning constant [-]
K_{POM}	POM-water distribution constant [L kg^{-1}]
L	Logarithmic hexadecane-air partitioning constant [-]
LDR	Linear dynamic range
LFER	Linear free-energy relationships
opLFER	One-parameter linear free-energy relationships
ppLFER	Poly-parameter linear free-energy relationships
LHAS	Leonardite Humic Acid Standard
LM	Langmuir model
LSER	Linear solvation energy relationships

m_s	Mass of sorbate sorbed on solid phase [µg]
m_T	Total mass of sorbate [µg]
m_w	Mass of sorbate in water [µg]
M_{nC60}	Mass of nC60 [kg]
M_{POM}	Mass of POM [kg]
m/z	Mass-to-charge ratio
MDL	Method detection limit
MRA	Multiple regression analysis
MS	Mass spectrometry
MV	Molar volume [cm^{-3}]
MW	Molecular weight [g mol^{-1}]
MWCNTs	Multi-walled carbon nanotubes
MWSE	Mean weighted square error
n	Freundlich exponent [-]
N	Number of data points
Naph	Naphthalene
NM	Nanomaterials
NOM	Natural organic matter
cOct	Cyclooctane
nOct	n-Octane
p	Number of fitting parameters
PAHs	Polycyclic aromatic hydrocarbons
PdI	Polydispersity index
Phen	Phenanthrene
PMM	Polanyi-Manes model
POM	Polyoxymethylene
POM-SPE	Polyoxymethylene solid-phase extraction
PPHAS	Pahokee Peat Humic Acid Standard
Pyr	Pyrene
Q_{max}	Maximum sorption capacity [µg kg^{-1}]
R	Universal gas constant [$8.314 \cdot 10^{-3}$ kJ mol^{-1} K^{-1}]
R^2	Coefficient of determination / Regression coefficient
RMSE	Root mean squared error

S	Dipolarity/polarizability
S_i	Subcooled liquid solubility
S_w	Aqueous solubility [mg L^{-1}]
S/N	Signal-to-noise ratio
SE	Standard error of estimates
SEM	Scanning electron microscopy
SMM	Single magnet mixer
SPDE	Solid phase dynamic extraction
SPE	Solid phase extraction
SPME	Solid-phase microextraction
nd-SPME	non-depletion Solid-phase microextraction
SS	Sum of squares
SSL	Split/splitless injector
SWCNTs	Single-walled carbon nanotubes
t_R	Retention time [min]
T	Absolute temperature [K]
TOC	Total organic carbon
Tol	Toluene
TOT	Time of transition
V	Molar volume
V_s	Bulk molar volume
V_w	Volume of water [L]
VOCs	Volatile organic compounds
WPHAR	Waskish Peat Humic Acid Standard
WSS_{res}	Weighted sum of squares residual
XPS	X-ray photoelectron spectroscopy
oXyl	o-Xylene
pXyl	p-Xylene
ZP	Zeta potential
ε	Sorption potential [kJ mol^{-1}]
ε_{sw}	Effective sorption potential [kJ mol^{-1}]
ρ	Density [g mL^{-1}]

8.4 List of Publications

Publications in peer-reviewed Journals

Hüffer, T.; Schroth, S.; Schmidt, T.C. *Is the Sorption Mode of Carbon Nanotubes affected by Natural Organic Matter?* Environmental Science & Technology, submitted.

Hüffer, T., Osorio, X.L.; Jochmann, M.A.; Schilling, B.; Schmidt, T.C. *Multi-walled carbon nanotubes as sorptive material for solventless in-tube microextraction (ITEX2) – A factorial design study*. Analytical and Bioanalytical Chemistry **2013,** 405 (26), 8387-8395.

Hüffer, T.; Kah, M.; Hofmann, T.; Schmidt, T.C. *How Redox Conditions and Irradiation Affect Sorption of PAHs by Dispersed Fullerenes (nC60)*. Environmental Science & Technology, **2013**, 47 (13), 6935-6942.

Oral presentations

Hüffer, T.; Kah, M.; Hofmann, T.; Schmidt, T.C. *Einfluss umweltrelevanter Parameter auf das Sorptionsverhalten kohlenstoff-basierender Nanomaterialien*, 18.Jahrestagung der SETAC GLB, 23.-26.09.2013, Essen, Germany.

Hüffer, T.; Kah, M.; Hofmann, T.; Schmidt, T.C. *Characterization of aqueous fullerene (nC60) after UV-assisted dispersion and during sorption with phenanthrene,* 23rd International Symposium on Polycyclic Aromatic Compounds (ISPAC23), 04.-08.09.2011, Münster, Germany.

Hüffer, T.; Schmidt, T.C. *Sorption of non-ionic organic compounds onto carbon-based nanomaterials*, Norman Workshop: Engineered Nanoparticles in the Environment, 19.-20.10.2010, Koblenz, Germany.

Hüffer, T.; Schmidt, T.C. *Sorption of non-ionic organic compounds onto carbon-based nanomaterials*, 5.Spätsommer Workshop der Wasserchemischen Gesellschaft, 29.09.-01.10.2010, Schloss Maurach, Bodensee, Germany.

Poster presentations

Hüffer, T.; Metzelder, F.; Schroth, S.; Schmidt, T.C. *Charakterisierung der Sorption nicht-ionischer organischer Verbindungen ab mehrwandigen Kohlenstoffnanoröhren mittels ppLFER*, 18.Jahrestagung der SETAC GLB, 23.-26.09.2013, Essen, Germany.

Hüffer, T.; Schmidt, T.C. *Einfluss von Huminstoffen auf den Sorptionsmodus an Kohlenstoffnanoröhren*, Jahrestagung der Wasserchemischen Gesellschaft, 06.-08.05.2013, Goslar, Germany.

Hüffer, T.; Osorio, X.L.; Schmidt, T.C.; Jochmann, M.A. *Carbon nanotubes as sorptive material for ITEX2 microextraction – A factorial design study*, ANAKON 2013, 04.-07.03.2013, Essen, Germany.

Hüffer, T.; Schmidt, T.C. *How natural organic matter affect the sorption behavior of carbon-based nanomaterials*, Gemeinsame Jahrestagung der Fachgruppe Umwelt-Chemie und Ökotoxikologie der GDCh und der SETAC GLB, 10.-13.09.2012, Leipzig, Germany.

Hüffer, T.; Kah, M.; Hofmann, T.; Schmidt T.C. *Influence of surface oxidation on the sorption behavior of nC60 suspensions*, Jahrestagung der Wasserchemischen Gesellschaft, 14.-16.05.2012, Neu-Ulm, Germany.

8.5 Curriculum Vitae

Der Lebenslauf ist in der Online-Version aus Gründen des Datenschutzes nicht enthalten.

8.6 Erklärung

Hiermit versichere ich, dass ich die vorliegende Arbeit mit dem Titel

„Sorption of non-ionic organic compounds by carbon-based nanomaterials – Systematic characterization, modeling, and application"

selbst verfasst und keine außer den angegebenen Hilfsmitteln und Quellen benutzt habe, und dass die Arbeit in dieser oder ähnlicher Form noch bei keiner anderen Universität eingereicht wurde.

Essen, im Oktober 2013